NEXT GENERATION ELECTROSPUN NANOFIBER ELECTRODES FOR HYDROGEN/AIR FUEL CELLS

By

John James Slack

Dissertation

Submitted to the Faculty of the

Graduate School of Vanderbilt University

in partial fulfillment of the requirements

for the degree of

DOCTOR OF PHILOSOPHY

in

Chemical Engineering

January 31, 2019

Nashville, Tennessee

Approved:

Peter Pintauro, Ph.D.

Kane Jennings, Ph.D.

Rizia Bardhan, Ph.D.

Janet Macdonald, Ph.D.

DEDICATION

Dedicated to my parents, Helen and Jerry Slack, my sister, Jackie Copenhaver, my brother, Eric Copenhaver, and my fiancé, Brittany Skelly, whose support has enabled the completion of this document.

ACKNOWLEDGEMENTS

I thank everyone who made contributions which were essential to the completion of this dissertation. Gratitude goes to my thesis advisor, Professor Peter N. Pintauro, for accepting me into his research group and supporting my studies at Vanderbilt. I thank Professors G. Kane Jennings, Rizia Bardhan, and Janet Macdonald, for providing valuable feedback on my research while serving on my thesis committee.

I also want to acknowledge all members of the Pintauro group for their support. Professor Ryszard Wycisk and his expertise in polymer chemistry was a useful resource in the laboratory. Thanks goes to Dr. Matthew Brodt for his guidance during my early years at Vanderbilt. I would like to especially thank and acknowledge Krysta Waldrop and Devon Powers whose friendship and collaboration were truly invaluable during my studies at Vanderbilt. Tori Trout and Brian Doney were undergraduate researchers who worked on various aspects of this project. Mr. Doney made substantial contributions to the studies on PtCo alloy catalysts.

Several collaborators made significant contributions to this work. Dr. Nilesh Dale, Dr. Amod Kumar, and Dr. Cenk Gumeci at Nissan Technical Center of North America have all helped tremendously in providing their insights as well as additional results through the use of their testing facilities in Novi, MI. Dr. Sanjeev Mukerjee and his research group as well as Pajarito Powder, LLC were critical in the study of PGM-free oxygen reduction reaction (ORR) catalysts for use in electrospun PEMFC cathodes. These groups provided the PGM-free catalysts and confirmed baseline performances. Dr. Karren More, Dr. David Cullen, and Dr. Brian Sneed at Oak Ridge National Laboratory (ORNL) were instrumental

during my visits to Oak Ridge National Laboratory in helping me obtain and analyze electron probe microscopy data on beginning of life and end of life membrane electrode assemblies (MEAs). Dr. Rangachary Mukundan, Dr. Rod Borup, Dr. Andrew Baker, and Dr. Natalia Macauley at Los Alamos National Lab (LANL) were also helpful for their independent evaluation and confirmation of the performance of our material as well as the accelerated stress test data that they provided for our materials.

I also want to thank several members of the Vanderbilt community for their diligent work which was vital for completion of my research. Mary Gilleran, Angie Pernell, Julie James, Felisha Baquera, and Julie Canada, provided friendly administrative assistance and were always prompt in processing my purchase requests and travel forms. Mark Holmes helped whenever there was an issue that arose with building equipment. Professor Anthony Hmelo was helpful in training me to use our scanning electron microscope, the MERLIN and he worked tirelessly to ensure laboratory facilities were available to the VINSE research community. Fellow graduate students and members of the Nashville community made my time spent at Vanderbilt unforgettable. Thanks to all of you for your friendship and kindness. Most importantly, I want to thank my family for their unwavering love and support. My parents and sister helped me put life in perspective throughout the highs and lows of graduate school.

This work was funded initially by the National Science Foundation (NSF EPS-1004083 through the TN-SCORE program under Thrust 2 and the United States Department of Energy (DE-EE0007215) and then by Fuel Cell Consortium for Performance and Durability DOE-EERE FC-PAD Project DE-EE0007653.

TABLE OF CONTENTS

Chapter Page

LIST OF TABLES

Page

LIST OF FIGURES

Page

CHAPTER 1

INTRODUCTION

1.1 Rationale

Fuel cells have been gaining attention as a means of sustainable energy conversion in recent years and are expected to grow much more in the near future.[1] This technology is an attractive option for both grid-level and automotive applications for a number of reasons including zero-carbon-emissions, high energy and power densities, and moderate operating temperature (80 – 110 °C).[2–4]

The limiting factor for sustainable energy usage at large and small scales is energy storage.[5] With the advent of renewable energy sources, the decentralization of electricity generation has brought about new challenges for electrical grids including the prevention of wasted electricity. Distributed electricity generation from solar, wind, and hydroelectric utility stations have caused variability and intermittency in power output and do not always match with demand. During peak output, power generation can be more than 60% over demand.[6] Without a storage solution, energy is wasted. An effective method for energy storage is through the generation of hydrogen via water-splitting and then recovery of that energy through the use of a fuel cell. The hydrogen generated from excess renewables may be utilized for either stationary (e.g. smart-grid) or portable power generation (e.g. electric vehicle).

In the process of decarbonizing the automotive industry, two primary electrochemical storage methods are being considered: fuel cells and batteries. While both have specific niches to fill, fuel cell electric vehicles (FCEVs) offer several benefits over

traditional battery-driven electric vehicles including a fast refueling rate, and much lower operation cost at long ranges. The first commercial FCEV, the Toyota Mirai, was released in 2015 and as of December 2017, 5,300 Mirais have been sold globally.[7] Since then, automakers all over the world including Honda, Hyundai, General Motors, Ford, Nissan, and more, have been developing their own FCEVs for release.

Widespread adoption of this technology has not been realized for several reasons.[8] These reasons include the low power output while operating at low (~40%) relative humidity (RH), and degradation of the fuel cell's membrane electrode assembly (MEA). The work included in this dissertation aims to mitigate these obstacles by designing fuel cell electrodes with electrospun nanofiber morphologies. Specifically, the studies presented herein will focus on improving power generation of nanofiber cathodes using platinum and platinum alloy catalysts and improving durability of nanofiber electrodes with platinum-free cathodes.

1.2 Current Obstacles in Fuel Cell Technology

1.2.1 Low Relative Humidity Operation

Conventional hydrogen/air fuel cells generate lower power at low relative humidity according to both modeling and experimental results.[9–12] This occurs for three reasons: (1) because of low ionic conductivity of the membrane and ionomer in the electrode binder[10,13–17], (2) reduced oxygen reduction activity at low RH[9,11,12,18], and (3) increased gas transport resistance through the ionomer in the binder[12,19]. Fuel cell MEAs require high ionic conductivity for optimal performance.[20] This ionic conductivity is highly dependent on the amount of water in the fuel cell electrode ionomer and membrane.[21–23] The ionomer and membrane used in fuel cells today are based on perfluorosulfonic acid

(PFSA) polymers such as Nafion®. The conductivity of Nafion varies significantly with water content which decreases with decreasing relative humidity at a given temperature.[21] For example, Nafion's conductivity at 80 °C in air at near full humidification is 0.1 S/cm and at 40% RH, Nafion's conductivity is 0.02 S/cm.[9] The operation of a fuel cell at low relative humidity has been shown to produce lower power at lower relative humidity due to the lower conductivity of the ionomer within the membrane electrode assembly (MEA).[13-17] In addition, the oxygen reduction kinetics at the cathode are also more sluggish at low relative humidity which can further reduce power generation.[11,12,18,19] Generally, for a proton exchange membrane fuel cell, several parameters are considered when evaluating the rate-limiting oxygen reduction reaction kinetics: open circuit voltage, exchange current density, and Tafel slope.[24] The relative humidity of a fuel cell will affect all of these parameters. As relative humidity decreases, open circuit voltage (OCV) increases due to its dependence on the concentration of oxygen at the catalyst sites; as water vapor in the feed is reduced, the partial pressure of oxygen is increased which increases OCV. Higher OCV generally improves the performance of a PEMFC MEA. This effect is overshadowed, however, by the effect of the exchange current density decreasing with relative humidity.[25]

Decreasing relative humidity not only affects ORR kinetics, but also impedes the mass transport of oxygen within a fuel cell electrode. The transport resistance of feed gas through the catalyst layer relative to moderate humidity is decreased because gas travels more quickly through hydrated ion clusters and channels in the polymer more quickly than through the polymer itself.[26] The effect of RH on mass transport properties is multifaceted and depends on the composition and structure of the fuel cell anode, membrane, and

cathode because at full humidification, water "flooding" may occur which can cause water to block catalyst sites in the cathode, causing sharp declines in voltage at high current.[24]

1.2.2 Low Catalyst Loading

The overall cost of platinum catalyst has decreased in relation to the total fuel cell stack design[8], but the catalyst metal remains expensive. Because of this, there has been an emphasis on reducing the amount of platinum in the fuel cell. Research has focused on several approaches to reduce platinum including developments in Pt-alloy catalysts, Platinum- and Platinum-Group-Metal-free catalysts, and intelligent electrode design.[27–38] Highly active catalysts have been synthesized and a lower total loading of these catalysts produce the same amount of power. Several groups including work performed by Markovic[35], Stamenkovic[37], Strasser[36], and more have examined new electrocatalysts that are platinum-based, but contain another transition metal (e.g. Ni, or Co). These groups have also improved the intrinsic catalytic activity for the oxygen reduction reaction by controlling the shape of the metal nanoparticles (e.g. octahedral, hollow, core/shell or nano-cage structures) rather than the conventional spherical nanoparticles.[39–41] Intrinsic catalytic activity in this case refers to the ability of a metal to adsorb the reactants (H_2 or O_2) strongly enough to facilitate a reaction but not so strongly that the catalyst becomes blocked by the reactant or product (H_2O). Each of the aforementioned strategies have resulted in significant improvements in power generation when testing in a rotating-disk-electrode (RDE) setup. While these experiments are valuable for screening materials for improved activity, RDE results often do not correlate with results in a real fuel cell membrane electrode assembly[42]. RDE results with PtCo nanoparticles suggest the current should be orders of magnitude larger than traditional Pt nanoparticles, but in an MEA, there

is a more modest ~30% improvement over conventional catalysts.[43,44] Nonetheless, this is a significant improvement. Incorporating PtCo/C into fuel cell MEAs will be discussed more in-depth in Chapters 4 and 5 of this dissertation.

A different strategy involving catalyst synthesis includes using a much less costly platinum-group-metal-free (PGM-free) catalyst.[27,28,31–33] This approach completely eliminates precious metal in a fuel cell cathode. PGM-free catalysts are typically pyrolyzed carbon based powders with metal/nitrogen/carbon (M-N-C) catalytic surface sites[27], where the metal ion is often cobalt or iron. In M-N-C catalysts, three types of active sites have been established – metal-nitrogen moieties embedded in carbon (MN_xC_y), nitrogen-carbon moieties (CN_x), and nitrogen doped carbon encapsulating inorganic metal species ($M@N_xC_y$). All three types of active sites co-exist in most pyrolyzed M-N-C materials. These types of catalysts have been developed by Atanassov[27], Dodelet[31,33], Zelenay[32], and Mukerjee[28]. This strategy creates a catalyst that has much lower mass activity (i.e. : ~1 $mA/mg_{PGM\text{-}free\ catalyst}$ vs. ~100 mA/mg_{Pt}), but is much less expensive, so higher loadings of catalyst can be used to make up for the reduction in activity. One type of PGM-free catalyst (synthesized by Pajarito Powder LLC) will be discussed more in depth in Chapter 3 of the dissertation.

1.2.3 PEMFC Membrane Electrode Assembly Durability

The cathode must exhibit sufficient durability as defined by targets set by the United States Department of Energy (DOE)[45] and the Fuel Cell Commercialization Conference of Japan (FCCJ)[46]. The durability targets were developed in collaboration with auto-makers and have set a goal for PEMFC MEA performance loss after defined accelerated stress tests (ASTs). These ASTs were designed to simulate processes that

would naturally occur during the lifetime of a fuel cell electric vehicle. These include starting and stopping the vehicle (a voltage cycling protocol from 1.0 V to 1.5 V which induces carbon corrosion) and accelerating and decelerating the vehicle (a voltage cycling protocol from 0.6 V to 0.95 V which induces metal dissolution).[46] The DOE durability performance targets for 2020 are that an MEA with >240 mA/cm^2 at 0.8V, >800 mW/cm^2 at rated power will experience <50% drop in ORR mass activity after 30,000 voltage cycles of 0.6 V – 0.95 V and <20% drop in voltage at 1.2 A/cm^2 after 5,000 voltage cycles from 1.0 V - 1.5 V and <30% loss in rated power after drive cycle durability.[45]

The start/stop accelerated stress test causes oxidation of the carbon catalyst support to form CO_2 or to partially oxidize the carbon surface. These effects result in a loss of surface area and catalyst layer collapse.[47] The metal dissolution AST will cause failure by dissolving catalyst metal and redepositing in the membrane, causing Pt to migrate and agglomerate forming larger particles, or dissolving and precipitate Pt onto larger metal particles (Ostwald ripening) which can decrease the electrochemically active surface area or decrease membrane conductivity.[41,48] These effects will increase the ionic resistance of the membrane and decrease the electrochemically active surface area which effectively reduces the ability of the cathode to catalyze the oxygen reduction reaction. If the catalyst metal is Pt alloyed with a transition metal (e.g. Cobalt or Nickel), transition metal leaching can occur which reduces catalyst activity and through deposition/interaction with the ionomeric binder and membrane, further reduces ionic conductivity of the MEA.[49]

The next chapter will discuss the fundamentals of fuel cell MEA analysis, the strategies used in the literature to overcome obstacles to widespread fuel cell adoption, and the objectives of this dissertation.

1.3 References

[1] I. Trends, Projected global fuel cell vehicle unit sales between 2015 and 2020 (in units) https://www.statista.com/statistics/644545/global-sales-of-fuel-cell-vehicles/ **2018**.

[2] Dimitrios Papageorgopoulos, *Fuel Cells R&D Overview. Office of Energy Efficiency and Renewable Energy*; Washington D.C., 2018.

[3] *Hydrog. Counc. Hydrog. scaling up A Sustain. Pathw. Glob. energy transition. www.hydrogencouncil.com* **2017**, 80.

[4] S. Satyapal, *Hydrogen and Fuel Cells Overview. Department Of Energy. 2018 Annual Merit Review*; 2017.

[5] B. K. Paul Denholm, Erik Ela, and M. Milligan, *The Role of Energy Storage with Renewable Electricity Generation*; 2010.

[6] K. Kimura, *Renew. Energy Inst.* **2016**.

[7] N. Release, Toyota sells 1.52 million electrified vehicles in 2017, three years ahead of 2020 target. *Toyota Glob. Newsroom* **2018**.

[8] J. Wang, H. Wang, Y. Fan, *Engineering* **2018**, *4*, 352.

[9] J. Zhang, Y. Tang, C. Song, Z. Xia, H. Li, H. Wang, J. Zhang, *Electrochim. Acta* **2008**, *53*, 5315.

[10] S. D. Knights, K. M. Colbow, J. St-Pierre, D. P. Wilkinson, *J. Power Sources* **2004**, *127*, 127.

[11] M. M. Saleh, T. Okajima, M. Hayase, F. Kitamura, T. Ohsaka, *J. Power Sources* **2007**, *164*, 503.

[12] J. H. Jang, W. M. Yan, H. Y. Li, Y. C. Chou, *J. Power Sources* **2006**, *159*, 468.

[13] A. V. Anantaraman, C. L. Gardner, *J. Electroanal. Chem.* **1996**, *414*, 115.

[14] V. Ramani, H. R. Kunz, J. M. Fenton, *Electrochim. Acta* **2005**, *50*, 1181.

[15] H. Xu, H. R. Kunz, J. M. Fenton, *Electrochim. Acta* **2007**, *52*, 3525.

[16] Y. Sone, *J. Electrochem. Soc.* **1996**, *143*, 1254.

[17] J. J. Sumner, *J. Electrochem. Soc.* **1998**, *145*, 107.

[18] T. Abe, H. Shima, K. Watanabe, Y. Ito, *J. Electrochem. Soc.* **2004**, *151*, A101.

[19] R. Jiang, H. Russell Kunz, J. M. Fenton, *Electrochim. Acta* **2006**, *51*, 5596.

[20] S. M. Haile, *Acta Mater.* **2003**, *51*, 5981.

[21] J. Fimrite, B. Carnes, H. Struchtrup, N. Djilali, *J. Electrochem. Soc.* **2005**, *152*, A1815.

[22] R. W. Kopitzke, C. A. Linkous, H. R. Anderson, G. L. Nelson, *J. Electrochem. Soc.* **2000**, *147*, 1677.

[23] M. Cappadonia, J. W. Erning, S. M. S. Niaki, U. Stimming, *Solid State Ionics* **1995**, *77*, 65.

[24] J. Z. Huamin Zhang, Jianlu Zhang, Jifeng Wu, *PEM Fuel Cell Testing and Diagnosis*; 2013.

[25] H. Xu, Y. Song, H. R. Kunz, J. M. Fenton, *J. Electrochem. Soc.* **2005**, *152*, A1828.

[26] T. Sakai, *J. Electrochem. Soc.* **1986**, *133*, 88.

[27] A. Serov, M. H. Robson, B. Halevi, K. Artyushkova, P. Atanassov, *Electrochem. commun.* **2012**, *22*, 53.

[28] J. Li, S. Ghoshal, W. Liang, M.-T. Sougrati, F. Jaouen, B. Halevi, S. McKinney, G. McCool, C. Ma, X. Yuan, Z.-F. Ma, S. Mukerjee, Q. Jia, *Energy Environ. Sci.* **2016**, *9*, 2418.

[29] M. K. Debe, A. K. Schmoeckel, G. D. Vernstrom, R. Atanasoski, *J. Power Sources* **2006**, *161*, 1002.

[30] A. Kongkanand, Z. Liu, I. Dutta, F. T. Wagner, *J. Electrochem. Soc.* **2011**, *158*, B1286.

[31] M. Lefèvre, E. Proietti, F. Jaouen, J.-P. Dodelet, *Science* **2009**, *324*, 71.

[32] G. Wu, K. L. More, C. M. Johnston, P. Zelenay, *Science (80-.).* **2011**, *332*, 443.

[33] E. Proietti, F. Jaouen, M. Lefèvre, N. Larouche, J. Tian, J. Herranz, J. P. Dodelet, *Nat. Commun.* **2011**, *2*.

[34] E. Antolini, J. R. C. Salgado, E. R. Gonzalez, *J. Power Sources* **2006**, *160*, 957.

[35] and V. R. S. Chen, C., Y. Kang, Z. Huo, Z. Zhu, W. Huang, H. L. Xin, J. D. Snyder, D. Li, J. A. Herron, M. Mavrikakis, M. Chi, K. L. More, Y. Li, N. M. Markovic, G. A. Somorjai, P. Yang, *Science (80-.).* **2014**, *343*, 1339.

[36] S. Koh, P. Strasser, *J. Am. Chem. Soc.* **2007**, *129*, 12624.

[37] V. Stamenkovic, B. S. Mun, K. J. J. Mayrhofer, P. N. Ross, N. M. Markovic, J. Rossmeisl, J. Greeley, J. K. Nørskov, *Angew. Chemie - Int. Ed.* **2006**, *45*, 2897.

[38] K. Takahashi, K. Kakinuma, M. Uchida, *J. Electrochem. Soc.* **2016**, *163*, F1182.

[39] C. Wang, N. M. Markovic, V. R. Stamenkovic, *ACS Catal.* **2012**, *2*, 891.

[40] M. Oezaslan, F. Hasché, P. Strasser, *J. Phys. Chem. Lett.* **2013**, *4*, 3273.

[41] S. Chen, H. A. Gasteiger, K. Hayakawa, T. Tada, Y. Shao-Horn, Platinum-Alloy Cathode Catalyst Degradation in Proton Exchange Membrane Fuel Cells:

Nanometer-Scale Compositional and Morphological Changes. *J. Electrochem. Soc.* **2010**, *157*, A82.

[42] S. A. Mauger, K. C. Neyerlin, S. M. Alia, C. Ngo, S. K. Babu, K. E. Hurst, S. Pylypenko, S. Litster, B. S. Pivovar, *J. Electrochem. Soc.* **2018**, *165*, F238.

[43] P. Yu, M. Pemberton, P. Plasse, *J. Power Sources* **2005**, *144*, 11.

[44] E. Antolini, J. R. C. Salgado, M. J. Giz, E. R. Gonzalez, *Int. J. Hydrogen Energy* **2005**, *30*, 1213.

[45] U.S. Department of Energy, *Annu. Prog. Rep.* **2014**.

[46] Atsushi Ohma, Kazuhiko Shinohara, Akihiro Iiyama, Toshihiko Yoshida, and A. Daimaru, *ECS Trans.* **2011**, *41*, 775.

[47] N. Macauley, D. D. Papadias, J. Fairweather, D. Spernjak, D. Langlois, R. Ahluwalia, K. L. More, R. Mukundan, R. L. Borup, N. Materials, O. Ridge, **2018**, *165*, 3148.

[48] A. V. Virkar, Y. Zhou, Mechanism of Catalyst Degradation in Proton Exchange Membrane Fuel Cells. *J. Electrochem. Soc.* **2007**, *154*, B540.

[49] H. Li, J. Gazzarri, K. Tsay, S. Wu, H. Wang, J. Zhang, S. Wessel, R. Abouatallah, N. Joos, J. Schrooten, *Electrochim. Acta* **2010**, *55*, 5823.

[50] J. S. Park, M. S. Shin, C. S. Kim, *Curr. Opin. Electrochem.* **2017**, *5*, 43.

[51] M. C. B. Kienitz, J. Kolde, S. Priester, C. Baczkowski, *Trans. E C S Soc. Electrochem.* **2011**, *41*, 1521.

[52] X. Zhu, H. Zhang, Y. Zhang, Y. Liang, X. Wang, **2006**, 14240.

[53] R. Wycisk, P. N. Pintauro, J. W. Park, *Curr. Opin. Chem. Eng.* **2014**, *4*, 71.

[54] J. Choi, K. M. Lee, R. Wycisk, P. N. Pintauro, P. T. Mather, *J. Mater. Chem.* **2010**, *20*, 6282.

[55] I. Ezzell, R. Bobby, L. Jackson, P. William, Low Equivalent Weight Sulfonic Fluoropolymers **1987**.

[56] C. Laberty-Robert, K. Vallé, F. Pereira, C. Sanchez, *Chem. Soc. Rev.* **2011**, *40*, 961.

[57] L. Dos Santos, M. Maréchal, A. Guillermo, S. Lyonnard, S. Moldovan, O. Ersen, O. Sel, H. Perrot, C. Laberty-Robert, *Adv. Funct. Mater.* **2016**, *26*, 594.

[58] C. S. Kim, Method for preparing catalyst layer by in-situ sol-gel reaction of tetraethoxysilate in nafion ionomer solution *2*.

[59] A. Rolfi, C. Oldani, L. Merlo, D. Facchi, R. Ruffo, *J. Power Sources* **2018**, *396*, 95.

[60] D. Spernjak, R. Mukundan, R. L. Borup, L. G. Connolly, B. I. Zackin, V. De Andrade, M. Wojcik, D. Y. Parkinson, D. L. Jacobson, D. S. Hussey, K. L. More, T. Chan, A. Z. Weber, I. V Zenyuk, *Appl. Energy Mater.* **2018**.

[61] J. V. and S. G. THOMAS A. ZAWODZINSKI, JOHN DAWY, *Ekctrochimica Acta* **1995**, *40*, 297.

[62] A. W. R. D. J. M. J. Newman, In *Handbook of Fuel Cells: Fundamentals and Survey of Systems*; 2010.

[63] A. Kusoglu, A. Z. Weber, *Chem. Rev.* **2017**, *117*, 987.

[64] M. Ji, Z. Wei, *Energies* **2009**, *2*, 1057.

[65] W. Schramm, Fuel Cells with Hydrogen Recycle **1992**.

[66] and J. Z. Huamin Zhang, Jianlu Zhang, Jifeng Wu, *PEM Fuel Cell Testing and Diagnosis*; Elsevier Science, 2013.

[67] M. U. Kento Takahashi, Ryo Koda, Katsuyoshi Kakinuma, *J. Electrochem. Soc.* **2017**, *164*, F235.

[68] Y. A. E. Xuhai Wang, Francis W. Richey, Kevin H. Wujcik, *J. Power Sources* **2014**, *264*, 42.

[69] S. Martin, P. L. Garcia-Ybarra, J. L. Castillo, *Int. J. Hydrogen Energy* **2010**, *35*, 10446.

[70] S. Kumaraguru, *Energy.gov Hydrog. Fuel Cells Progr. Annu. Merit Rev.* **2018**, *1*, 1.

[71] A. Kongkanand, N. P. Subramanian, Y. Yu, Z. Liu, H. Igarashi, D. A. Muller, *ACS Catal.* **2016**, *6*, 1578.

[72] W. Zhang, P. N. Pintauro, *ChemSusChem* **2011**, *4*, 1753.

[73] M. Brodt, R. Wycisk, P. N. Pintauro, *J. Electrochem. Soc.* **2013**, *160*, F744.

[74] M. Brodt, T. Han, N. Dale, E. Niangar, R. Wycisk, P. Pintauro, *J. Electrochem. Soc.* **2015**, *162*, F84.

[75] M. Brodt, R. Wycisk, N. Dale, P. Pintauro, *J. Electrochem. Soc.* **2016**, *163*, F401.

CHAPTER 2

BACKGROUND

The term "fuel cell" refers to several types of electrochemical devices including but not limited to the proton exchange membrane fuel cell, the anion exchange membrane fuel cell, direct methanol fuel cells, the phosphoric acid fuel cell, and the solid-oxide fuel cell.[1] Each converts the chemical potential of incoming reactants into electrical potential which may be used to move electrons and perform work. The type of fuel cell that this dissertation will focus on is the proton exchange membrane fuel cell (PEMFC) which utilizes hydrogen and oxygen as the incoming reactant species.[2] The PEMFC is chosen instead of the other types of fuel cells because of its low operating temperature, low weight/volume, and only needing a hydrogen storage tank and oxygen from the air to operate.[3] This chapter is organized into two parts where the first will outline the details regarding PEMFC operation, sources of performance loss, and analysis techniques. The second part of this chapter will summarize electrospinning as it pertains to PEMFCs as well as how this dissertation builds upon prior research performed by Pintauro and co-workers including Zhang and Brodt.

2.1 Proton Exchange Membrane Fuel Cell Theory

2.1.1 Governing Reactions

There are two electrochemical half-cell reactions that take place within a PEMFC.[2] These are the hydrogen oxidation reaction (HOR) (Reaction 1) and the oxygen reduction reaction (ORR) (Reaction 2) which take place at the anode and cathode respectively as is depicted in Figure 2.1

$$H_2 \rightarrow 2H^+ + 2e^- \qquad \text{(Reaction 1)}$$

$$\tfrac{1}{2}O_2 + 2H^+ + 2e^- \rightarrow H_2O \qquad \text{(Reaction 2)}$$

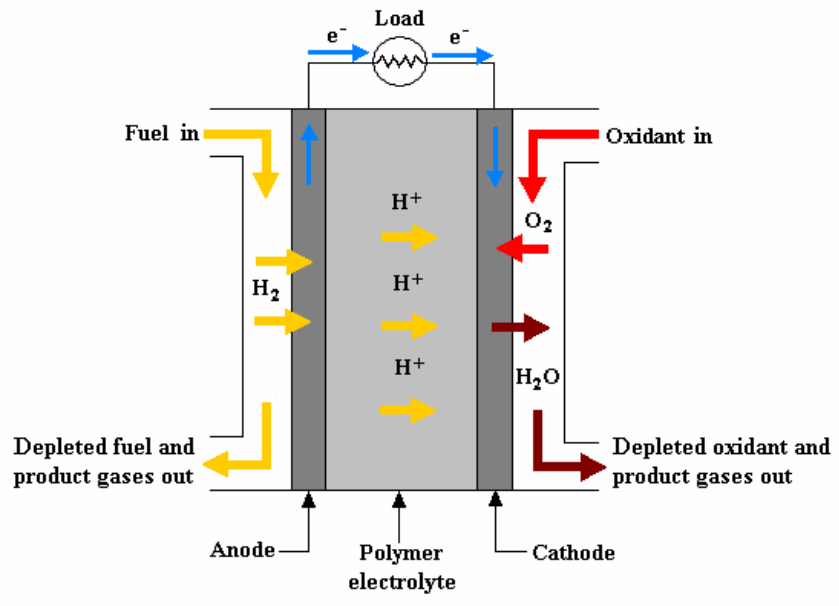

Figure 2.1: Schematic diagram of a PEMFC MEA. Adapted from Reference [4].

A schematic representation of a hydrogen/air PEMFC is shown in Figure 2.1. As feed-gases diffuse through the anode and cathode compartments, Reactions 1 and 2 take place. The protons generated from reaction 1 travel through the polymer electrolyte membrane and the electrons travel through an external circuit.

The kinetics of the ORR are several orders of magnitude slower than the HOR and so the majority of catalyst and electrode research has focused on the cathode.[5] There is some research, however, that points to the importance of anode hydration with regard to overall water management.[6–8] These studies have focused on increasing the hydration of

the anode to prevent anode drying which can lead to drying of the membrane and significant increases in resistance across the cell.[8] This topic will be covered in greater detail in Chapter 5 of this dissertation.

The coupling of Reaction 1 and Reaction 2 is spontaneous and has chemical potential energy associated with it.[9] This chemical potential is equal to the enthalpy of formation of water from its constituents (H_2 and O_2) minus a temperature dependent entropy term (Gibbs free energy).[10] At standard temperature, this energy is equal to 237.3 kJ/mole of water for complete combustion.[9] Because free electrons are involved in this reaction, the chemical potential may be associated with a proportional electrical potential which is given by Equation 2.1.

$$E_{cell}^{o} = -\frac{\Delta G^{o}}{nF} \qquad \text{(Equation 2.1)}$$

Where F is Faraday's constant (96485 C/mol) and n is the number of electrons involved in the reaction per mole of water generated (n = $2e^-/mol_{H2O}$). Substituting all values into Equation 1 yields E_{cell}^{o} equal to 1.23 V vs. the standard hydrogen electrode (SHE) which is equivalent to Reaction 1 and is defined as having a standard reduction potential of 0.0 V. This value is based off of the coupling of Reaction 1 and Reaction 2 vs SHE. This electrical potential is the driving force for current generation in a fuel cell.[11] As current is drawn, there are sources of voltage loss (also referred to as overpotential).[5] There are three primary sources of overpotential that correspond to three different physical phenomena which occur during fuel cell operation. These sources will be discussed in the following sections.

2.1.1 Overpotential

When a fuel cell membrane electrode assembly produces current, it is moving away from its equilibrium state.[12] The voltage of the cell may be expressed by Equation 2.2.

$$E_{cell} = E_{T,P}^{OCV} - \eta_{activation} - \eta_{ohmic} - \eta_{mass\ transport} \qquad \text{(Equation 2.2)}$$

In this equation, $E_{T,P}^{OCV}$ represents the cell's open circuit voltage (OCV) at a given temperature and pressure. The OCV of a cell deviates from the theoretical value of 1.23 for several reasons including hydrogen crossover from the anode to the cathode[13], mixed potential at the cathode caused by electrochemical side reactions[14], and the activation of Pt from PtO[15]. Each η value represents one of the three types of overpotential: activation, ohmic, and mass transport. Each of these sources of overpotential is dependent on the current drawn. Each source of overpotential may be expressed as a term that depends on current density. Equation 3 expresses the cell's potential at a given current density.[9]

$$E_{cell} = E_{T,P}^{OCV} - \frac{RT}{\alpha F} \cdot \ln\left(\frac{i}{i_0}\right) - (i) \cdot R_i - \frac{RT}{nF} \cdot \ln\left(\frac{i_L}{i_L - i}\right) \qquad \text{(Equation 3)}$$

In this equation, the expression for activation overpotential is derived from the Butler-Volmer equation[16] where i = current density (mA/cm^2), R = gas constant 8.314 J/(mol·K), T = temperature (K), α = transfer coefficient, i_0 = exchange current density (A/cm^2), the ohmic overpotential is simply linear and is derived from Ohm's law (R_i = total MEA resistance (Ω)), and finally the mass transport overpotential is derived from the Nernst equation (i_L = limiting current density A/cm^2).[17] The three sources of voltage loss are plotted in Figure 2.1 (a) and the curve resulting from the cumulative sum of the losses is plotted in Figure 2.1 (b).

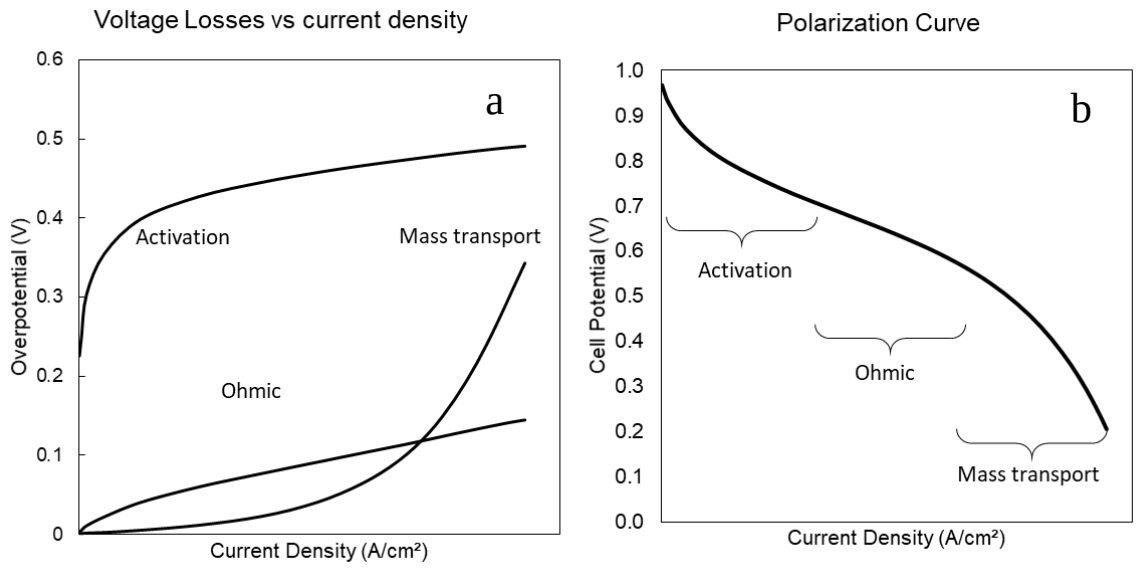

Figure 2.1 (a) Example of overpotential sources as a function of current density (b) polarization curve with each region labeled.

The curve on the right is obtained by collecting and plotting current-voltage data in an operating fuel cell. The three labeled regions in Figure 2.1b designate where each of the voltage losses dominate, but as is seen in Figure 2.1a, there is some contribution of each overpotential at all current densities. The plot in Figure 2.1b is known as a polarization curve and is used to calculate power at a given current density or voltage (power density = voltage · current density).

2.2 Analysis Techniques

In addition to collecting polarization data as just described, there are a number of useful analysis techniques which provide additional diagnoses to characterize the MEA as a whole, only the membrane, or only the cathode or anode. These are useful in decoupling the impact of a particular MEA component on the power density at a given voltage or current density. The analyses are linear sweep voltammetry (LSV), mass activity

determination, cyclic voltammetry (CV, to determine electrochemically active surface area), and electrochemical impedance spectroscopy (EIS).[18]

Linear Sweep Voltammetry

Membranes that are used in hydrogen/air fuel cell MEAs ideally conduct protons and perfectly separate the anode and cathode compartments.[19] In reality, there is some degree of gas permeation through the membrane (crossover) that occurs during the operation of the fuel cell.[14] While both hydrogen and oxygen permeation occurs, the latter occurs at a much slower rate and therefore, hydrogen crossover is of primary interest.[20] When hydrogen gas is present at the cathode, the mixed potential of the reactants lowers the open circuit voltage. Efficiency is also lowered because no electrical work is captured even though the reactant is consumed by the chemical reaction of H_2 and O_2 at the cathode catalyst site.[9] Additionally, when hydrogen crosses over and reacts directly with oxygen at the cathode, locally generated heat may lead to the formation of membrane pin-holes.[21] For these reasons, hydrogen crossover must be minimized. Linear sweep voltammetry (LSV) is a method that is used to quantify the degree of hydrogen crossover from the anode to the cathode.[22] In this experiment, hydrogen gas is fed to the anode and the cathode (working electrode) is purged with an inert gas such as nitrogen. A potentiostat is then used to apply a voltage from low to high. This forward voltage scan will oxidize any hydrogen present. At high enough voltages, hydrogen will instantly oxidize at the mass-transfer limiting condition.[23] The current that is generated from the LSV may be correlated directly to the amount of hydrogen present in the cathode compartment by Equation 4.

$$\frac{moles\ H_2}{s} = \frac{I_L}{nF} \qquad \text{(Equation 4)}$$

In this equation, I_L is the measured current from the LSV, n is 2 mols of electrons per mol of hydrogen, and F is Faraday's constant. The flux of hydrogen across the membrane will affect $E_{T,P}^{OCV}$ from Equation 3 by inducing a mixed potential.[14]

Mass Activity

The electrocatalytic activity of a cathode in an MEA is specified by the US Department of Energy as the current generated at 0.9 V vs SHE, 80 °C and 100% RH, normalized by the mass of the active catalyst.[24] If the current is normalized by area, it is referred to as specific activity. The potential of 0.9 V is chosen as the standard for activity measurement because it is a sufficiently high voltage that activation overpotential dominates (i.e. ohmic and mass transport overpotentials only minimally interfere with the generated current). In a mass activity measurement the voltage is measured across two decades of current (i.e. from 1 A to 0.01 A).

To eliminate the influence of ohmic and mass transport overpotentials, several steps are taken. The effect of mass transport overpotential is accounted for by using pure oxygen as the cathode feed gas with a back pressure of 150 kPa absolute at the cathode, 100 sccm flow rates for both anode and cathode feeds, 80 °C, and full humidification. 150 kPa pressure is used to ensure that the partial pressure of oxygen at the cathode surface is near unit activity (since saturated water vapor at 80 °C has a partial pressure of 47.373 kPa ≅ 50 kPa).

To account for the effect of ohmic overpotential losses, the measured current is first corrected by adding the current loss due to hydrogen crossover, as determined by LSV. Measured voltages are corrected by measuring the high frequency resistance (HFR) in an

electrochemical impedance spectroscopy (EIS) experiment and then using the HFR value to correct the voltage for ohmic overpotential at a given current (where the overpotential was found by multiplying the HFR and current). After obtaining both corrected current and corrected voltage, they are plotted against each other to yield Figure 2.2 (a) and (b).

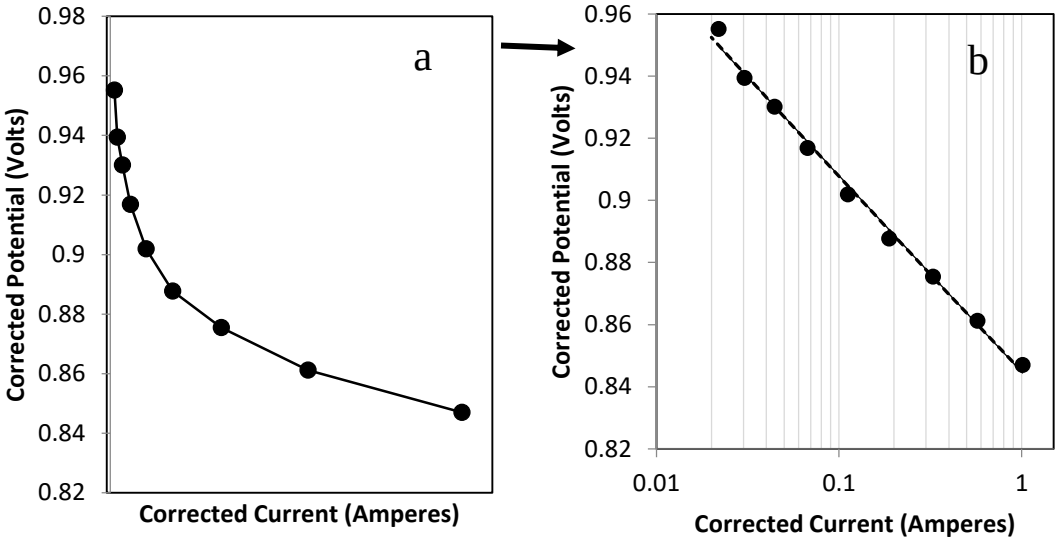

Figure 2.2 Corrected current and corrected voltage collected from a mass activity measurement plotted (a) on a linear x-axis and (b) on a log-scale x-axis.

This set of points is essentially the activation region of the polarization curve, but with corrected values of voltage and current. Plotting this data on a log scale yields a plot such as Figure 2.2 (b). Interpolation of this curve allows for an exact determination of the current produced at 0.9 V. Dividing this current by the mass of platinum in the electrode yields the final mass activity with units of (mA/mg_{Pt}). The slope obtained from Figure 2.2 (b) is known as the Tafel slope and is indicative of the ORR kinetics. Tafel slopes that are steeper indicate a greater activation overpotential as is required to generate a given current density according to the Butler-Volmer equation.[25]

Electrochemical Surface Area

The actual surface area of platinum accessible to catalyze the HOR and ORR is usually less than the total theoretical surface area of the Pt nanoparticles due to poor contact between the ionomer, feed gases, and catalyst sites. The accessible catalyst surface area is known as the electrochemically active surface area (ECSA) and can be measured by cyclic voltammetry (CV). In a CV experiment, a PEMFC MEA is cycled between 0.05 V to 0.90 V at a scan rate of 0.01 V/s. Hydrogen is oxidized as voltage increases during the forward scan and protons are reduced as the voltage is decreased during the reverse scan. The electroreduction of protons, the backwards direction of Reaction 3, occurs from 0.06V to 0.4V of the reverse voltage scan (as depicted by the region between the vertical dotted lines in Figure 2.3) and is used to calculate the active electrochemical surface area.

$$Pt–H_{ads} \leftrightarrow Pt + H^+ + e^- \qquad \text{(Reaction 3)}$$

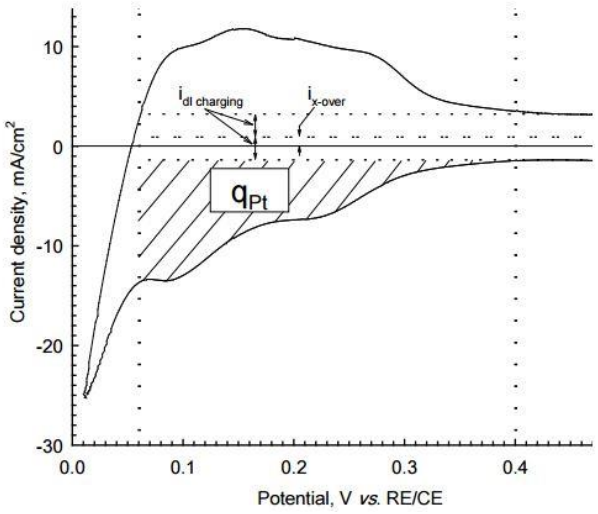

Figure 2.3 Example of Cyclic Voltammogram of PEM fuel cell catalyst layer for ECSA analysis.

The shaded area in Figure 2.3 is equal to the hydrogen adsorption charge density (q_{Pt}). This shaded region neglects the charge associated with non-faradaic processes present in a fuel cell to avoid overestimating q_{Pt} – therefore, the reverse double layer charging current density (i_{dl}) is subtracted from this region.[22] The voltage is scanned at a known rate *v* (0.04 Volts/second) across a known voltage range V_1-V_2 (0.06 Volts to 0.40 Volts). Therefore, the time to scan across the voltage range is equal to the following: $t = (V_1-V_2)/v$ = 8.5 seconds in this example. Because of this, it would be equivalent to plot the shaded region between 0 and 8.5 seconds.

Integration of the current density (with units of: $C/s \cdot cm^2$) from 0.06V to 0.40V is equivalent to integrating with respect to time (s) which results in charge density (C/cm^2). The electrochemical surface area (Equation 5) of an electrode is calculated from three values: the hydrogen adsorption charge density (q_{Pt}) (units of: C/cm^2), the charge required to reduce a monolayer of protons on Pt (designated as "Γ", with a value of 210 $\mu C/cm^2$), and the Pt loading in the electrode (designated as L) (with units of mg_{Pt}/cm^2).

$$ECSA\ (cm_{Pt}^2/g_{Pt}) = \frac{q_{Pt}}{\Gamma \cdot L} \qquad \text{(Equation 5)}$$

Electrochemical Impedance Spectroscopy (EIS)

Another important metric for hydrogen/air PEMFC performance is the high frequency resistance (HFR) which provides a measure of the ohmic resistance of an MEA membrane and the contact resistance between the membrane and electrodes. This includes the ionic contributions to ohmic resistance. The HFR of an MEA is determined through EIS. This method applies a small sinusoidal perturbation to a fixed current within a specified range of frequencies (1 mHz to 10 kHz for the Scribner 850e test station). The

current used in this experiment is chosen to be in the ohmic-dominated region of the polarization curve, but the resistance generally does not deviate greatly between different current densities. Using frequency response analysis software, the resultant signal magnitude and phase shift are presented graphically, often as a Nyquist plot as shown in Figure 2.4, with real and imaginary impedances as the abscissa and ordinate, respectively. The characteristic shape of two overlapping semicircles can be observed.

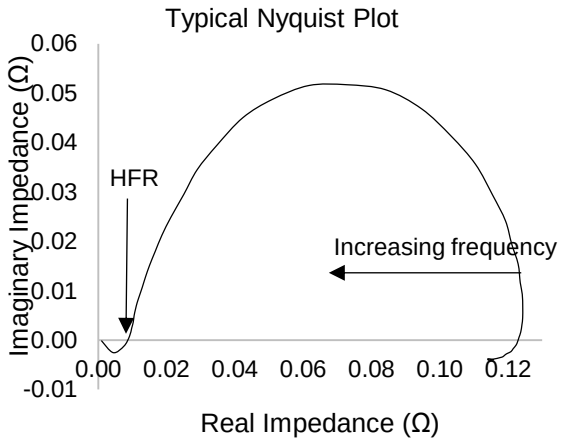

Figure 2.4 Typical Nyquist plot used to determine the high frequency resistance.

2.3 Electrospinning and its use in PEMFCs

Electrospinning involves pumping a polymer solution or polymer melt out of a metal needle spinneret in the presence of a strong electric field between the needle tip and a grounded fiber collector surface. This setup is shown in Figure 2.6.

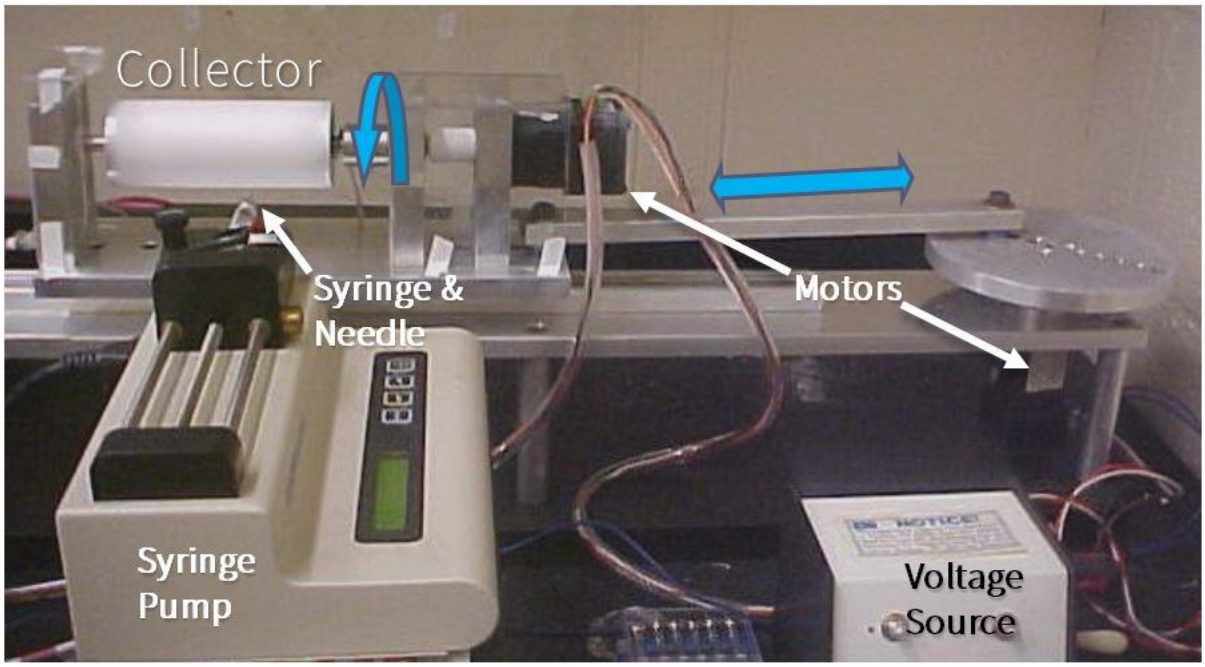

Figure 2.5 An image of the electrospinning setup that is used to generate nanofiber electrode mats.

The electric field overcomes the surface tension of the polymer solution and the "Taylor cone" forms. A jet emerges from the Taylor cone; as the jet dries, it rapidly accelerates toward the grounded collector where the resulting polymeric nanofibers deposit.

In the case of electrospinning PEMFC electrodes, the polymer solution will also contain catalyst particles, as has been demonstrated by Angela Zhang and Matthew Brodt.[26–29] The polymer/particle/solvent dispersion will henceforth be referred to as an electrode ink. An ink is composed of solvent, an ion conducting polymer (e.g. Nafion), a carrier polymer for electrospinning, such as poly(acrylic acid) (PAA) or polyvinylidene fluoride (PVDF), and catalyst particles; each of these components must be compatible with each other to successfully electrospin an electrode. A carrier polymer is added because

Nafion does not have sufficient polymer chain entanglements and thus cannot be electrospun alone in solution.

There are several conditions important for electrospinning a polymer-based solution which can affect the quality of the nanofibers or if the nanofibers form at all.[30] These conditions include the bias voltage, the distance from the spinneret to the collector surface, the relative humidity, the rate at which the ink is pumped out of the needle, the boiling point of the solvent system, the dielectric properties of the ink[31], the ratio of "carrier" polymer to other components[32], and the molecular weight of the polymers used.[33] Adjusting these parameters will result in changes in electrospin-ability of the solution (i.e. the wrong conditions and the result is electrosprayed droplets or bead-on-fiber structures) as well as the final fiber diameter and the uniformity of the fiber diameter.[30]

In 2011, Zhang and Pintauro fabricated and tested the first Nafion/catalyst nanofiber-structured cathodes for proton exchange membrane H_2/air and H_2/O_2 fuel cell MEAs with poly(acrylic acid) (PAA) as the carrier polymer for Nafion electrospinning.[29] In this paper, the nanofiber structure was found to exhibit excellent beginning of life performance including high power (524 mW/cm^2 at 0.6 V, 0.1 mg_{Pt}/cm^2, 80 °C, and ambient pressure) and high mass activity (0.23 A/mg_{Pt}) as well as improved durability. These results laid the groundwork for future studies to be performed in the Pintauro group by Matthew Brodt. In 2013, Brodt et al. showed that electrospun nanofiber cathodes provide high power at very low catalyst loading. With a Pt loading of 0.055 mg/cm^2 the nanofiber cathode MEA produced a maximum power density of 906 mW/cm^2 at 80 °C and 300 kPa pressure with fully humidified 500 standard cubic centimeters per minutes (sccm) H_2 and 2000 sccm air.[28] It was also shown that there was less carbon corrosion when using

the nanofiber electrode structure using Nafion/PAA as a binder compared to a standard sprayed electrode. Brodt et al. also showed that the addition of PAA to a conventional painted electrode significantly decreased the fuel cell power output due presumably to a decrease in ionic conductivity of the binder. After attempting to remove the PAA in boiling acid and peroxide, he concluded that it was not possible.[27] Brodt showed that nanofiber diameter between 250 nm and 520 nm does not affect power density and that the nanofiber electrode morphology can be used to improve the performance of commercial Pt/C powders.[27] Subsequently in 2016, Brodt et al. showed that Nafion-PVDF binders appear to suppress carbon corrosion in a hydrogen/air PEMFC by increasing the nanofiber hydrophobicity, thus decreasing the concentration of water at the Pt/C catalyst surface.[26] The work contained in this dissertation builds upon these prior nanofiber electrode works.

2.4 Strategies in the Literature for Overcoming Current Obstacles

As was stated in Chapter 1 of this dissertation, there are several key obstacles to overcome for widespread adoption of fuel cell technology in the market. Below is a brief discussion of work that has been done to improve power density at realistic operating conditions.

2.4.1 Approaches to Improve Performance at Low RH

To combat the deleterious effects of low RH operation, several design principles have been utilized to create MEAs that perform better at low RH.[34] These include decreasing the membrane thickness[35,36], using a low equivalent weight (high ion exchange capacity) perfluorosulfonic acid polymer for the membrane [32,37–40], and the electrode binder[41,42], changing the composition of the gas diffusion layer[43], and fuel cell operational strategies (e.g. asymmetric humidification of the anode and cathode)[8]. These

strategies take into consideration the water flux through an MEA and try to mitigate unwanted drying in the anode and unwanted flooding in the cathode. Anode drying occurs because of electroosmotic drag which is the flux of water induced by the movement of protons across the polymer electrolyte membrane.[44] Electroosmotic drag delivers more water to the cathode than what is dictated by stoichiometry through the reduction of oxygen alone: between 1 and 2.5 water molecules are dragged across the membrane with each proton.[45] Thus, for every water molecule generated, there are between 2 and 5 water molecules dragged from the anode to the cathode.[45],[46,47] The electroosmotic drag of water is countered by the back-diffusion of water[44] where back diffusion is dependent on the concentration gradient of water from the cathode to the anode as well as the thickness of the membrane.[35] Operational considerations such as asymmetric humidification of the anode and cathode[8] and recirculation of the anode feed[48] to recover both H_2 and water are other ways of improving performance at low relative humidity. Chapter 5 of this dissertation focuses on a nanofiber anode/cathode design that produces high power at low RH.

2.4.2 Electrode Design for Lowered Pt Content and Improved Durability

Electrode design affects the performance of an MEA by affecting three phenomena: (1) the activation of the oxygen reduction reaction, (2) electronic and ionic conductivity, and (3) the transport of feed gasses to catalyst sites and the expulsion of water away from the catalyst sites.[49] This section will discuss several prominent electrode fabrication techniques and the benefits of each approach.

2.4.2.1 Electrosprayed Electrodes

Using a technique to electrospray the cathode catalyst layers to improve performance while using very low amounts of platinum has been utilized by several groups including Uchida[50,51], Elabd[52], and Castillo.[53] These groups observed an improvement in catalyst utilization, an improvement of electrochemically active surface areas over baseline air-sprayed catalyst layers, an increase in catalyst layer uniformity, and an increase in electrode porosity relative to slurry electrodes. Overall, the electrodes showed improvements in power generation over slurry electrodes. Uchida and coworkers observed that at full humidification, a very high max power of 1010 mW/cm^2 was generated using a Pt loading of 0.056 mg_{Pt}/cm^2 with operating conditions of 100 kPa absolute, 80 °C. However, the electrosprayed cathodes' current generation show a strong dependence on RH (decreasing by nearly 80% from 100% RH to 40% RH). In the work performed by Elabd and coworkers, they employ a technique of simultaneously electrospinning nanofibers of Nafion and poly(acrylic acid) and electrospraying droplets of Nafion and Pt/C. This combination nanofiber/nanospray electrodes, the maximum power obtained at 0.052 mg_{Pt}/cm^2 was 656 mW/cm^2 in H_2/air feed gas at 80 °C, and 272 kPa absolute pressure.

2.4.2.2 Nanostructured Thin Film (NSTF)

The nanostructured thin film (NSTF) catalyst electrodes developed by 3M Company are platinum "nano-whiskers" which contain no carbon or ionomer binder.[54] These structures exhibited more stable electrochemical surface area compared to their control electrode when an accelerated stress test of voltage cycling from 0.6 V – 1.2 V was applied.[54] The authors conclude that the absence of carbon in the catalyst layer is the

reason for the improved durability when being cycled at high voltages (> 1.0 V). While the stability improves, this structure struggles to generate high current densities due to an issue with water management.

The following table is a compilation of recent literature for new fuel cell MEA designs along with the power density, catalyst loading, and fuel cell operating conditions for each MEA. Kumaraguru et al.[55] use a high ion exchange capacity ionomer (825EW perfluorosulfonic acid) for the anode and cathode binder and a membrane that is 12 microns thick (half as thick as a standard Nafion 211 membrane) and a PtCo/C catalyst at the cathode to achieve 1.3 W/cm^2 at fuel cell operating conditions listed in Table 1.1. Kongkanand et al.[56] achieve similarly high power by utilizing a new catalyst type with a Pt monolayer shell around a core of Pd supported on carbon. This paper used low catalyst loading (0.05 mg_{Pt}/cm^2) and observed very good power generation at high current densities.

Table 1.1 List of competitive power densities obtained at given conditions and catalyst loadings.

Reference	Strategy	Operating Conditions	Cathode Catalyst loading (mg_{Pt}/cm^2)	Maximum Power Density (mW/cm^2)
Uchida[50]	Electrosprayed electrodes Cathode: Pt/C Membrane: N/A Anode: Pt/C	P = 100 kPa T = 80 C RH = 100% Flow Rates = (N/A)	0.056	1010
Kumaraguru[55]	Optimized slurry cast electrodes Cathode: PtCo/HSC Membrane: 12 µm 825 PFSA Anode: Pt/C	P = 250 kPa T = 80 C RH = 65% Flow Rates = Stoic. 1.5/2.0	0.1	1300
Kongkanand[56]	Pt-monolayer/Pd/C core−shell cathode Cathode ionomer: 900 EW PFSA Membrane: Nafion 211 Anode: Pt/C 900 EW PFSA	P = 150 kPa T = 80 C RH = 100% Flow Rates = Stoic. 1.5/2.1	0.05	1100

2.5 Objectives and Remaining Dissertation Format

To improve the power density of previously reported fuel cell membrane electrode assemblies initially and/or after stress tests, this dissertation details the preparation and characterization of (1) nanofiber cathodes which incorporate platinum-free cathode catalysts and a Nafion/polyvinylidene fluoride binder (Chapter 3), (2) nanofiber cathodes which utilize PtCo/C as the catalyst with a Nafion/poly(acrylic acid) binder (Chapter 4), (3) nanofiber anodes and cathodes which are electrospun from a Nafion/polyethylene oxide ink and then the polyethylene oxide is removed (Chapter 5), (4) Nafion/PVDF binder nanofiber cathodes samples which are analyzed at Oak Ridge National Laboratory for thickness collapse and porosity after a carbon corrosion accelerated stress test (Chapter 6), and (5) a nanofiber cathode in which a sulfonated-silicate network is formed from a sol-gel reaction that takes place before, during, and after electrospinning (Chapter 7). In each of these works, the nanofiber electrodes are compared to a conventional slurry or sprayed electrode from Nissan Technical Center of North America or Los Alamos National Laboratory. The remaining chapters of this dissertation will discuss in detail each of the numbered points above and provide physical and electrochemical characterization of nanofiber cathodes and anodes.

References

[1] L. Carrette, K. A. Friedrich, *ChemPhysChem* **2000**, *1*, 162.

[2] S. J. Peighambardoust, S. Rowshanzamir, M. Amjadi, *Review of the proton exchange membranes for fuel cell applications*; Elsevier Ltd, 2010; Vol. 35.

[3] FuelCellTehcnologyOffice, Comparison of Fuel Cell Technologies. Office of Energy Efficiency and Renewable Energy. *Comp. Fuel Cell Technol. Off. Energy Effic. Renew. Energy. Energy.gov* **2018**, 1–3.

[4] M. S. Rahman, S. Paul, R. R. Riadh, *Electr. Comput. Eng. An Int. J.* **2015**, *4*, 43.

[5] H. J. J. K. Nørskov,* J. Rossmeisl, A. Logadottir, L. Lindqvist, J. R. Kitchin, T. Bligaard, *J. Phys. Chem. B* **2004**, *108*, 17886.

[6] S. Hou, H. Su, H. Zou, D. Dang, H. Song, X. Li, S. Liao, *Int. J. Hydrogen Energy* **2015**, *40*, 15613.

[7] L. Xin, F. Yang, J. Xie, Z. Yang, N. N. Kariuki, D. J. Myers, J.-K. Peng, X. Wang, R. K. Ahluwalia, K. Yu, P. J. Ferreira, A. M. Bonastre, D. Fongalland, J. Sharman, *J. Electrochem. Soc.* **2017**, *164*, F674.

[8] M. M. Saleh, T. Okajima, M. Hayase, F. Kitamura, T. Ohsaka, *J. Power Sources* **2007**, *164*, 503.

[9] F. Barbir, *PEM Fuel Cells: Theory and Practice*; 1st ed.; Elsevier Ltd: Burlington, MA, 2005.

[10] A. D. Le, B. Zhou, *J. Power Sources* **2008**, *182*, 197.

[11] M. Gasik, *Mater. Today Rev. Featur.* **2003**, 24.

[12] U. Chakraborty, *Energies* **2018**, *11*, 1851.

[13] S. A. Vilekar, R. Datta, *J. Power Sources* **2010**, *195*, 2241.

[14] J. Z. Huamin Zhang, Jianlu Zhang, Jifeng Wu, *PEM Fuel Cell Testing and Diagnosis*; 2013.

[15] S. G. Tom A. Zawodzinski, *Advances in Electrochemical Science and Engineering*,; Wiley-VCH: Wiley-VCH, 1995.

[16] R. F. Mann, J. C. Amphlett, B. A. Peppley, C. P. Thurgood, *J. Power Sources* **2006**, *161*, 775.

[17] P. T. Nguyen, T. Berning, N. Djilali, *J. Power Sources* **2004**, *130*, 149.

[18] J. Wu, X. Z. Yuan, H. Wang, M. Blanco, J. J. Martin, J. Zhang, *Int. J. Hydrogen Energy* **2008**, *33*, 1735.

[19] and J. S. Y. Shyam S. Kocha, J. Deliang Yang, *Wiley Intersci.* **2006**, *52*, 1916.

[20] M. Inaba, T. Kinumoto, M. Kiriake, R. Umebayashi, A. Tasaka, Z. Ogumi, *Electrochim. Acta* **2006**, *51*, 5746.

[21] H. M. Yu J, Matsuura T, Yoshikawa Y, Islam MN, *Electrochem. Solid State Lett.* **2005**, *8*, A156.

[22] K. Cooper, *Fuel Cell Mag. Scribner Assoc. Inc.* **2008**, 1.

[23] L. Bard, A.J. and Faulkner, *Electrochemical Methods: Fundamentals and Applications*; Wiley & Sons: New York, NY.

[24] H. A. Gasteiger, S. S. Kocha, B. Sompalli, F. T. Wagner, Activity benchmarks and requirements for Pt, Pt-alloy, and non-Pt oxygen reduction catalysts for PEMFCs.

Appl. Catal. B Environ. **2005**, *56*, 9–35.

[25] C. Song, J. Zhang, *PEM Fuel Cell Electrocatal. Catal. Layers Fundam. Appl.* **2008**, 89.

[26] M. Brodt, R. Wycisk, N. Dale, P. Pintauro, *J. Electrochem. Soc.* **2016**, *163*, F401.

[27] M. Brodt, T. Han, N. Dale, E. Niangar, R. Wycisk, P. Pintauro, *J. Electrochem. Soc.* **2015**, *162*, F84.

[28] M. Brodt, R. Wycisk, P. N. Pintauro, *J. Electrochem. Soc.* **2013**, *160*, F744.

[29] W. Zhang, P. N. Pintauro, *ChemSusChem* **2011**, *4*, 1753.

[30] J. Doshi, D. H. Reneker, *J. Electrostat.* **1995**, *35*, 151.

[31] S. V. Fridrikh, J. H. Yu, M. P. Brenner, G. C. Rutledge, *Phys. Rev. Lett.* **2003**, *90*, 4.

[32] J. Choi, K. M. Lee, R. Wycisk, P. N. Pintauro, P. T. Mather, *J. Mater. Chem.* **2010**, *20*, 6282.

[33] J. S. Lee, K. H. Choi, H. Do Ghim, S. S. Kim, D. H. Chun, H. Y. Kim, W. S. Lyoo, *J. Appl. Polym. Sci.* **2004**, *93*, 1638.

[34] J. S. Park, M. S. Shin, C. S. Kim, *Curr. Opin. Electrochem.* **2017**, *5*, 43.

[35] M. C. B. Kienitz, J. Kolde, S. Priester, C. Baczkowski, *Trans. E C S Soc. Electrochem.* **2011**, *41*, 1521.

[36] X. Zhu, H. Zhang, Y. Zhang, Y. Liang, X. Wang, **2006**, 14240.

[37] R. Wycisk, P. N. Pintauro, J. W. Park, *Curr. Opin. Chem. Eng.* **2014**, *4*, 71.

[38] I. Ezzell, R. Bobby, L. Jackson, P. William, Low Equivalent Weight Sulfonic Fluoropolymers **1987**.

[39] C. Laberty-Robert, K. Vallé, F. Pereira, C. Sanchez, *Chem. Soc. Rev.* **2011**, *40*, 961.

[40] L. Dos Santos, M. Maréchal, A. Guillermo, S. Lyonnard, S. Moldovan, O. Ersen, O. Sel, H. Perrot, C. Laberty-Robert, *Adv. Funct. Mater.* **2016**, *26*, 594.

[41] C. S. Kim, Method for preparing catalyst layer by in-situ sol-gel reaction of tetraethoxysilate in nafion ionomer solution *2*.

[42] A. Rolfi, C. Oldani, L. Merlo, D. Facchi, R. Ruffo, *J. Power Sources* **2018**, *396*, 95.

[43] D. Spernjak, R. Mukundan, R. L. Borup, L. G. Connolly, B. I. Zackin, V. De Andrade, M. Wojcik, D. Y. Parkinson, D. L. Jacobson, D. S. Hussey, K. L. More, T. Chan, A. Z. Weber, I. V Zenyuk, *Appl. Energy Mater.* **2018**.

[44] J. V. and S. G. THOMAS A. ZAWODZINSKI, JOHN DAWY, *Ekctrochimica Acta* **1995**, *40*, 297.

[45] A. W. R. D. J. M. J. Newman, In *Handbook of Fuel Cells: Fundamentals and Survey*

of Systems; 2010.

[46] A. Kusoglu, A. Z. Weber, *Chem. Rev.* **2017**, *117*, 987.

[47] M. Ji, Z. Wei, *Energies* **2009**, *2*, 1057.

[48] W. Schramm, Fuel Cells with Hydrogen Recycle **1992**.

[49] and J. Z. Huamin Zhang, Jianlu Zhang, Jifeng Wu, *PEM Fuel Cell Testing and Diagnosis*; Elsevier Science, 2013.

[50] K. Takahashi, K. Kakinuma, M. Uchida, *J. Electrochem. Soc.* **2016**, *163*, F1182.

[51] M. U. Kento Takahashi, Ryo Koda, Katsuyoshi Kakinuma, *J. Electrochem. Soc.* **2017**, *164*, F235.

[52] Y. A. E. Xuhai Wang, Francis W. Richey, Kevin H. Wujcik, *J. Power Sources* **2014**, *264*, 42.

[53] S. Martin, P. L. Garcia-Ybarra, J. L. Castillo, *Int. J. Hydrogen Energy* **2010**, *35*, 10446.

[54] M. K. Debe, A. K. Schmoeckel, G. D. Vernstrom, R. Atanasoski, *J. Power Sources* **2006**, *161*, 1002.

[55] S. Kumaraguru, *Energy.gov Hydrog. Fuel Cells Progr. Annu. Merit Rev.* **2018**, *1*, 1.

[56] A. Kongkanand, N. P. Subramanian, Y. Yu, Z. Liu, H. Igarashi, D. A. Muller, *ACS Catal.* **2016**, *6*, 1578.

[57] M. Bass, A. Berman, A. Singh, O. Konovalov, V. Freger, *Macromolecules* **2011**, *44*, 2893.

CHAPTER 3

PGM-FREE CATALYST POWDER AND NAFION/PVDF BINDER

3.1 PGM-free catalyst in Nanofibers with Nafion/PVDF

A variety of strategies are being pursued to lower the platinum content in proton exchange membrane fuel cells. These include the use of Pt-alloy, core-shell and shape-controlled platinum catalysts which exhibit very high oxygen reduction reaction (ORR) activity. Another approach is focused on inexpensive platinum-group-metal-free (PGM-free) powders as the cathode catalyst. PGM-free catalysts are typically carbon based powders with metal/nitrogen/carbon (Me/Nx/Cy) catalytic surface sites, where the metal ion is often cobalt, or iron.[1-3] The ORR activity of these catalysts is lower than that of Pt, but they can be cost effectively used at higher loadings to compensate for slower oxygen reduction kinetics. Additionally, prior studies have reported poor durability of MEAs with non-PGM catalysts in hydrogen/air fuel cells due to several effects including loss of the carbon support material, loss of metal ions from the catalyst which lowers catalytic activity and binder conductivity, water flooding which impedes oxygen transport, and the generation of peroxide species which degrades the catalyst and binder.[4-6]

The present study was initiated to obtain preliminary fuel cell performance and durability data on one type of PGM-free catalyst powder in particle/polymer nanofiber mat cathodes. The catalyst used in this study was a metal organic framework (MOF)-derived Fe–N–C catalyst with 0.5 wt.% Fe, a BET surface area of 1362 m2/g, and a reported RDE mass based kinetic current density of 7.78 $A/g_{catalyst}$ at 0.8 V.[7] MEAs with electrospun and conventional sprayed cathodes were examined and their performance compared. Pintauro and coworkers[8-10] have shown that an electrospun nanofiber cathode with a conventional

Pt/C catalyst performs well in a hydrogen/air proton exchange membrane fuel cell with high power at low Pt loadings and good performance after accelerated carbon corrosion and Pt dissolution tests. Carbon corrosion was significantly suppressed by using a Nafion:PVDF mixture, with some degree of hydrophobicity depending on the Nafion:PVDF weight ratio, as the binder in cathode mat nanofibers.[10]

Top-down SEM images of electrospun nanofiber mats containing PGM-free catalyst, before and after hot-pressing at 4 MPa and 140 °C are shown in Figure 3.1 (a and b). The average fiber diameter, as determined by mapping digitized SEM images using ImageJ software, is ~750 nm. The porosity of the hot pressed fiber mat was estimated to be ~50%, as determined by comparing the measured density of the compressed mat (0.86 g/cm^3 from the fiber mat mass and volume) to the theoretical density based on the fiber composition and the known densities of catalyst and binder (1.75 g/cm^3).

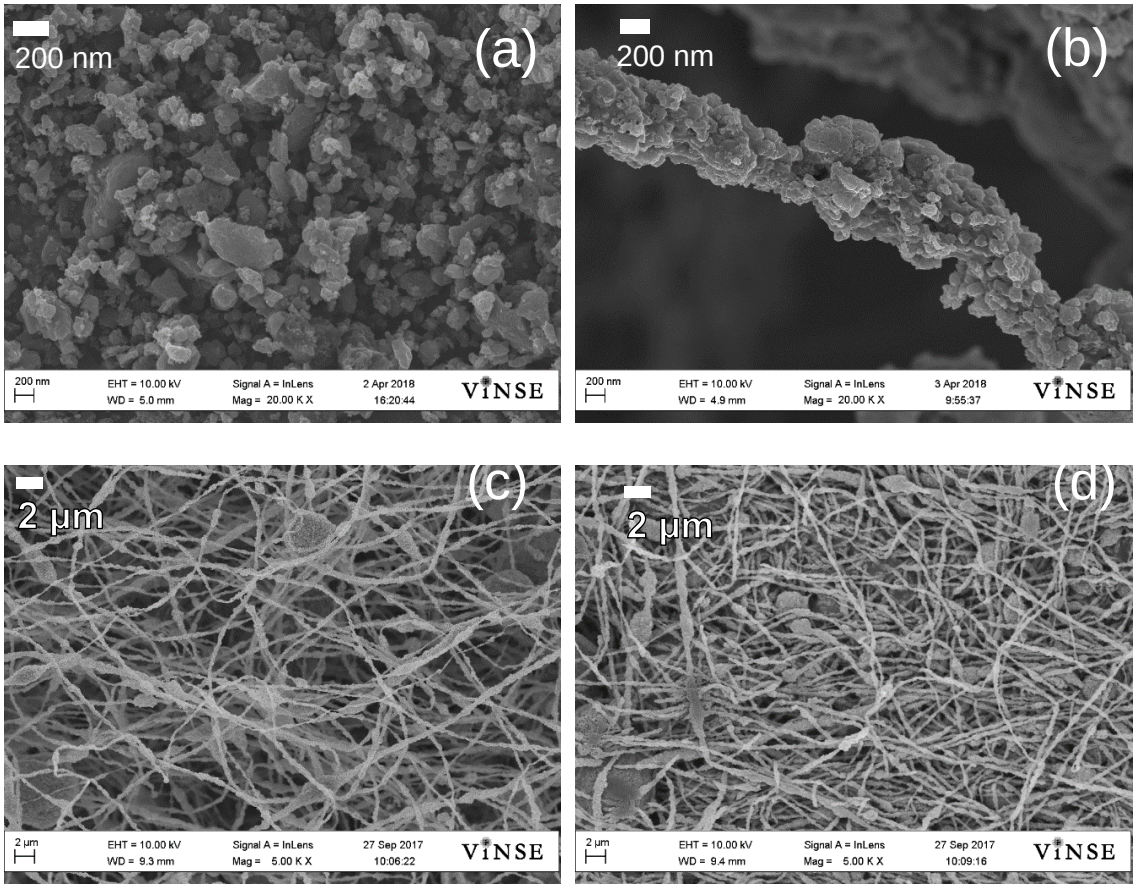

Figure 3.1 Top down SEM images of (a) the PGM-free catalyst particles after ultrasonicating to break up agglomerates (b) a nanofiber composed of PGM-free catalyst:Nafion:PVDF (70:10:20 weight ratio) (c) an electrospun mat of the same composition at 5,000x magnification (d) an electrospun mat of the same composition after hot pressing at 140 °C and 4 MPa.

Figure 3.2 (a and b) shows polarization curves taken immediately upon loading an MEA into the fuel cell test fixture and after 50 hours of operation at a constant voltage of 0.5 V, for one nanofiber and two sprayed cathodes with humidified hydrogen and air feeds. The nanofiber cathode binder was a 1:1 weight ratio blend of Nafion:PVDF (a catalyst:Nafion:PVDF weight ratio of 70:15:15) and the sprayed cathodes employed either a neat Nafion binder or a 1:1 weight ratio Nafion:PVDF blend. The initial time data was collected with no MEA break-in protocol. The neat Nafion sprayed GDE initially

outperformed the nanofiber MEA, with power densities that are comparable to data in the literature, e.g., 120 mW/cm^2 at 0.5 V in Figure 3.2 a vs 100 mW/cm^2 at 0.5 V from reference 5 and 150 mW/cm^2 at 0.5 V in references 1, and 11. After 50 hours, the power output of the neat Nafion sprayed cathode decreased (as observed by previous literature[5,12]), whereas the performance of the nanofiber cathode MEA increased. The initial power output of the sprayed cathode MEA with a 1:1 Nafion/PVDF binder was very low, with a modest improvement in performance after 50 hours of constant voltage operation. Thus, the observed (unexpected) increase in power over 50 hours of operation for the two Nafion:PVDF binder MEAs is due to binder composition effects (a slow break in period for a Nafion:PVDF binder), whereas the high power of the nanofiber cathode MEA after 50 hours is attributed to the fiber morphology.

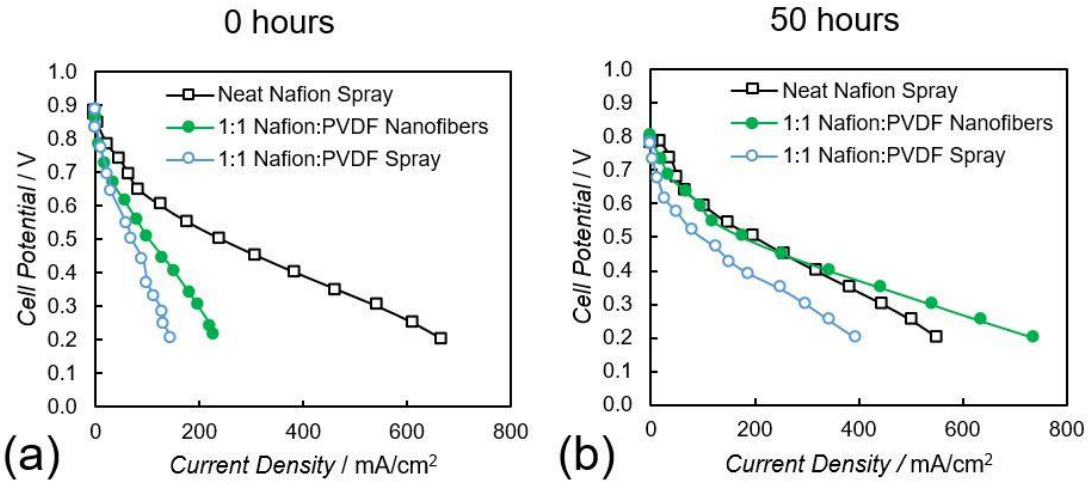

Figure 3.2 H_2/air fuel cell polarization curves for nanofiber and sprayed cathodes MEAs with a PGM-free cathode catalyst (3.0 mg/cm2), a Nafion 211 membrane, and a Pt/C sprayed anode (0.1 mg/cm2 with a neat Nafion binder). (a) Initial fuel cell performance and (b) Fuel cell performance after 50 hours of constant voltage operation at 0.5 V. Fuel cell operating conditions: 80ºC, 100% relative humidity, 1 atm_g backpressure, and 125/500 sccm H_2/air feed gas flow rates. All MEAs have an anode of Johnson Matthey 40% Platinum on carbon with a loading of 0.1 mg_{Pt}/cm^2.

The transient behavior of two nanofiber cathode MEAs (with 1:1 and 1:2 Nafion:PVDF weight ratio binders) and two slurry cathode MEAs (neat Nafion and 1:1 Nafion:PVDF binders) during 300 hours of fuel cell operation is summarized in Figure 3.3, where the power density at 0.5 V is plotted vs. time. The current was measured across the entire timespan at a rate of 1 point every 10 minutes. The results show the beneficial effects of both binder composition and electrode morphology on MEA performance. As expected, based on data in the literature,[5] the initial high performance from a slurry electrode MEA degraded over time, with a 63% decrease in power density at 0.5 V after 300 hours, due presumably to catalyst degradation.[4] The power output of the slurry electrode MEA with a 1:1 weight ratio Nafion:PVDF binder increased after start-up, reached a maximum power density at approximately 150 hours of operation, and then slowly declined for the remainder of the test, with a final power density of only 47 mW/cm^2. The low but stable power is associated with the hydrophobicity of the binder. Initially, there is insufficient water at the catalyst surface for fast oxygen reduction kinetics. During fuel cell operation the catalyst surface becomes more hydrated due to the generation of water during oxygen reduction and the power rises and then stabilizes. There is a slow increase in binder conductivity as the electrode becomes more hydrated. This is evidenced by a decrease in high frequency resistance (from an initial value of 225 $m\Omega \cdot cm^2$ to 115 $m\Omega \cdot cm^2$ after 150 hours) throughout the voltage hold.

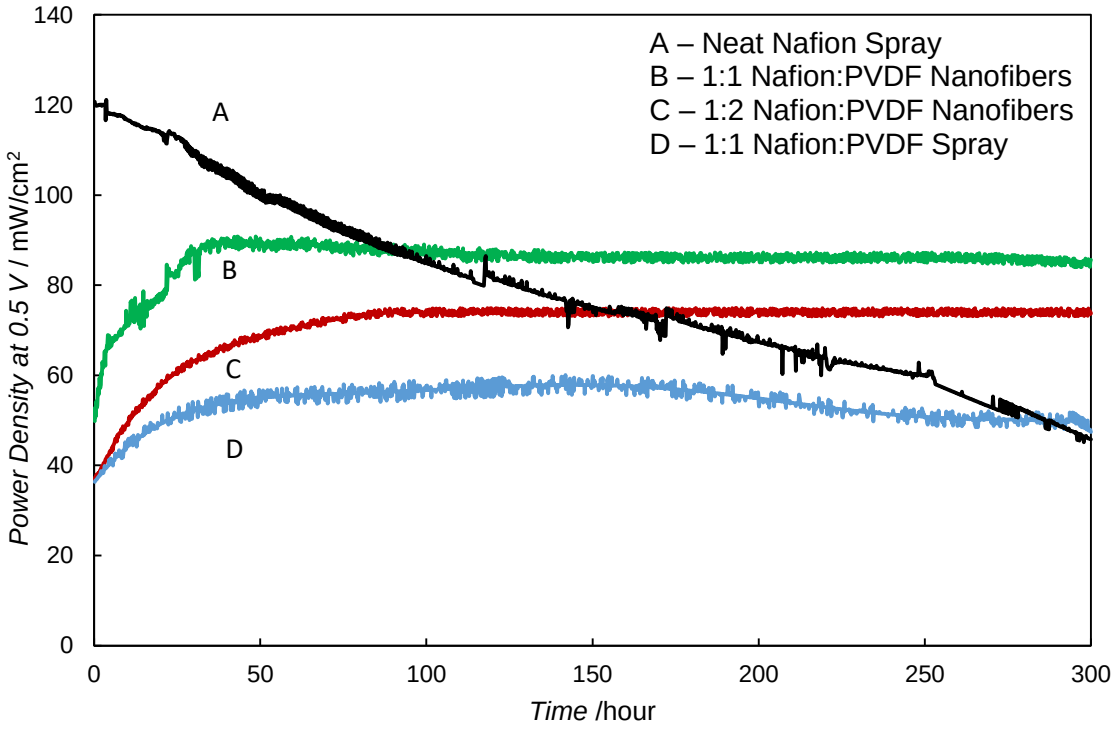

Figure 3.3 H_2/air fuel cell power density at 0.5 V vs time for 300 hours with MEAs using PGM-free catalyst at 3.0 mg/cm2 and either a nanofiber cathode (with a 1:1 or 1:2 Nafion:PVDF binder) or a sprayed cathode (with neat Nafion or a 1:1 Nafion:PVDF binder). All MEAs had a Nafion 211 membrane and a sprayed anode with Nafion binder and Johnson Matthey Pt/C HiSpec 4000 at 0.1 mgPt/cm2¬. Fuel cell operating conditions: 80ºC, 100% relative humidity, 1atmg backpressure, and 125/500 sccm H_2/air feed gas flowrates.

The water content in the Nafion:PVDF binder remains lower than that in a Nafion cathode, which allows for better catalyst stability and constant power operation between 150 and 300 hours. The benefits of a nanofiber cathode morphology is clearly seen in Figure 3.3, for the two Nafion:PVDF binder MEAs. Power output was essentially constant from 150-300 hours for the 1:1 Nafion:PVDF binder with a 72% improvement in power density at 0.5 V after 300 hours (86 mW/cm2 vs. 50 mW/cm2 comparing the nanofiber and slurry cathode MEAs with a 1:1 Nafion:PVDF binder). A similar power density

improvement for a nanofiber vs. sprayed cathode MEA was seen previously with a Pt/C catalyst,[8-10] which was attributed to intrafiber and/or interfiber voids in a fiber mat and good mixing of catalyst and binder with a thin and uniform coating of binder on all catalyst particles (which allows for facile O_2 access to catalyst sites and water removal from the electrode). When the nanofiber cathode binder was made more hydrophobic by using a 1:2 Nafion:PVDF binder, there was a slower rise in power during the initial stages of the test (the power did not stabilize until 100 hours of constant voltage operation) and a 15% decrease in the long-term power density (73 mW/cm2 vs. 86 mW/cm^2 at 300 hours). This result suggests that there may be an optimum PVDF binder content ($\leq$ 50 wt.% PVDF), where the beneficial effects of PVDF regarding catalyst stability are balanced by its adverse effects on power output (decreasing the concentration of water at the catalyst surface and lowering the proton conductivity of the binder). Further work is needed to optimize the Nafion:PVDF weight ratio of the binder for PGM-free ORR catalysts; such experiments were not part of the present study but they are being planned and will be the subject of a future publication.

Carbon corrosion voltage cycling (from 1.0 – 1.5 V vs. SHE) accelerated stress tests (ASTs) were performed on all MEAs after 300 hours of operation at 0.5 V. It is well known that exposing cathodes with PGM-free-based catalysts to potentials above 1.2 V vs. SHE results in extreme degradation.[13-14] The results of these experiments are summarized in Figure 3.4 a, where the maximum H_2/air fuel cell power output at 80 °C, 1 atm back pressure, and 100% relative humidity, measured intermittently over the course of 500 carbon corrosion voltage cycles is shown. The fuel cell polarization plots used to generate this data are shown in Figure 3.4 (b and c).

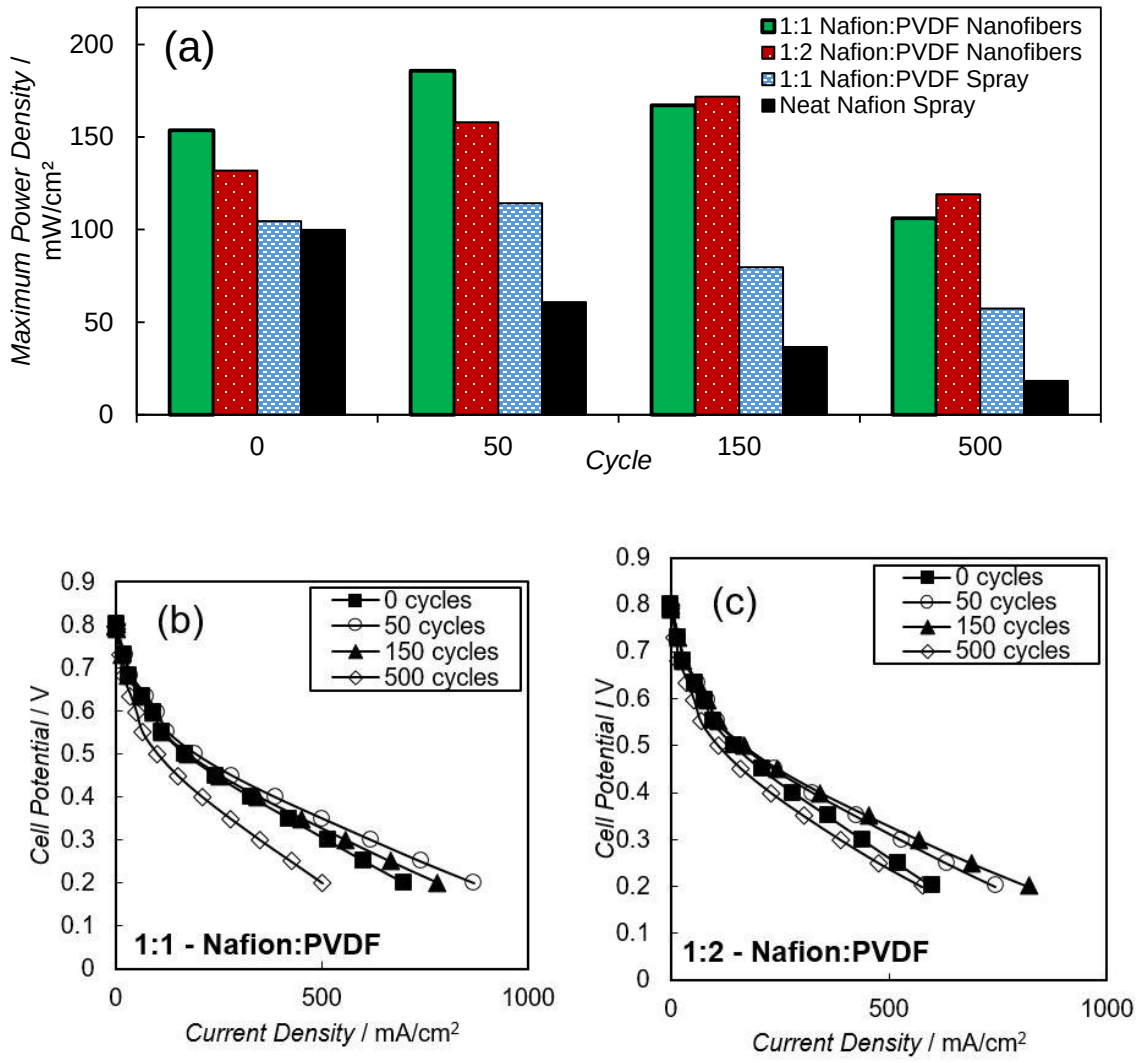

Figure 3.4 Results from the start/stop carbon corrosion voltage cycling accelerated stress test for MEAs with a nanofiber cathode (3.0 mg/cm^2 with 1:1 or 1:2 Nafion:PVDF binders) a sprayed cathode (3.0 mg/cm^2 with a 1:2 Nafion:PVDF binder), and a neat Nafion sprayed cathode with 3.0 mg/cm² cathode loading. (a) Change in the maximum power density with voltage cycle number. (b) fuel cell polarization curves during the stress test for the nanofiber cathode MEA with a 1:1 Nafion:PVDF binder. (c) Fuel cell polarization curves during stress test for the nanofiber cathode MEA with a 1:2 Nafion:PVDF binder. Voltage cycling was between 1.0 and 1.5 V in a triangular waveform at 500mV/s. Fuel cell operating conditions: 80 ºC, 100% relative humidity, 1 atm_g backpressure, and 125/500 sccm H_2/air feed gas flow rates. All MEAs had a Nafion 211 membrane and a sprayed anode with Nafion binder and Johnson Matthey Pt/C HiSpec 4000 at 0.1 mg_{Pt}/cm^2.

The results are significant in that all three PGM-free cathodes with PVDF survived the AST. I.e., each retained greater power after 500 voltage cycles compared to the neat Nafion sprayed cathode. For the neat Nafion sprayed cathode MEA, there was a sharp decline in maximum power with voltage cycling. In contrast, both nanofiber MEAs exhibited an increase in power output after 150 voltage cycles, followed by a gradual decrease in MEA performance for the duration of the test. The difference in results between the two binder compositions demonstrates the effect of hydrophilicity at the beginning of life (BOL) and end of life (EOL). At BOL, the MEA with more PVDF produces lower power compared to the 1:1 Nafion:PVDF and at EOL, the MEA with more PVDF produces higher power. The increase in power during the initial stages of the carbon corrosion AST is consistent with prior studies on the carbon corrosion durability of Pt/C-containing nanofiber cathodes, when the Nafion:PVDF binder weight ratio was < 0.5. As explained in reference 10, the presence of hydrophobic PVDF in a cathode binder with Nafion limits water contact with the catalyst surface, resulting in less carbon corrosion but poor/slow kinetics for the oxygen reduction reaction (a low ORR catalytic mass activity). With continued voltage cycling, hydrophilic carbon oxidation species (e.g., C=O and C-OH) are formed on the catalyst and result in an improvement in power output. Normally, for a conventional cathode structure, this increase in hydrophilicity results in cathode flooding and a loss in power which is observed in Figure 3.4a for the sprayed electrode with a 1:1 weight ratio Nafion:PVDF binder. The nanofiber cathode mat morphology with the same composition, however, allows for the rapid expulsion of water from the sub-micron diameter fibers, so that power losses by cathode flooding are less significant. After 150 voltage cycles, the benefits of further increasing cathode hydrophilicity and water content

at the catalyst surface are overwhelmed by carbon losses/oxidation and water flooding. This explanation of the sprayed and nanofiber cathode behavior in Figure 3.4a is further substantiated by the measured carbon loss from the cathode during the AST (as determined from the measured CO_2 concentration and flow rate in the air exhaust). Carbon corrosion was affected by binder composition (less carbon loss for a binder with more PVDF) and not by cathode morphology. Nanofiber vs sprayed cathodes with the same composition had nearly the same percent carbon loss after 500 voltage cycles (9% for the sprayed electrode with a 1:1 Nafion:PVDF binder and 8% for the nanofiber cathode with a 1:1 Nafion:PVDF binder). The nanofiber morphology, however, does play an important role in that it minimizes the deleterious effect of catalyst surface hydrophilicity on cathode flooding.

SEM images were taken of Nafion/PVDF fibers that were poorly electrospun as well and are shown in Figure 3.5. The importance of these images is to indicate the way this poor dispersion of particles on the nanofibers was resolved. The PGM-free catalyst had primary particle sizes that were quite large and with normal ink preparation resulted in large agglomerates of catalyst along the length of the fiber and large sections of fiber that were devoid of any catalyst particles at all. To solve the problem of large agglomerates of catalyst particles, the catalyst was first dispersed in a sufficient amount of DMF and then had to be ultra-sonicated in an ice bath using a sonication horn and not simply a sonication bath. The sonication horn was used for a period of 5 minutes and this process was repeated 3 times for a total of 15 minutes of ultra-sonication. The process was broken into three separate events because otherwise the solution became quite hot and some of the solvent evaporated.

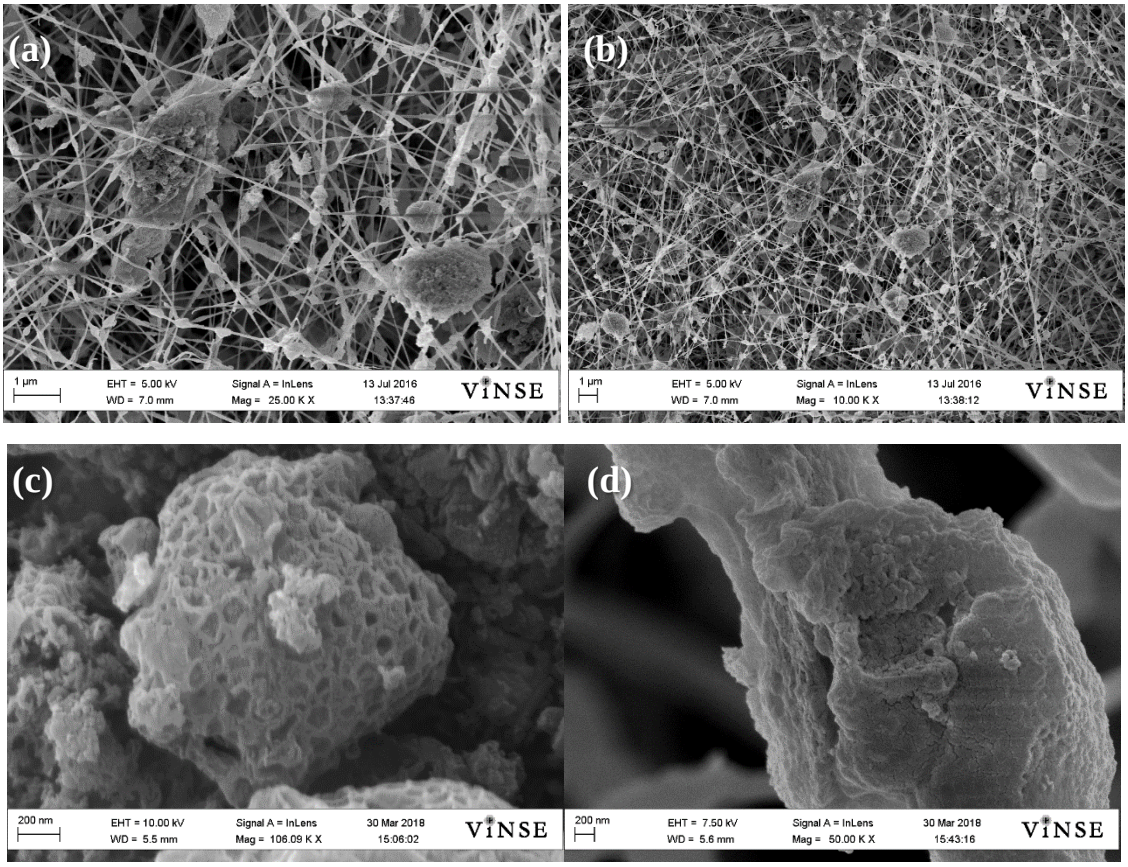

Figure 3.5 Poorly formed Nafion/PVDF nanofibers using Pajarito Powder PGM-free catalyst (a) 25kx magnification (b) 10kx magnification (c) particle of PGM-free catalyst at 100,000 x magnification and (d) poorly formed fiber at 50,000 x magnification.

Experimental Section

Non-PGM catalyst was synthesized at Pajarito Powder, LLC, using a method developed by Mukerjee and Dodelet.[7,15] Specifically, zinc oxide (calcinated 400 °C), 2-methylimidazole, and ammonium sulfate were ball milled for one hour in the presence of isopropyl alcohol, water, and surfactant to form the metal organic framework (ZIF-8). The addition of $(NH_4)_2SO_4$ promotes the reaction between ZnO and 2-methylimidazole (the ligand which forms the ZIF-8 structure) via protonation of imidazolium groups. Further addition of iron sulfate and 1,10-phenanthroline monohydrate was followed by two hours

of ball mixing. The resulting powder (FePhenMOF) was pyrolyzed at 1035 °C under flowing nitrogen for 60 minutes with a ramping rate of 15 °C per minute and then cooled to room temperature. The pyrolyzed powder was ball milled, heat treated in ammonia at 950 °C for 30 minutes, and then allowed to cool down to room temperature before obtaining the final powder (FePhenMOF-ArNH3).

All anodes were prepared by spraying gas diffusion electrodes with an ink composed of 35 wt.% Nafion and 65 wt.% Johnson Matthey Pt/C powder (HiSpec4000) in a 2:1 (w:w) water:isopropanol mixture. For electrospun fiber cathodes, two inks were prepared with a catalyst:Nafion:PVDF wt.% composition of 70:15:15 and 70:10:20, where the solvent was a 7:3 (w:w) mixture of dimethylformamide (DMF) and acetone and the solvent content of the ink was 85 wt.%. Electrospinning inks were prepared by the following three-step procedure: (1) a dispersion of PGM-free catalyst powder in a mixed solvent of 7:3 (w:w) DMF:acetone was mixed by ultrasonic agitation for 30 minutes (Sonics & Materials Inc. VibraCell ultrasonicator), (2) a Nafion/solvent dispersion (20 wt.% 1100 EW Nafion resin, obtained by drying an Ion Power Liquion 115 solution, in 7:3 (w:w) DMF:acetone solvent) was added to the catalyst solution followed by an additional 30 minutes of sonication, and (3) a 10 wt.% PVDF solution was added to the ink mixture (Kynar® HSV 900 PVDF from Arkema, Inc. in 7:3 (w:w) DMF:acetone) followed by 12 hours of mechanical stirring.

Two electrode inks for conventional sprayed cathodes were also prepared, with either 70:15:15 wt.% catalyst:Nafion:PVDF (same composition used in a nanofiber cathode) or 65:35 catalyst:Nafion in a 2:1 (w:w) water:isopropanol solvent. These inks were prepared in a similar way to the nanofiber inks, but the sprayed inks were much more

dilute (97.5 wt.% solvent) to facilitate spraying. Conventional sprayed cathodes were made by airbrush spraying ink directly onto a Sigracet® 29 BC series carbon paper gas diffusion layer (GDL), where the catalyst loading was fixed at 3.0 mg/cm^2.

The apparatus and general procedure for electrospinning cathode mats with PGM-free catalyst are similar to those reported previously for Pt/C catalyst powders.[8-10] Fiber mats were electrospun under controlled humidity conditions using a single needle syringe as the spinneret (22 gauge needle) and a rotating and laterally oscillating drum fiber collector. Electrospinning conditions for producing well-formed particle/polymer fibers with PGM-free catalyst and Nafion:PVDF binder were: 75% relative humidity air at 23 °C, a syringe pump flow rate of 0.2 mL/h, an applied voltage of 12 kV, and a spinneret-to-collector distance of 8 cm. Fibers were electrospun on aluminum foil. Sufficient ink was used to generate a fiber mat with a catalyst loading of 1.5 mg/cm^2.

Electrospun nanofiber mats were cut into 5 cm^2 free-standing cathodes. Two electrospun fiber mats (each at 1.5 mg/cm^2) were stacked and pressed together during MEA fabrication to achieve a catalyst loading of 3.0 mg/cm^2. Fiber cathodes were then hot-pressed together with a Nafion 211 membrane, an anode (0.1 mg$_{Pt}$/cm^2), and two Sigracet® 29 BC Series carbon paper GDLs at 140 ºC at 4 MPa for 10 minutes. The same membrane and hot pressing conditions were used for the sprayed cathode MEAs.

Fuel cell tests were performed using a Scribner Series 850e test station with mass flow, temperature, and backpressure control. The fuel cell test fixture housed a single MEA and contained a single serpentine flow channel for both the anode and cathode. Polarization curves in H_2/air were collected at 80 ºC, 100% relative humidity, 1 atm$_g$ backpressure, and feed gas flow rates of 125 sccm for H_2 and 500 sccm for air. The durability of MEAs was

evaluated in a sequence of two experiments: (1) measuring the H_2/air fuel cell output current over a time period of 300 hours for a constant voltage of 0.5 V and then immediately thereafter (2) performing a carbon corrosion accelerated stress test using the DOE's start-stop potential cycling protocol (triangular wave voltage cycles between 1.0 and 1.5 V vs. SHE at a scan rate 500 mV/s). During the carbon corrosion cathode cycling test, the fuel cell test fixture was supplied with 100 sccm H_2 at the anode and 100 sccm N_2 at the cathode (both feed gases were fully humidified at ambient pressure). During the carbon corrosion test, CO_2 in the air exhaust was monitored to gauge carbon loss. A non-dispersive infrared CO_2 detector (CO_2 Meter Inc. – Model No. CM-0152) in the air exhaust generated CO_2 (ppm) vs. time data, which was then integrated to yield the total carbon loss from the cathode.

3.2 PGM-free Catalyst in Nanofibers with Nafion/Polyethylene Oxide

The catalyst obtained from Pajarito Powder LLC was also used to electrospin fibers that used a Nafion/PEO electrode binder. The power density observed from this electrode was higher at the beginning of life (before any voltage hold). An increase in power density was observed for this electrode structure as well, however, it was not as stable as the electrodes that contained Nafion/PVDF as the binder. The trend after 300 hours is shown in Figure 3.6. The fuel cell operating conditions during this voltage hold were 80 ºC, 100% relative humidity, 200 kPa backpressure, and 125/500 sccm H_2/air feed gas flow rates. This MEA had a PGM-free catalyst cathode loading of 3.0 mg/cm^2 and also had a Nafion 211 membrane and a sprayed anode with Nafion binder and Johnson Matthey Pt/C HiSpec 4000 at 0.1 mgPt/cm^2.

The results of this experiment show that the Nafion/PEO-based PGM-free catalyst electrode produces only slightly lower power after 300 hours than the BOL neat Nafion slurry electrode using the same PGM-free catalyst for the cathode. The results of the power density at BOL and EOL are summarized in Table 3.1.

Table 3.1 Power densities of various PGM-free cathode MEAs

	Neat Nafion Spray	1/1 - Nafion/PVDF Spray	1/1 - Nafion/PVDF Nanofibers	Nafion/PEO Nanofibers
Power at 0 hours (mW/cm^2)	120	37	37	159
Power at 150 hours (mW/cm^2)	75	58	85	155
Power at 300 hours (mW/cm^2)	45	48	85	106
(Power 300h)/(Power 0h)	38%	130%	230%	67%

While the Nafion/PVDF nanofibers do show a greater relative improvement in power density after 300 hours compared to the other systems, the Nafion/PEO nanofibers show the greatest absolute power density at the end of the 300 hour voltage hold – more than two times the power density of the neat Nafion slurry at 300 hours.

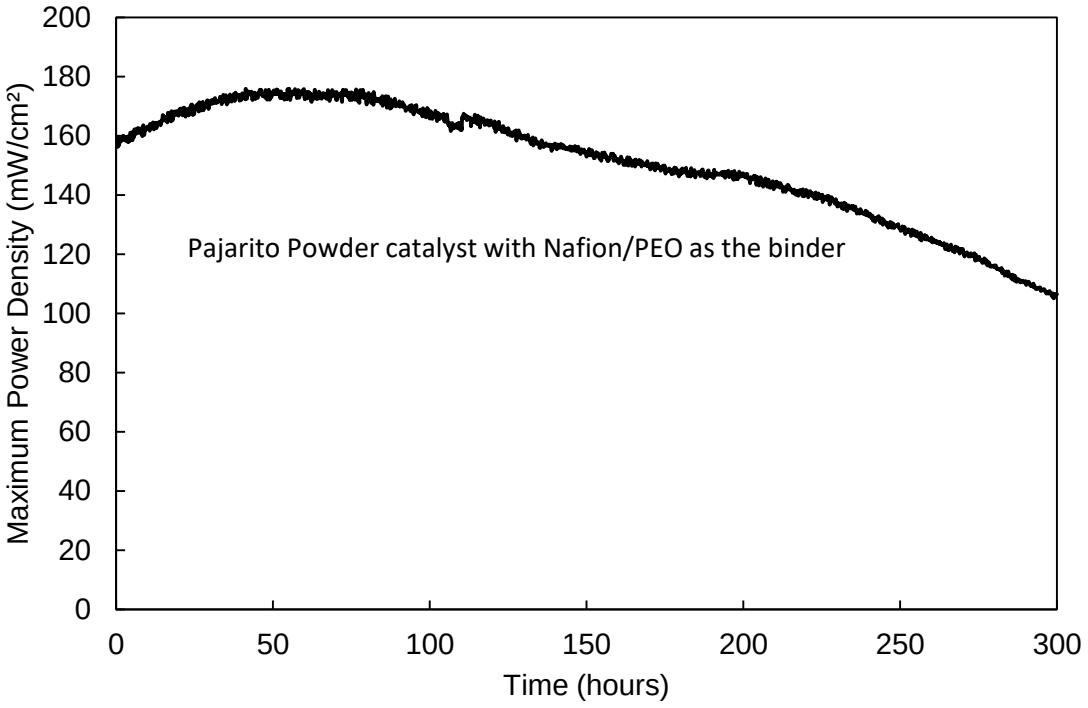

Figure 3.6 Maximum Power vs. Time for an MEA containing Nafion/PEO as the binder.

3.3 Conclusions

In summation, sprayed and nanofiber cathode MEAs with a MOF-derived Fe–N–C PGM-free cathode catalyst (at 3.0 mg/cm^2) were investigated in an H_2/air fuel cell. The use of a Nafion:PVDF binder allowed for stable long-term (300 hour) power output for both nanofiber and sprayed cathode MEAs; this result is much different from that observed for a neat Nafion binder (sprayed cathode morphology) where there was a sharp decline in power. Thus, a particle/polymer nanofiber mat cathode with PGM-free catalyst and a 1:1 weight ratio Nafion:PVDF binder exhibited a stable maximum power density of 153 mW/cm^2 at 80 °C and 1 atm backpressure for 300 hours. The nanofiber MEA cathode also exhibited excellent resistance to the deleterious effects of carbon corrosion, with a maximum power density increase from 150 to 186 mW/cm^2 after 50 voltage cycles (from

1.0 to 1.5 V) followed by a slow but steady power loss to 106 mW/cm2 after 500 cycles. The 1:1 weight ratio Nafion:PVDF binder produced more power after 300 hours of operation, but the power density decreased more rapidly during a carbon corrosion accelerated stress test, as compared to a nanofiber cathode with a binder of 1:2 Nafion:PVDF. The excellent performance of the nanofiber cathode was attributed to the combined effects of the somewhat hydrophobic Nafion:PVDF binder, which minimized catalyst degradation, and the nanofiber morphology which allows for facile oxygen access to catalyst sites and the efficient expulsion of water, where the latter allowed for reasonable power output after a carbon corrosion test. Furthermore, the use of a Nafion/PEO binder has shown to yield the greatest absolute power after a 300 hour voltage hold.

3.4 References

[1] F. Jaouen, E. Proietti, M. Lefevre, R. Chenitz, J. Dodelet, G. Wu, H. T. Chung, C. M. Johnston, P. Zelenay. Energy Environ. Sci. 2011, 4, 114-130.

[2] A. L. Bouwkamp-Wijnoltz, W. Visscher, J. A. R. V. Veen, E. Boellaard, A. M. V. D, Kraan, S. C. Tang. The Journal of Physical Chemistry B. 2002, 106 (50), 12993–13001.

[3] M. Lefèvre, J. P. Dodelet, P. Bertrand, Journal Physical Chemistry B 2002, 106 (34), 8705–8713.

[4] D. Banham, S. Ye, K. Pei, J.-i Ozaki, T. Kishimoto, Y. Imashiro, Y. J. Power Sources 2015, (285), 334−348

[5] M. Shao, Q. Chang, J.-P. Dodelet, R. Chenitz. Chem. Rev. 2016 (116) 3594-3657.

[6] J. C. C. H. Zagal, F. Bedioui, J. P. Dodelet. Springer Science Business Media, LLC: New York, NY, 2006. pp. 130-139.

[7] J. Li, S. Ghoshal, W. Liang, M-T. Sougrati, F. Jaouen, B. Halevi, S. McKinney, G. McCool, C. Ma, X. Yuan, Z-F. Ma, S. Mukerjee, Q. Jia. Energy Environ. Sci. 2016, 9, 2418-2432.

[8] W. Zhang, P. N. Pintauro, ChemSusChem 2011, 4 (12), 1753–1757.

[9] M. Brodt, R. Wycisk, P. N. Pintauro. Journal of the Electrochemical Society 2013, 160 (8). F744-F749.

[10] M. Brodt, R. Wycisk, N. Dale, P. N. Pintauro. Journal of The Electrochemical Society. 2016, 163 (5). F401-F410.

[11] G. Wu, K. L. More, C. M. Johnston, P. Zelenay. Science 2011, 332 (6028), 443–447.

[12] D. Zhao, J-L. Shui, C. Chen, X. Chen, B. M. Reprogle, D. Wang, D-J. Liu. Chem. Sci., 2012, 3, 3200-3205

[13] A. Serov, M. J. Workman, K. Artyushkova, P. Atanassov, G. McCool, S. McKinney, H. Romero, B. Halevi, T. Stephenson. Journal of Power Sources. 2016. (327) 557-564.

[14] S. Mukerjee, FY 2012 Annual Progress Report DOE Hydrogen and Fuel Cells Program. 2012. V-143 – V148.

[15] E. Proietti, F. Jaouen, M. Lefevre, N. Larouche, J. Tian, J. Herranz, J-P. Dodelet. Nat. Commun. 2011, 2, 146, 1-9

CHAPTER 4

NANOFIBER FUEL CELL CATHODES WITH PLATINUM COBALT AND A NAFION/PAA BINDER

4.1 Introduction

The development of sustainable energy storage and conversion technologies is an important technological and societal challenge. The hydrogen/air proton-exchange membrane fuel cell (PEMFC) is a promising energy conversion device due to its high power output, high-energy conversion efficiencies and moderate operating temperature.[1,2] These characteristics make the PEMFC well suited for automotive applications, but the cost and durability of Pt-based catalyst electrodes are still issues that require further attention.

In 2011, Zhang and Pintauro published the fabrication method and superior performance of a nanofiber electrode mat for a fuel cell cathode.[3] In three following papers, Brodt et al. extended this work.[4–6] They showed that the nanofiber electrode morphology provides inter-fiber and intra-fiber void-space for facile oxygen access to cathode catalyst sites and for rapid product water removal. In Reference 6, the hydrophobicity of the cathode was altered by using a binder composed of Nafion and polyvinylidene fluoride (PVDF), which lowered the rate of carbon corrosion in an accelerated stress test.

A variety of strategies are being pursued to lower the Pt content in proton exchange membrane fuel cell membrane-electrode-assemblies (MEAs), including the use of core-shell and Pt-alloy catalysts which exhibit very high oxygen reduction reaction (ORR)

activity.[7,8] Recently, a number of studies have shown that PtCo/C catalysts are particularly attractive for use in a hydrogen/air fuel cell due to their very high mass activity.[8–11]

In the present study, commercial PtCo catalyst supported on porous carbon supplied by Tanaka Kikinzoku Kogyo (TKK) were incorporated into nanofiber cathode MEAs using a Nafion/poly(acrylic acid) (PAA) cathode binder. The performance and durability of these MEAs were assessed in a hydrogen/air fuel cell at a cathode catalyst loading of 0.1 mg_{Pt}/cm^2. The PtCo/C nanofiber cathode MEAs were compared to spray cathode MEAs with the same catalysts and with neat Nafion binder.

4.2 Experimental

4.2.1 Electrode Preparation

Electrospinning inks were prepared at Vanderbilt University by dispersing a carbon supported catalyst with Nafion dispersion (Liquion 1115 1100 EW) and 450 kDa PAA (Sigma Aldrich). The catalyst powder was either 40 wt.% Pt/Vulcan carbon (Johnson Matthey HiSPEC 4000) or a 52 wt.% PtCo on porous carbon (Tanaka Kikinzoku Group: TEC36E52). Inks were made with an isopropyl alcohol/water solvent. The solids content of the inks for nanofiber electrodes was 15 wt.% - much higher than the solids content for spray inks (4.6 wt.%).[4] Spray inks require low viscosity to achieve even distribution from atomization[12] and nanofiber inks require high viscosity for sufficient polymer chain entanglement during the electrospinning process described previously.[3] Electrospinning inks were prepared by the following steps. First, catalyst powder was added to water and sonicated for 30 minutes in an ice bath. Next, Nafion was added followed by an additional 30 minutes of ice bath sonication. Finally, the carrier polymer, PAA, was added and the mixture was mechanically stirred for two days.

Electrospinning was carried out using a single stainless steel needle tipped syringe as the spinneret, with a rotating and horizontally oscillating drum collector, as described in References 3–6. Nanofiber mats were electrospun by controlling the voltage bias between the needle tip and the grounded drum collector, the ink flow rate, relative humidity, and distance from needle tip to collection drum. The final platinum loading of the electrode was controlled by the duration of the electrospinning process. The conditions to electrospin with Nafion and PAA were: 12 kV, 0.75 mL/hr, 40% RH, and 8 cm from tip to collector. The Pt-alloy dry fiber mat composition was 65:23:12 catalyst:Nafion:PAA; this correlates to an ionomer to carbon (I/C) ratio of 1.108 where the ionomer in this case is defined as (Nafion + PAA).

Spray inks were prepared at Nissan Technical Center of North America (NTCNA). Typically, the catalyst inks were made by mixing water, n-proponol and Nafion ionomer dispersion (20 wt.%). The mass-based ionomer/carbon (I/C) ratio in the ink was kept constant at 1.2, and the water/alcohol weight ratio was 1/1. The obtained ink was well-mixed using a homogenizer (Ika T25) for 4 hours. Then, the electrocatalyst cathode layer was sprayed onto gas diffusion layers (GDLs) using an automated robotic spray system (Asymtek, Nordson). The spray electrodes from Nissan also had a layer of Nafion sprayed onto their surface (at 0.5 mg_{Nafion}/cm^2) in order to facilitate hot pressing of the electrode and membrane.

Membrane-Electrode-Assembly (MEA) Preparation

A series of different nanofiber and spray electrode MEAs were prepared. The anode and cathode Pt loadings for all nanofiber MEAs were 0.1 ± 0.01 mg_{Pt}/cm^2. Therefore, the total MEA platinum loading was 0.2 ± 0.02 mg_{Pt}/cm^2. All MEAs with a nanofiber

cathode also had a nanofiber anode. Nanofiber anodes contained Johnson Matthey 40% Pt/C on HiSpec 4000 catalyst and a catalyst:Nafion:PAA wt. ratio of 65:23:12. For anode/cathode spray electrode MEAs, the binder was neat Nafion (no PAA). The spray cathode loading was ~0.1 mg_{Pt}/cm^2 and the sprayed anode loading was 0.4 mg_{Pt}/cm^2, resulting in a total MEA loading of ~0.5 mg/cm^2. The sprayed anode loading above 0.1 mg_{Pt}/cm^2 should not affect MEA performance.

All nanofiber MEAs were prepared at Vanderbilt University by hot pressing the anode and cathode onto opposing sides of a Nafion NR211 membrane, with Sigracet 29 BC anode and cathode gas diffusion layers. Nanofiber electrodes were hot pressed at 2 MPa and 140 °C for 5 minutes. Sprayed electrode MEAs were prepared at Nissan Technical Center of North America (NTCNA) by hot pressing gas diffusion electrodes at 2 MPa and 130 °C for 10 minutes.

4.2.2 Procedures for Fuel Cell Testing

All Nanofiber and spray electrode MEAs that were studied at NTCNA had an active area of 10 cm^2 and used parallel channel flow fields. Hydrogen/air fuel cell polarization data were collected at 80 °C, 200 kPa absolute and either 40% or 90% relative humidity. H_2/air feed flow rates were 4000/8000 standard cubic centimeters per minute (sccm). Oxygen reduction reaction mass activities were obtained using methodologies in the literature[13] at 80 °C and 0.9 V, under fully humidified hydrogen/oxygen at 150 kPa absolute with anode and cathode flow rates of 4000/8000 sccm H_2/O_2, respectively. The electrochemical surface area (ECSA) of cathodes was determined from cyclic voltammograms of H_2 generation/stripping with stagnant H_2 gas at ambient pressure and 30 °C as is standard procedure.[14] Oxygen gas transport resistance in cathodes was

determined using a limiting current method described in reference [15]. Limiting currents were measured under the conditions shown in Table 4.1

Table 4.1. Oxygen limiting current experimental conditions used to determine the gas transport resistance (GTR).

Experimental Parameter	**Condition**
Anode Gas / Flow Rate (sccm)	H_2 / 4000
Cathode Gas / Flow Rate (sccm)	Diluted O_2 with balanced N_2 / 8000
Pressure (kPa absolute)	100, 150, 200, 250
Cell Temperature (°C)	80
Anode Dew Point (°C)	77.4
Cathode Dew Point (°C)	77.4

PtCo/C nanofiber cathode MEAs were subject to additional testing at Los Alamos National Lab in a 5 cm^2 differential cell following the procedure reported by Baker et al.[16] This cell was subjected to a repeated recovery protocol[17] in order to maximize mass activity and fuel cell performance. The recovery protocol was applied four times after conditioning at 0.6 V for 16 hours in order to achieve the maximum initial performance and then to recover the performance after 15,000 and 30,000 square wave (0.6 V and 0.95 V for 3 seconds) accelerated stress test (AST) voltage cycles. The specific recovery protocol consisted of a 1.0 hour hold at 0.1 V in H_2/air with the cell at 35 °C and the humidifier bottles for H_2 and air at 40 °C, which provides sufficient water to wash out impurities from the catalyst. Next, the MEA was subjected to a pumping current of 0.1 A/cm^2 for 1.0 hour with H_2 anode gas and N_2 cathode feed gas resulting in a zero or mildly negative voltage to desorb impurities from the catalyst surface.

To determine the gas transport resistance of Nafion on catalyst particles, the limiting O_2 reduction current must be obtained at varying oxygen concentrations and varying total pressures. The limiting currents were obtained by linear sweep voltammetry using an external potentiostat in the potential window of 0.1 V – 0.95 V at a scan rate of 10 mV/s for 4 cycles while supplying diluted oxygen to the working electrode (cathode) and pure hydrogen to the counter electrode (anode). The experiments were conducted with a cathode feed gas at five different concentrations of oxygen balanced with nitrogen: 0.000%, 0.525%, 0.787%, 1.838% and 2.625% O_2. The gases were supplied at a high flow rate to minimize the in-plane reactant gas concentration differential. The reactant gas (O_2) concentration was controlled by mixing it with N_2 gas by means of mass flow controllers. The relative humidity (RH) of inlet gases (O_2 mixtures and H_2) was set at 90%. At higher RH conditions (RH 100%), a decrease in the limiting current due to flooding was observed. In contrast, at lower RH conditions (~70%), the limiting current was not clearly obtained due to an increase in the IR drop across the membrane and the catalyst layer. As a result, 90% was considered as the optimal RH condition for this study. This procedure is similar to that performed in previous studies.[18–20]

Electrochemical impedance spectroscopy (EIS) measurements were performed at 0.45 V (DC) from 15 kHz to 0.1 Hz with an AC amplitude of 10 mV, and a cell temperature of 80 °C at 100% RH, where the fuel cell was supplied with H_2 at the anode and N_2 at the cathode (both at 500 sccm).

4.2.3 Accelerated Stress Tests

To simulate acceleration/deceleration events in an automotive setting, the Fuel Cell Commercialization Conference of Japan (FCCJ) established a square-wave voltage cycling

protocol of 0.6 V to 0.95 V.[21] This subjects catalyst particles to electrochemical degradation such as formation of platinum oxide species, agglomeration of particles in the catalyst layer by Ostwald ripening, and dissolution/migration/isolation of particles into the membrane.

The protocol utilizes fully humidified feed gases of hydrogen/nitrogen. An external potentiostat was used to apply 0.6 V for three seconds, then 0.95 V for three seconds, constituting one cycle. Tests were carried out using a Gamry Instruments Reference 3000 Potentiostat. To meet the standards of the United States Department of Energy, this accelerated stress test (AST) was applied for 30,000 square wave voltage cycles.

4.3 Results and Discussion

4.3.1 PtCo/C Nanofiber Structure

Nanofiber mats were imaged using a Zeiss Merlin scanning electron microscope (SEM) at the Vanderbilt Institute of Nanoscale Science and Engineering, with an accelerating voltage of 10 kV (as was used in the past to analyze this type of sample)[3] and a working distance of 8 mm. Figure 4.1 shows scanning electron micrographs of (PtCo/C)/Nafion/PAA fiber mats where the carbon support is high surface area carbon. The surface of the fibers is uniformly roughened due to the high catalyst particle content and there are no large electro-spray droplets. The average diameter of the fibers is approximately 600 nm, as determined by Fiji/ImageJ analysis of digitized micrographs. Typically, uniform, roughened fibers are thought to give rise to improved access to active sites and improved durability. The SEM image in Figure 4.1a is similar to those observed by both Brodt et al. (shown in Figure 4.1c)[4,5] and Zhang et al. (shown in Figure 4.1d)[3] These SEM images provides evidence that the use of PtCo alloy supported on high surface

area carbon does not significantly alter the fiber structure from the perspective of the electrode as a whole.

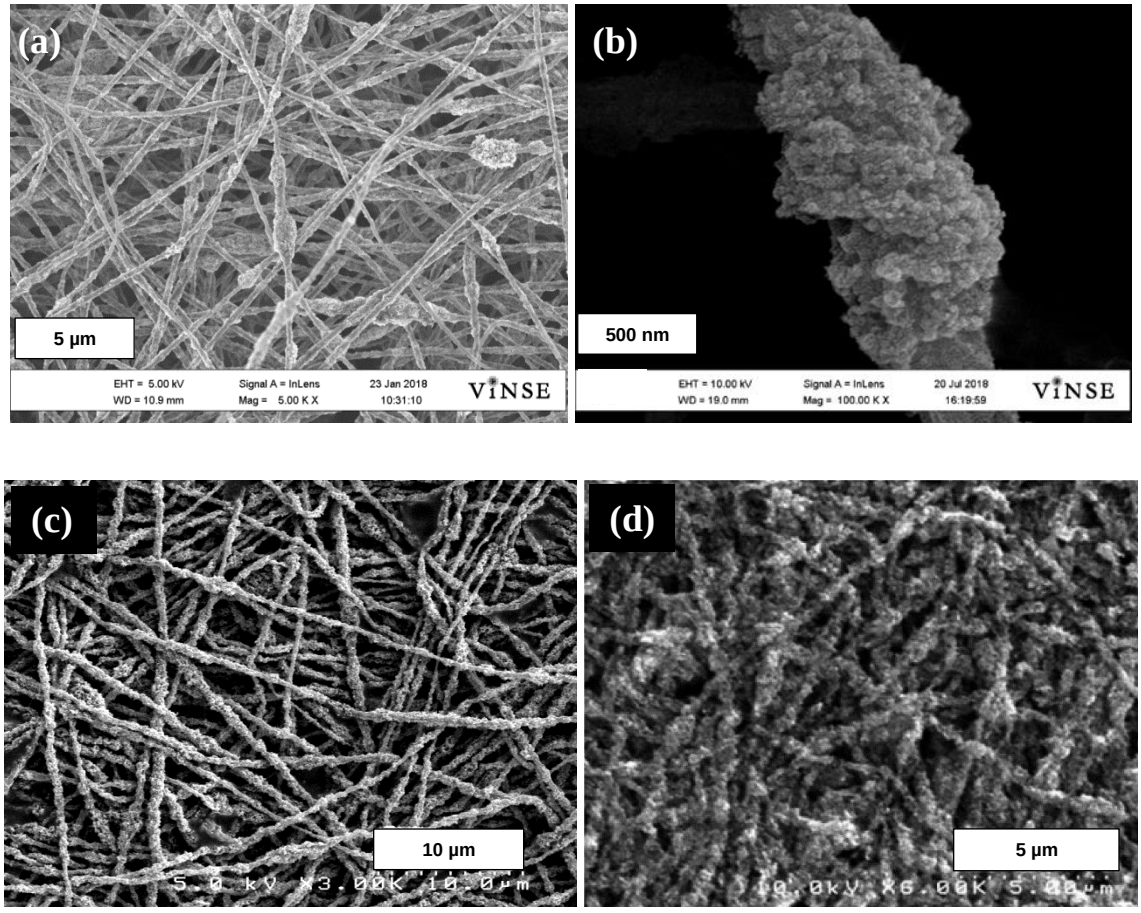

Figure 4.1 SEM images of nanofiber mat with a binder of Nafion/PAA containing PtCo/C at (a) (5000x), and (b) PtCo/C (100,000x) (c) Pt/C (3000x) nanofiber mat with a binder of Nafion/PAA from reference [5] and (d) Pt/C (6000x) nanofiber mat with a binder of Nafion/PAA from reference [3].

Scanning Transmission Electron Microscopy and Energy Dispersive X-ray Spectroscopy

Scanning transmission electron microscopy (STEM) tomography was performed using a 200kV FEI Talos F200X STEM at Oak Ridge National Laboratory (ORNL) with a Gatan High Tilt tomography holder for FEI instruments. The holder was plasma-cleaned for 5 minutes prior to use, after which the sample was loaded and a 20 minute ozone

cleaning treatment (10 minutes/side) was used to reduce possible hydrocarbon deposition (contamination). Bright field (BF) and high angle annular dark field (HAADF) image pairs (1024 by 1024 pixels) were acquired in 5° tilt increments over a tilt range of ±75° (150° total). This results in a series of STEM images referred to as a "tilt series". Tilt series alignment and tilt-axis corrections were performed manually for each image stack using computer software (Fiji/ImageJ and Tomviz (tomviz.org)). A 3D reconstruction of a 2 micron length of a single nanofiber was performed for the bright field tilt series using a bright-field model-based iterative reconstruction algorithm (MBIR) which accounts for diffraction contrast. Figure 4.2 shows images relating to the STEM analysis of the nanofiber structure including an example of the STEM dark field image of the nanofiber during the tilt-series (4.2a), the length-wise fiber cross section generated from these images (4.2b) and the resultant reconstruction (4.2c)

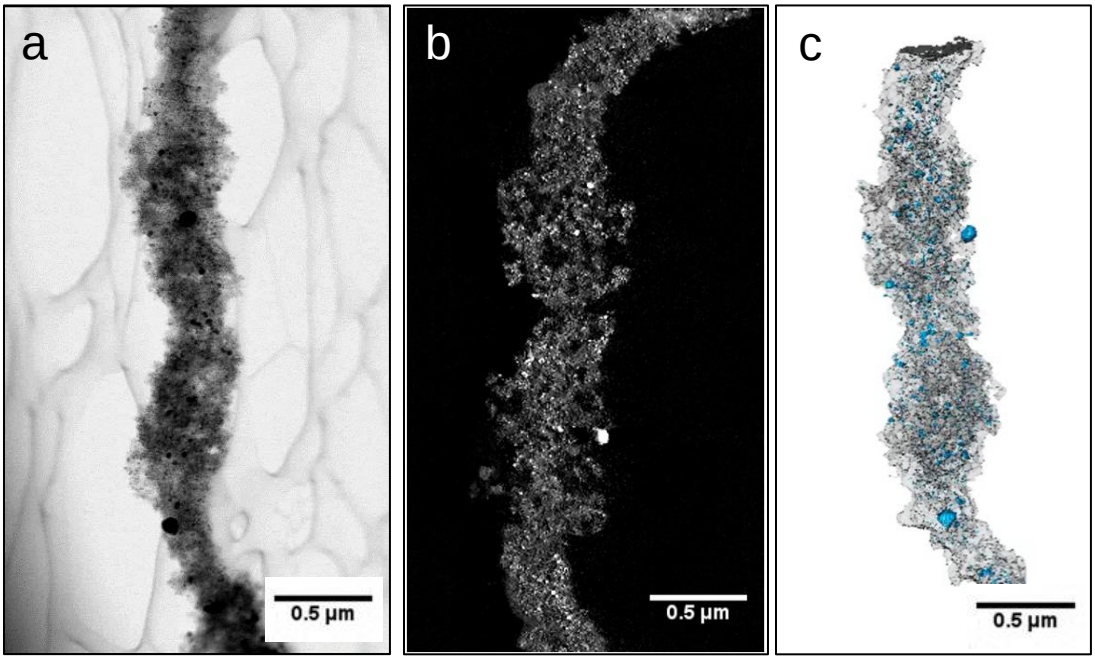

Figure 4.2 (a) The STEM-image of the 2 micron length of nanofiber at the beginning of the tilt series (75° from perpendicular) (b) The length-wise cross-section of the nanofiber

generated from the 3D reconstruction. The bright spots are metal particles, the gray areas are Nafion, PAA, or carbon, and the black is void-space (c) the total 3D reconstruction showing PtCo particles in blue, Nafion/PAA/C in gray, and void space in white.

The results of the reconstruction from STEM imaging show that there is a uniform distribution of the catalyst along the length of the fiber. Additionally, a significant portion of the nanofiber was void-space, as can be seen in Figure 4.2 b.

Next, the total amount of surface area generated by the internal void-space and surface roughness of the nanofiber was visualized and quantified. Visualizations of the 3D reconstructed single nanofiber, 2 microns in length, are shown in Figure 4.3. These visualizations were obtained using FEI's Aviso (v. 9.1.1) software. Figure 4.3a is the fiber reconstruction that includes the internal void-spaces and outer roughness. Figure 4.3b is the fiber reconstruction where the software filled the internal void-spaces. Figure 4.3c is the fiber reconstruction where the software filled the internal void-spaces and smoothed the outer roughness of the fiber length.

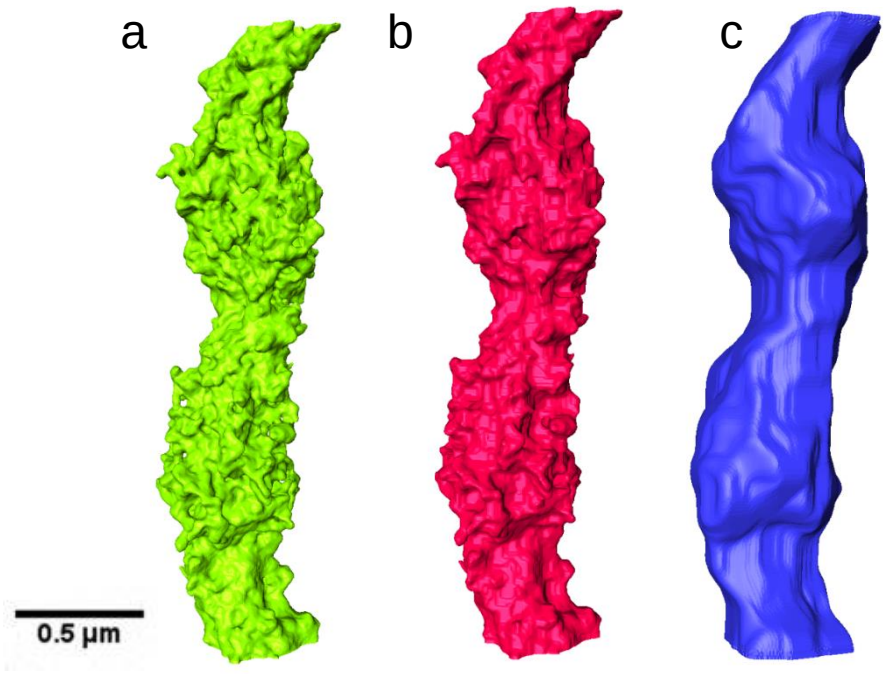

Figure 4.3 Three-dimensional reconstructions of nanofibers with TKK PtCo/C. (a) reconstructed nanofiber with void-spaces and surface roughness, (b) reconstructed nanofiber with void-spaces filled, (c) reconstructed nanofiber with void-spaces filled and surface roughness smoothed.

The Aviso software also computed the total surface area that resulted from Figure 4.3a, 4.3b, and 4.3c. These surface areas are provided in Table 4.2.

Table 4.2. Surface area per micron of nanofiber calculated from the 3D reconstructions obtained from Avisio software.

	Calculated Surface Area (nm^2)/micron length of fiber
Figure 4.3a (nanofiber reconstruction)	5.10×10^6
Figure 4.3b (void space filled)	3.51×10^6
Figure 4.3c (void space filled & outer roughness smoothed)	2.99×10^6

The surface area generated from Figure 4.3b is 31% lower than the surface area calculated from Figure 4.3a. This indicates that the intra-fiber voids contribute 31% to the

total fiber surface area. Comparing the surface areas generated from 4.3b and 4.3c, it was determined that an additional 15% of the fiber's surface area comes from the outer-fiber's roughness. Therefore, if the nanofiber was completely dense and smooth, it would have 41% less surface area than it does being rough and filled with void-spaces.

This STEM reconstruction provides information regarding total surface area from all components (including platinum, carbon, Nafion, and PAA). However, not all of this surface area can be used to facilitate the oxygen reduction reaction (ORR). Catalyst sites must be accessible to oxygen, protons, and electrons in order to facilitate the ORR. This requires a close proximity of catalyst particles and Nafion binder.[22] For this reason, in addition to the nanofiber's total surface area, it is also beneficial to determine the distribution of Nafion and platinum in the electrode.

The FEI Talos STEM microscope also has the capability to perform energy-dispersive x-ray spectroscopy (EDS) which was used to analyze the Nafion and platinum distribution across a fiber cross-section and along a fiber segment. EDS analysis results in an image that differentiates the signals of fluorine and platinum by color as is seen in Figure 4.4a and Figure 4.4b. The fluorine signals (green) indicate the locations of Nafion (since this is the only component that contains fluorine) and the platinum signals (red) indicate the location of the catalyst particles.

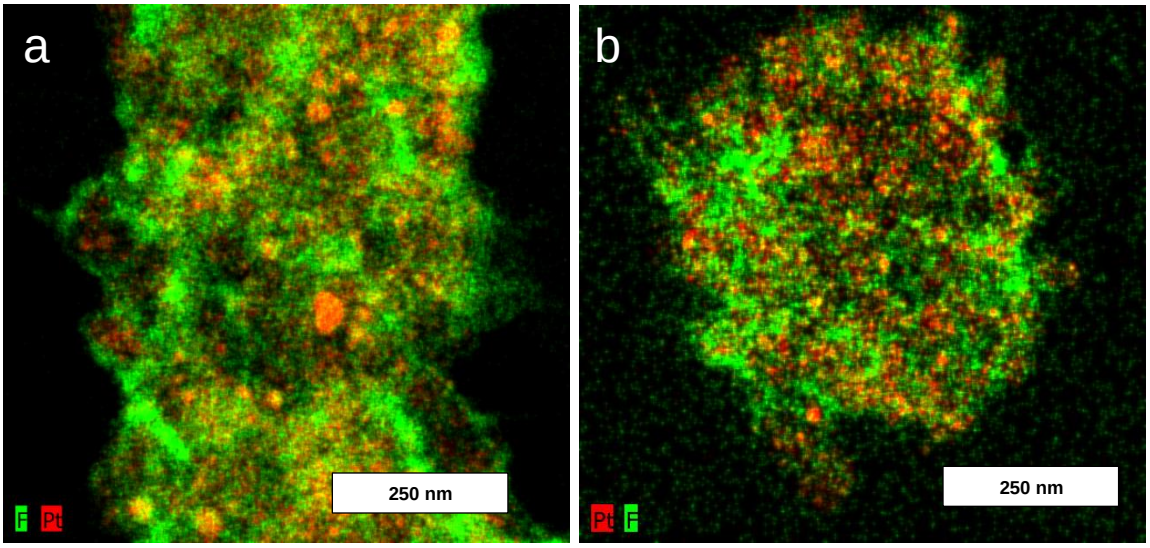

Figure 4.4 Fluorine and Pt signals from energy dispersive X-ray spectroscopy for (a) the length of the nanofiber and (b) the fiber cross section.

The images in Figure 4.4 show elemental maps that come from the EDS experiment. As is seen in Figure 4.4a, the Nafion and Pt are evenly distributed throughout the nanofiber length and as seen in Figure 4.4b the Nafion and Pt are evenly distributed across the diameter of the fiber. Any yellow pixels are due to overlap of the green and red signals indicating that Nafion and catalyst are co-located.

To quantify the platinum and fluorine signals, part of the elemental map may be selected with the FEI Talos' software, to create "line scan" across a fiber selection. Line scans report the x-ray counts associated with each element as a function of position across the sample selection. An example of this type of selection and resultant line scan is shown in Figure 4.5. For a single nanofiber roughly 3 microns in length. The area selected is denoted by the yellow box around the fiber with the center of the box having a thin yellow horizontal line.

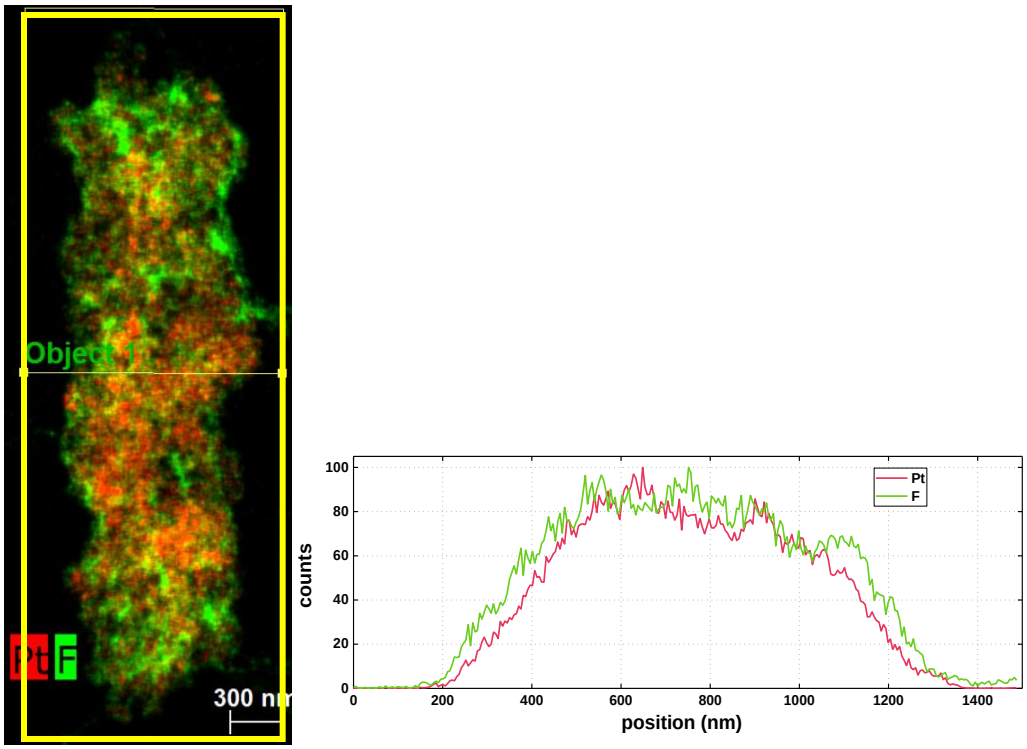

Figure 4.5 EDS analysis results showing (a) elemental map of platinum and fluorine and (b) the line scan result showing the Pt and F signals as a function of position.

4.3.2 Electrochemical Characterization

Polarization data was collected for cathode catalysts of PtCo/C from TKK (TECE3652) and Pt/C from TKK (TEC10E50E). This was done for both painted electrodes (shown in Figure 4.6a) and nanofiber electrodes (shown in Figure 4.6b) All MEAs had a loading of 0.1 mg_{Pt}/cm^2, used a Nafion 211 membrane, and Sigracet 29BC gas diffusion layers. For the painted slurry electrodes, the composition was 65/35 wt.% catalyst/Nafion. MEAs that had painted slurry cathodes also had a painted slurry anode with a composition of 65/35 wt.% (Pt/C)/Nafion. For the nanofiber electrodes shown in Figure 4.6b, the composition was 65/20/15 wt.% – catalyst/Nafion/PAA. Both nanofiber cathode MEAs had nanofiber anodes that were 65/20/15 wt.% (Pt/C)/Nafion/PAA. The PtCo/C cathode

catalyst MEA in both painted slurry electrode MEAs and nanofiber electrode MEAs generated >30% higher power density at 0.65V compared to Pt/C cathode catalyst MEAs. In the literature[11,23,24] PtCo/C also generate ~30% higher power in sprayed cathodes with neat Nafion binder compared to Pt/C cathode catalysts. The high frequency resistance (HFR), which measures the resistance of the membrane and contact resistance of the electrodes, was near ~60 (mΩcm²) for all MEAs indicating that the contact resistance was not significantly different.

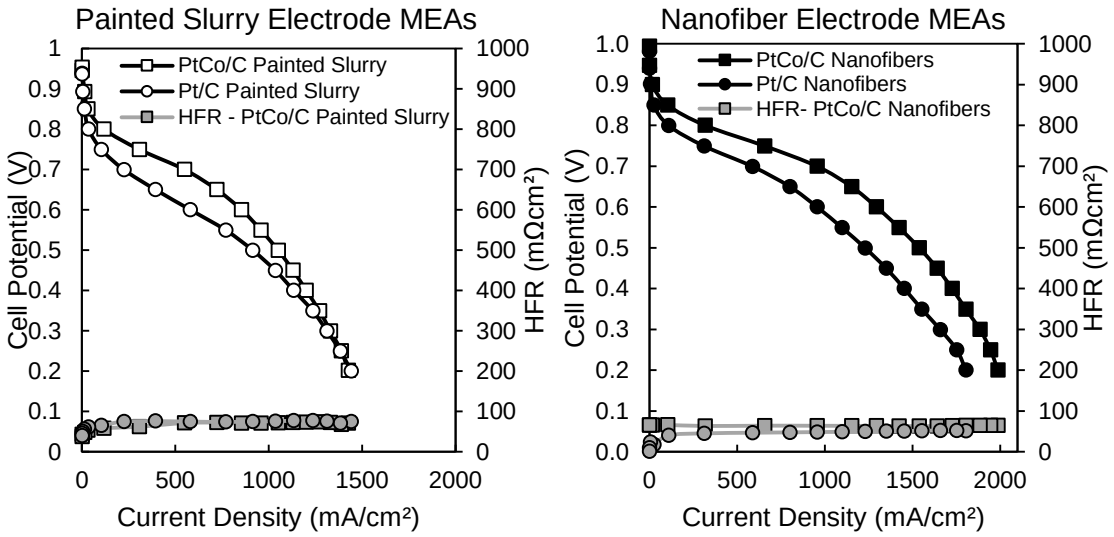

Figure 4.6 H_2/air fuel cell polarization data comparing two types of cathode catalysts using nanofiber electrode MEAs (PtCo/C and Pt/C) at 100% RH, 80 °C and 200 kPa absolute with 125/500 sccm H_2/air. MEAs with a nanofiber cathode used a nanofiber anode. MEAs with a slurry cathode used a slurry anode. All MEAs had an active area of 5 cm^2. Polarization data was collected at Vanderbilt University.

Changing catalyst from Pt/C to PtCo/C in both a painted slurry electrode and a nanofiber electrode results in higher power at higher voltages (0.8 V – 0.65 V). The nanofiber electrode MEA with PtCo/C maintained this increased power density vs. Pt/C. This is likely due to improved transport properties of the nanofiber vs. painted slurry electrodes.

The accessible catalyst surface area to protons, electrons, and feed gas is known as the electrochemically active surface area (ECSA) and can be measured by cyclic voltammetry (CV). As was explained in more detail in Chapter 1 of this dissertation, the charge density associated with hydrogen adsorption onto a Pt surface can be obtained from a CV experiment. From this value (in C/cm^2), the loading of Pt used (in mg_{Pt}/cm^2) and the known he charge required to reduce a monolayer of protons on Pt (210 $\mu C/cm^2$), ECSA is determined. The CV curve is shown in Figure 4.7 for a painted slurry electrode MEA (dashed line) and a nanofiber electrode MEA (solid line) using Pt/C catalyst. The area associated with hydrogen adsorption onto Pt is greater for a nanofiber electrode (as represented by the shaded region in Figure 4.7) than for a painted slurry electrode.

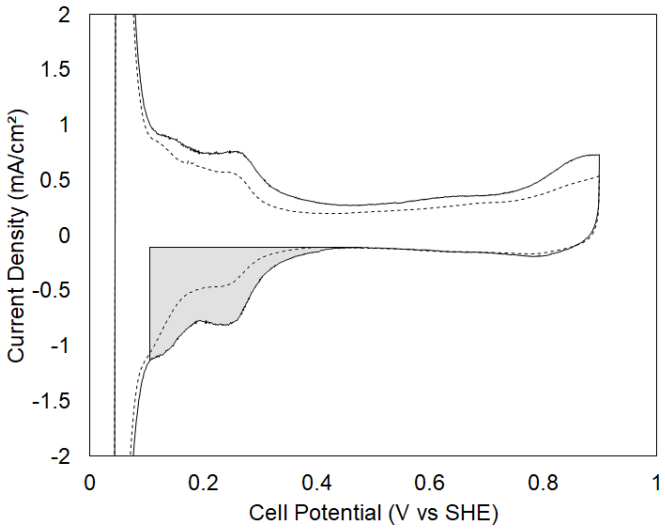

Figure 4.7. Cyclic voltammogram for a nanofiber cathode MEA and a painted slurry MEA used in calculating the electrochemically active surface area (ECSA). Both MEAs use a Pt/C catalyst at a loading of 0.1 mg_{Pt}/cm^2. The integration area for the nanofiber cathode MEA is shaded.

A quantitative comparison of ECSA and mass activity for nanofiber electrode MEAs and painted slurry electrode MEAs is shown in Figure 4.8 for both PtCo/C and Pt/C catalysts.

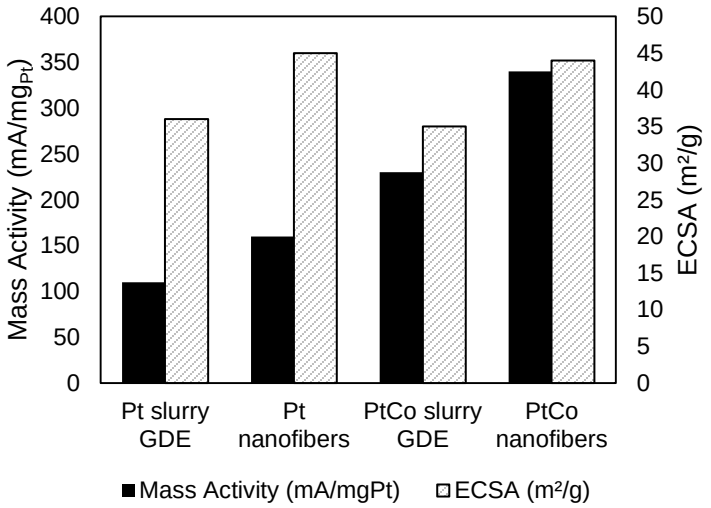

Figure 4.8. Mass Activity and Electrochemically active surface area measured at Vanderbilt University. All electrodes use a catalyst loading of 0.1 mg_{Pt}/cm^2, have a Nafion 211 membrane, and use 29BC Sigracet GDLs. MEAs with a painted slurry cathode have a painted slurry anode of 65/35 – (Pt/C)/Nafion. MEAs with a nanofiber cathode have a nanofiber anode of 65/20/15 – (Pt/C)/Nafion/PAA.

These measurements show that ECSA does not depend on the catalyst type, but instead depends on the morphology (i.e. whether the electrode is a painted slurry or nanofiber). However, mass activity depends both of catalyst type and the morphology. In a nanofiber mat structure, the measured PtCo/C mass activity of 297 mA/mgPt was 130% higher than that of Pt/C in a slurry electrode with Nafion. The relative increase from Pt/C to PtCo/C in a slurry and a nanofiber is the same (~45% increase from Pt/C to PtCo/C). However, the absolute increase in mass activity is greater for nanofibers which gained 110 mA/mg_{Pt} from Pt/C to PtCo/C, compared to a painted slurry electrode MEA which gained 50 mA/mg_{Pt} mg_{Pt} increase from Pt/C to PtCo/C. This means that changing both catalyst

and morphology is more beneficial than changing catalyst alone. The percentage increase in mass activity (for both slurry and nanofiber electrode MEAs) is also consistent with the observations that the PtCo metal exhibits significantly higher intrinsic catalytic activity as measured by RDE.[8,25]

The mass activity does not correlate 1:1 to an increase in power density throughout the polarization curve; this is observed in MEAs in the literature as well.[11,26] The mass activity measured for the PtCo/C catalyst falls within the range of MEA mass activities reported in the literature.[7,8,26] Table 4.3 summarizes the results of mass activity and ECSA measurements from Brodt et al.[4] and this dissertation. Brodt et al. used Johnson Matthey Pt/C catalyst and in this dissertation, TKK Pt/C and TKK PtCo/C were used. Brodt et al. used a 63/22/15 (Pt/C)/Nafion/PAA wt. ratio composition and this dissertation used a 65/20/15 wt.% (Pt/C)/Nafion/PAA. The average fiber diameter was 589 nm for Brodt et al. while the fiber diameter was similar (552 nm) in this dissertation. In a separate publication, Brodt et al.[5] varied the diameter of the nanofibers in the electrode mat from 250 nm to 520nm and found that the diameter had little impact on the fuel cell performance as determined by nearly identical polarization data. These data substantiate that using the same type of catalyst in a nanofiber structure is reproducible and also shows that changing the catalyst to PtCo/C in a nanofiber structure is approaching the 2020 DOE mass activity target.

Table 4.3. Electrochemical surface area and mass activity for nanofiber electrode MEAs where the cathode loading for all MEAs is 0.1 mg_{Pt}/cm^2 and the anode catalyst is Pt/C at a loading of 0.1 mg_{Pt}/cm^2.

Catalyst Type – (Measured by)	ECSA (m^2/g_{Pt})	Mass Activity (mA/mg_{Pt})
JM Pt/C – (Brodt et al.)[4]	41	160

TKK Pt/C – (this dissertation)	45	160
TKK PtCo/C – (this dissertation)	48	340
DOE 2020 Target[27]	–	440

In addition to painted slurry electrode MEAs made at Vanderbilt, sprayed electrode MEAs were made and tested at Nissan Technical Center of North America (NTCNA). These electrodes were prepared by spraying catalyst ink onto a gas diffusion layer to form a gas diffusion electrode (GDE). Anode and cathode GDEs were sprayed with a layer of Nafion (at 0.5 mg_{Nafion}/cm^2) and were hot-pressed onto a Nafion 211 membrane. The cathode catalyst used was TKK PtCo/C at a loading of 0.1 mg_{Pt}/cm^2 and the anode catalyst was TKK Pt/C at a loading of 0.4 mg/cm^2. All MEAs tested at NTCNA had an active area of 10 cm^2. When testing an MEA at NTCNA, the operating conditions were 80 °C, 200 kPa absolute, and 4000/8000 sccm H_2/air.

Polarization data from PtCo/C cathode MEAs for both Nissan spray and nanofiber electrode morphologies are shown in Figure 4.9 and summarized in Table 4.4. This data was collected at NTCNA. The PtCo/C nanofiber cathode MEAs generated higher power, as compared to spray MEAs at 100% relative humidity, but slightly underperformed the sprayed electrode MEA at 40% relative humidity.

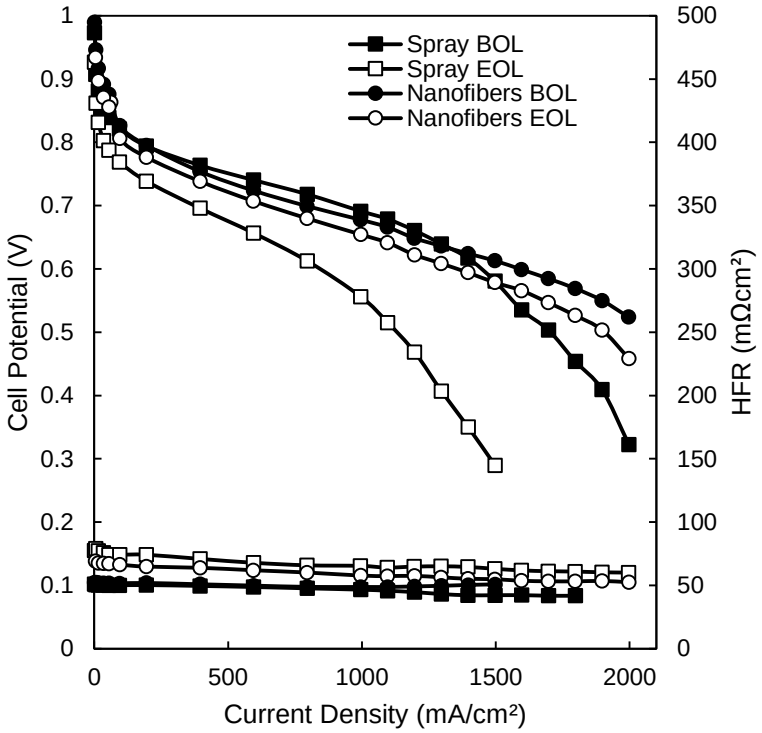

Figure 4.9. Measured at NTCNA, 10 cm^2 MEAs. H_2/air fuel cell polarization data for nanofiber electrode MEAs using PtCo/C cathodes and Pt/C anodes at 80 °C and 200 kPa absolute with feed gas flow rates of 4000/8000 sccm H_2/air.

The improved power densities of the nanofiber electrode MEA at high RH are attributed to the high inter-fiber void-space which allows for fast removal of product water. Water removal is particularly important at maximum power where the current density is high and flooding can occur. The effect of relative humidity will be discussed in the next chapter of this dissertation (Chapter 5) more thoroughly.

Table 4.4. Comparison of power densities at 40% RH and 100% RH for PtCo/C in spray and nanofiber electrode MEAs. Power data was collected at 200 kPa_{abs} and 80 °C and 4000/8000 sccm H_2/air. Cathode loadings in both cases were 0.1 mg_{Pt}/cm^2. Anode loading for nanofiber electrode MEA was 0.1 mg_{Pt}/cm^2. Anode loading for sprayed electrode MEA was 0.4 mg_{Pt}/cm^2.

	40% RH Power Density (mW/cm^2)		**100% RH Power Density (mW/cm^2)**	
	Maximum	0.65 V	Maximum	0.65 V
Spray TKK PtCo/C	597	388	835	715
Fiber TKK PtCo/C	590	255	1026	751

Brodt et al. showed that MEAs with Pt/C nanofiber cathode MEAs (with a Nafion 211 membrane and a conventional painted slurry anode) generated 52% less power at 0.65 V and 40% RH compared to spray.[5] In the present work, the PtCo/C nanofibers generated 35% less power at 0.65V and 40% RH as compared to a sprayed electrode MEA. This indicates that the nanofiber morphology affects performance similarly for Pt/C and PtCo/C catalyst. The high gas flow rates used by NTCNA (4000/8000 sccm H_2/air) dry out the nanofiber electrodes with Nafion/PAA at low relative humidity as was previously observed.[5]

In addition to testing 10 cm^2 MEAs at NTCNA, 25 cm^2 MEAs were fabricated and tested at Vanderbilt using a triple serpentine flow field channel. These results are shown in Figure 4.10.

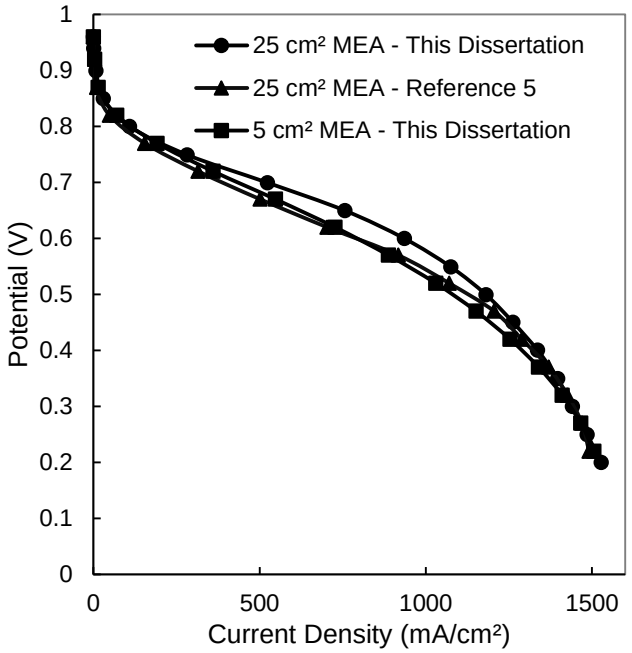

Figure 4.10. 25cm^2 nanofiber MEAs tested at Vanderbilt University using Johnson Matthey Platinum supported on HiSPEC4000. 500/2000 standard cubic centimeters per minute

H_2/air, 80 °C, ambient pressure, 100% relative humidity. The loading was 0.1mg_{Pt}/cm^2 loading and the membrane was Nafion 211.

The purpose of this experiment was to reproducibly prepare 25 cm^2 Pt/C nanofiber cathode MEAs with a Nafion/PAA binder as well as to show that 5 cm^2 MEAs generated the same polarization curves. This is important because industry generally uses larger MEAs (e.g. 25 cm^2 or 50 cm^2).[15,28–30] Figure 4.10 shows that MEAs produced a maximum power density that was within 5% of each other and provides evidence that results obtained from 5cm^2 MEAs scale well to larger MEAs.

A fuel cell electrode contains a catalyst on carbon support and ionomer. The relative amount of ionomer to carbon is important to fuel cell power generation as this ratio impacts (1) contact between the ionomer and Pt particles which promotes proton transport, (2) electron resistance, and (3) gas transport resistance.[31,32] The effect of ionomer to carbon ratio on power density generation was studied in nanofiber electrodes containing PtCo/C and Nafion. The initial results are shown in Figure 4.11. In the present study, "ionomer" is defined as the total binder content (i.e. Nafion+PAA). Two ionomer/carbon (I/C) ratios were examined, I/C = 1.0 and I/C = 1.6.

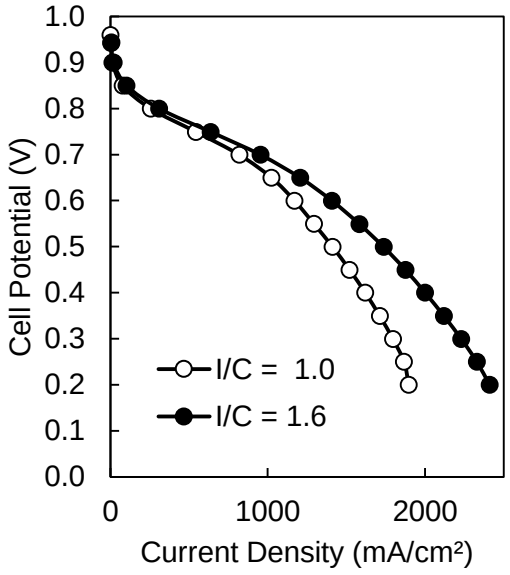

Figure 4.11. Polarization data for two different ionomer/carbon ratios in nanofiber electrodes containing (PtCo/C)/Nafion/PAA. Both MEAs have 5 cm^2 electrodes that use a catalyst loading of 0.1 mg_{Pt}/cm^2, have a Nafion 211 membrane, and use 29BC Sigracet GDLs. Both MEAs have an anode of 65/20/15 – (Pt/C)/Nafion/PAA. Polarization conditions for this experiment were 80 °C, 200 kPa, and 500/2000 sccm H_2/air.

The difference in performance between these two I/C ratio electrode MEAs suggests that at a low I/C ratio, the ionic resistance of the electrode hinders the power generation above ~1000 mA/cm^2 as seen in the polarization data. This is in agreement with Gasteiger and coworkers.[32] With only two I/C ratios, future work is needed to determine if an optimal amount of ionomer in a nanofiber electrode will produce more power than presented in this dissertation.

The effect of cathode flowrate and cathode/anode backpressure on PtCo/C nanofiber electrode MEA power density with Nafion/PAA was also investigated. Figure 4.12 shows the effect of increasing cathode feed gas flow rate on the measured power density where the total back pressured was set to 300 kPa absolute. Power density increases with increasing air flow rate. Flow rates above 2.0 L/min were not tested because this was the

limit of the Scribner fuel cell test station. The anode flow rates were always one fourth the rate of the cathode flow rate.

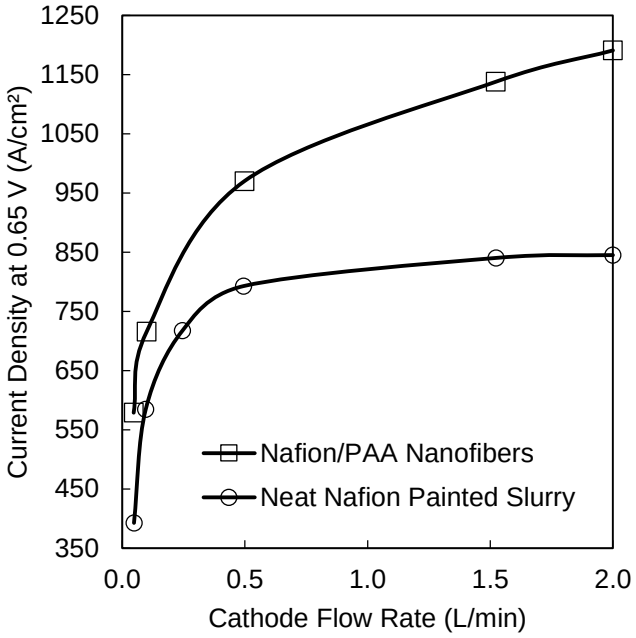

Figure 4.12. The effect of flow rate on power density for 5 cm^2 MEAs in a single serpentine flow channel. The nanofiber MEA had a composition of 65/20/15 – (PtCo/C)/Nafion/PAA. The painted slurry electrode had a composition of 65/35 catalyst/Nafion. All MEAs had a loading of 0.1 mg_{Pt}/cm^2 and a Nafion 211 membrane. Operating conditions were 100% RH, 80 °C, and 300 kPa absolute.

It should be noted that the pressure may have been above 300 kPa at high flow rates due to the use of a test fixture with a serpentine flow channel. Since the pressure was not measured, the results above 500 sccm are showing the effects of both flow rate and cathode back pressure on cathode performance. This backpressure effect applies to both the painted slurry electrode MEA and the nanofiber electrode MEA. The data, thus, show that inter and intra fiber porosity can be exploited in a nanofiber mat cathode to increase power at higher flow rates and backpressures.

Rated Power: In a fuel cell, the chemical potentials of H_2 and O_2 are converted into electricity and heat. The deviation of the V-i curve from a voltage of 1.23 V is a measure of the losses when converting chemical potential into electricity. As more power is drawn from a fuel cell, more heat is produced. In a vehicle, this heat must be expelled using a water-cooled radiator. The size of the radiator is limited and is governed by the amount of heat to be removed (Q) and the temperature difference (ΔT) during heat transfer.

According to automotive industry standards, the U.S. Department of Energy (DOE)[33] has generated a correlation equation for H_2/air fuel cells where the heat expulsion (Q) and ΔT of the radiator is related to the power, the operating voltage, and temperature of a fuel cell stack. It has been established that the radiator size will be acceptable for a Q/ΔT of 1.45 kW/°C.[34,35] Thus, from Equation 1 and this value of Q/ΔT, one can relate the operating voltage to the stack power, stack temperature, and ambient temperature. This calculated voltage is defined as the stack voltage at "rated power".

$$Q/\Delta T = \frac{\left[Stack\ Power\ (kW) \times (1.25 - V\ @\ rated\ power) \Big/ V\ @\ rated\ power \right]}{Cell\ Operating\ Temperature\ (^{o}C) - Ambient\ Temperature\ (^{o}C)} \qquad \text{(Equation 4.1)}$$

Using Equation 4.1 where the stack power is 90 kW and the ambient temperature is 40 °C (values agreed upon by the automotive industry and the DOE)[36], Figure 4.13 shows the relationship between voltage at rated power and cell operating temperature.

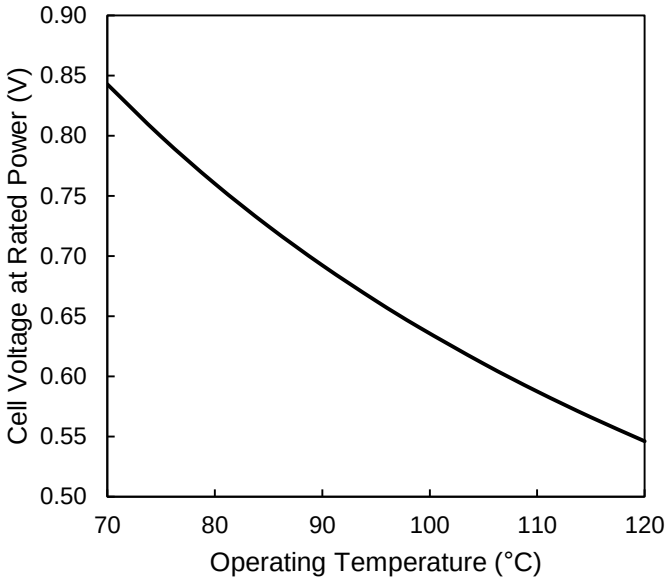

Figure 4.13. Cell voltage at rated power vs. temperature according to Equation 1 for a stack power of 90 kW, an ambient temperature of 40 °C, and a Q/ΔT of 1.45 kW/°C.

The rated power of an MEA with a PtCo/C:Nafion:PAA nanofiber cathode is shown in Table 4.5 for three different temperatures. The rated power increases with increasing temperature. Higher temperature allows for a lower fuel cell operating voltage to be utilized (according to Equation 4.1) which improves the rated power. Fuel cell operating temperature was set to either 80°C, 95°C, or 99°C. Polarization curves for these experiments are shown in Figure 4.14. Dotted lines show the associated rated power voltage/current data points at a given temperature.

Table 4.5. Rated power at three different operating temperatures for a nanofiber electrode MEA with a TKK PtCo/C cathode. Anode and cathode loadings were both $0.1 mg_{Pt}/cm^2$. Feed gas flow rates: 500 sccm H_2, 2000 sccm air; Membrane: Nafion 211, Relative Humidity: 100%, pressure: 150 kPa (absolute). Voltage was calculated from Equation 1.

Temperature (°C)	Potential (V)	Performance at Rated Power (mW/cm^2)
80	0.771	667
95	0.674	784
99	0.652	908

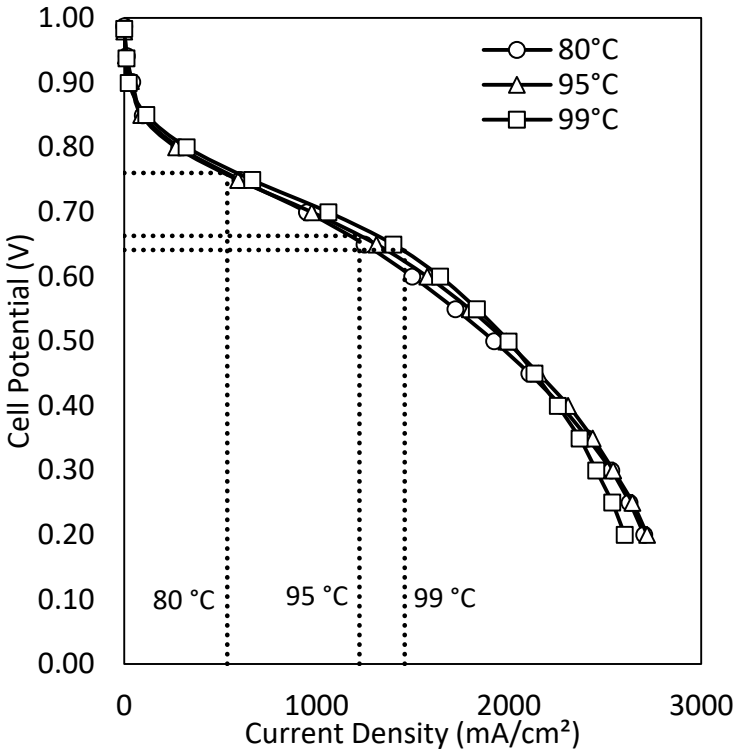

Figure 4.14. Rated Power polarization curves at 80 °C, 95 °C, and 99 °C. For ease of viewing, the voltage and current calculated from each of these curves is identified by a dotted line.

Electrochemical Impedance Spectroscopy (EIS) – EIS data were collected at LANL for cathode gas feeds of air and HelOx ($21\%O_2$, Bal: Helium), in order to quantify kinetic and mass transport losses. Figure 4.15(a) illustrates the EIS spectra (1 Hz to 5000 Hz) obtained at a low current density (0.2 A/cm^2, representative of the kinetic region) and high current density data (2.0 A/cm^2, representative of the mass transport region) are shown in Figure 4.15(b). The measured EIS data is represented by the filled (BOL) and open (30,000 cycles)

symbols whereas the equivalent circuit fit is represented by the solid (BOL) and dashed (30,000 cycles) lines. A simple equivalent circuit model reported earlier[28] was used to fit the data and quantify a high frequency resistance (HFR) and a kinetic and mass transport resistance. The HFR is constant throughout the experiment at a value of ≈ 0.55 $\Omega \cdot cm^2$ indicating no changes to the conductivity of the membrane. In the kinetic region, the performance is identical in Air and HelOx with the kinetic resistance increasing after 30,000 cycles. This increased kinetic resistance is due to both loss in electrocatalyst active surface area and leaching of Co, resulting in a reduced mass activity. After 30,000 cycles this resistance increases to 0.35 $\Omega \cdot cm^2$ at 0.2 A/cm^2), reaching a constant value of around 0.18 $\Omega \cdot cm^2$ at a current density > 0.8 A/cm^2. The mass transport component of the resistance develops near 1 A/cm^2 and increases with increasing current. The resistance is significantly lower in HelOx than in Air with the BOL mass transport resistance at 2 A/cm^2 of 0.14 $\Omega.cm^2$ in Air and only 0.04 $\Omega \cdot cm^2$ HelOx. Moreover, the mass transport loss also increases with cycling and is 0.31 $\Omega.cm^2$ and 0.08 $\Omega.cm^2$ in Air and HelOx respectively after 30,000 cycles. The amount of mass transport losses that can be recovered in HelOx is indicative of the pressure dependent transport term and still dominates the transport resistance (≈ 70% of the total transport resistance). The pressure independent transport resistance (as evidenced by GTR) also increases with cycling but is only a small portion of the overall transport resistance as indicated by the HelOx measurements. Therefore, in addition to the increases in local O_2 transport resistance caused by decreased catalyst surface area, molecular diffusion resistance also increases with catalyst cycling AST.

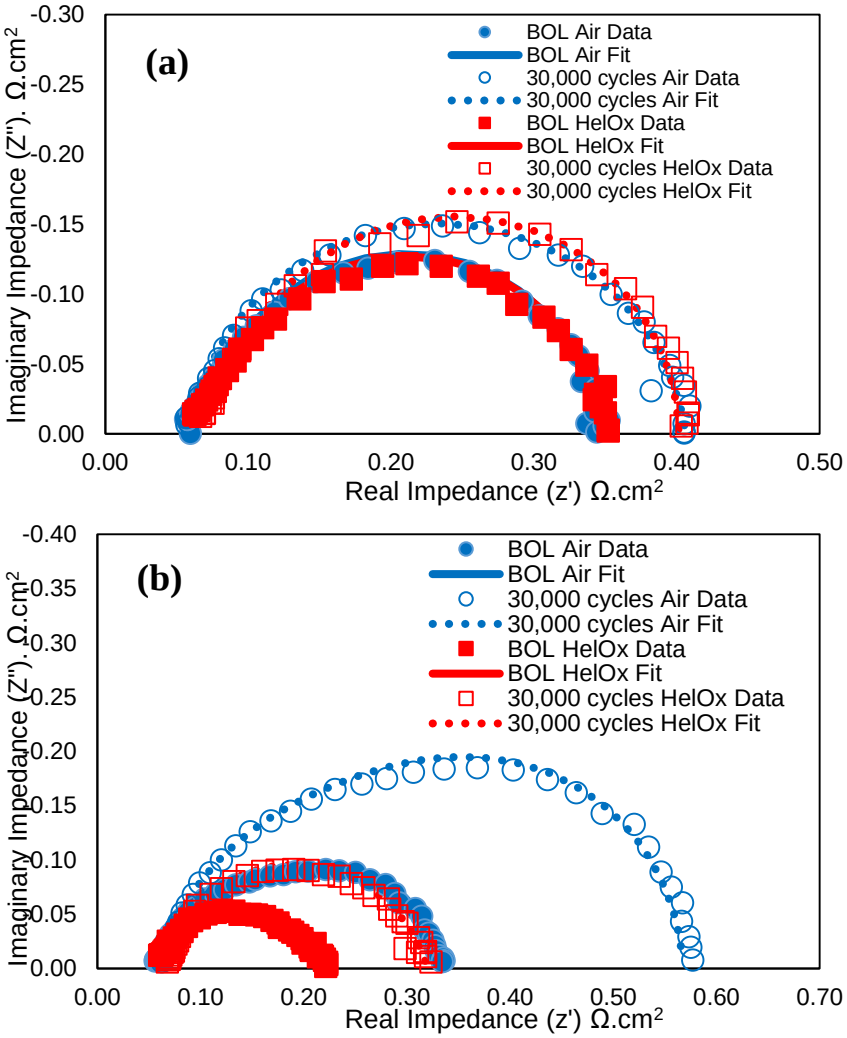

Figure 4.15. Electrochemical Impedance Spectra (EIS) of a 5 cm^2 nanofiber electrode MEAs with a PtCo/C cathode in Air and HelOx before and after 30,000 cycles of catalyst AST. (a) 0.2 A/cm^2 and (b) $2A/cm^2$. The equivalent circuit fit is given by the solid and lines; experimental data is shown by the markers.

4.3.3 Metal Dissolution Accelerated Stress Tests

Square wave voltage cycling metal dissolution accelerated stress tests (ASTs) were performed at NTCNA with nanofiber electrode and sprayed electrode MEAs. The metal dissolution AST voltage cycling protocol is shown in Figure 4.16

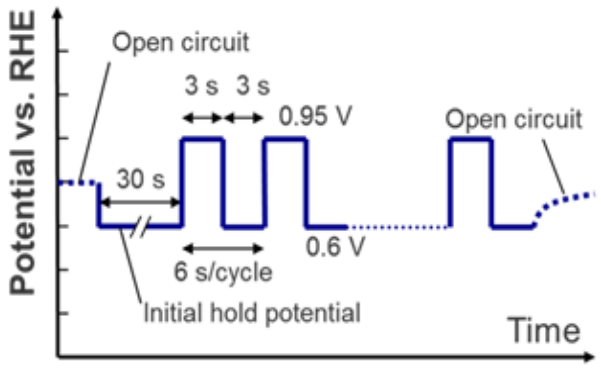

Figure 4.16. Metal dissolution accelerated stress test protocol. Anode/cathode feed gas are H_2/N_2 – 500/500 sccm at 80 °C and 100% RH.

Fuel cell polarization curves for nanofiber electrode MEAs and spray electrode MEAs with PtCo/C cathode catalyst at Beginning of Life (BOL) and after 30,000 metal dissolution voltage cycles are shown in Figure 4.17. The spray electrode lost 32% of its maximum power, as compared to less than 10% power loss for the nanofiber cathode MEA. The nanofiber electrode generated 1034 mW/cm^2 max power density at BOL and 955 mW/cm^2 max power density at EOL. Brodt et al.[5] showed that a spray and a nanofiber MEAs with Pt/C cathode catalyst exhibited similar durability after a metal dissolution voltage cycling AST to 10,000 cycles.[5] Brodt et al. observed a 5% loss in power at 0.65 V after 10,000 cycles. In the present study, the power density loss at 0.65 V after 30,000 cycles was 32% for the sprayed electrode MEA and 8% for the nanofiber electrode MEA.

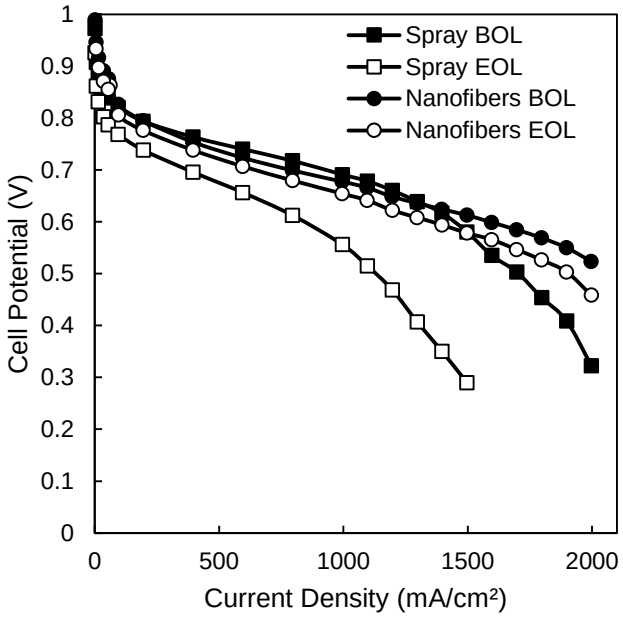

Figure 4.17. H_2/air fuel cell polarization data before and after metal dissolution of nanofiber and spray MEAs (EOL after 30,000 voltage cycles, 0.6 V to 0.95 V) at 100% RH, 80 °C and 200 kPa absolute, 4000/8000 sccm.

Table 4.6 presents beginning of life and end of life mass activity and electrochemically active surface area (ECSA) for MEAs. Beginning of life ECSA was similar between the spray and nanofiber morphologies, but after 30,000 voltage cycles the nanofiber electrodes retained more area (15% loss vs. 25% loss). The nanofiber EOL mass activity was 50% greater compared to spray due to the agglomeration and growth of catalyst particles as shown above.

Table 4.6. Electrochemically active surface area and mass activity of nanofiber and spray electrode MEAs at beginning and end of life (after 30,000 metal dissolution cycles).

	BOL ECSA (m^2/g_{Pt})	EOL ECSA (m^2/g_{Pt})	BOL Mass Activity (mA/mg_{Pt})	EOL Mass Activity (mA/mg_{Pt})
PtCo/C Spray	44	33	248	144
PtCo/C Nanofibers	48	41	270	219

Table 4.7 shows a comparison of the results found in the literature regarding metal dissolution durability for MEAs containing PtCo/C cathode catalysts. These results suggest that a standard sprayed electrode MEA loses ~20% of the initial power density at 0.65 V after 30,000 cycles. This is less than what was observed in the present study with a NTCNA sprayed electrode MEA.

Table 4.7. Literature values comparing performance and durability after a metal dissolution AST.

Reference	EOL/BOL Power density at 0.65V (mW/cm^2)	AST conditions
Yu et al.[11]	83%	24000 square wave cycles 30 seconds per cycle. 0.84 V - 1.2 V
Myers et al.[42]	82%	30,000 square wave cycles (20s / cycle) 0.4V - 0.95V
Ahluwalia et al.[43]	78%	30,000 square wave cycles (6s / cycle) 0.6V - 0.95V
This study (Nissan sprayed GDEs w/ Nafion coating)	68%	30,000 square wave cycles (6s / cycle) 0.6V - 0.95V
This study (nanofiber electrodes)	92%	30,000 square wave cycles (6s / cycle) 0.6V - 0.95V

To explain the small (<10%) loss of electrochemical performance after 30,000 metal dissolution cycles, post-mortem analyses of both sprayed electrode and nanofiber electrode MEAs were performed at Oak Ridge National Laboratory using Scanning Transmission Electron Microscopy (STEM) and Energy-Dispersive X-ray Spectroscopy (EDS).

The goal of this analysis is to determine the size and composition of the metal PtCo nanoparticles in the catalyst layer before and after the metal dissolution AST. First, STEM

images of the metal PtCo nanoparticles, such as in Figure 4.18a, are obtained. These contain 20 to 50 nanoparticles per image; enough are taken so that there is sample size of ~200 nanoparticles. Next, these images must be binarized in ImageJ, such as in Figure 4.18b. Each particle is then numbered and the software determines an area for each particle. From this area, an effective radius of the particle is determined assuming each particle is spherical. Figure 4.18 is an example of end of life catalyst particles in a sprayed electrode. From these types of images, particle diameter was obtained.

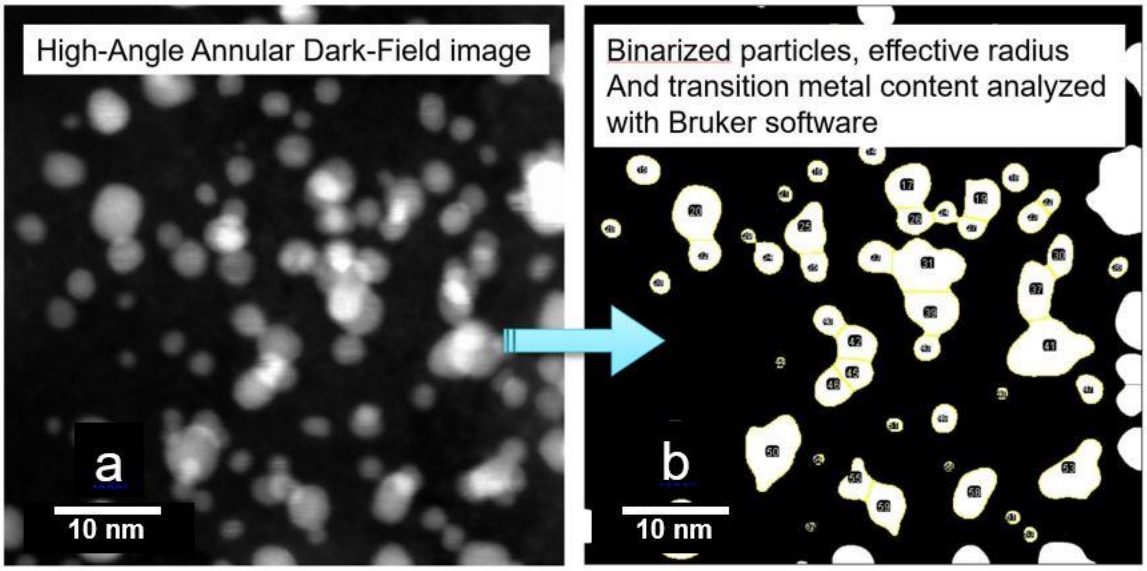

Figure 4.18. STEM image converted to a "binary" image that only contains white and black pixels such that imageJ can calculate an area for each particle. These metal nanoparticles of PtCo are within a sprayed electrode at EOL. Particle agglomeration is observed.

To obtain the relative amount of Pt and Co in each nanoparticle, energy dispersive x-ray spectra was taken simultaneously with the STEM image (as in Figure 4.18a). This EDS spectra is then interpreted by Bruker® software and each individual metal nanoparticle has a Pt and Co percentage ascribed to it. From this combined analysis, it is possible to determine the amount of cobalt loss and particle growth after the metal dissolution AST. Figure 4.19 shows that there was (1) a greater retention of cobalt in

individual nanoparticles and (2) less particle growth in a nanofiber cathode MEA relative to the sprayed cathode MEA.

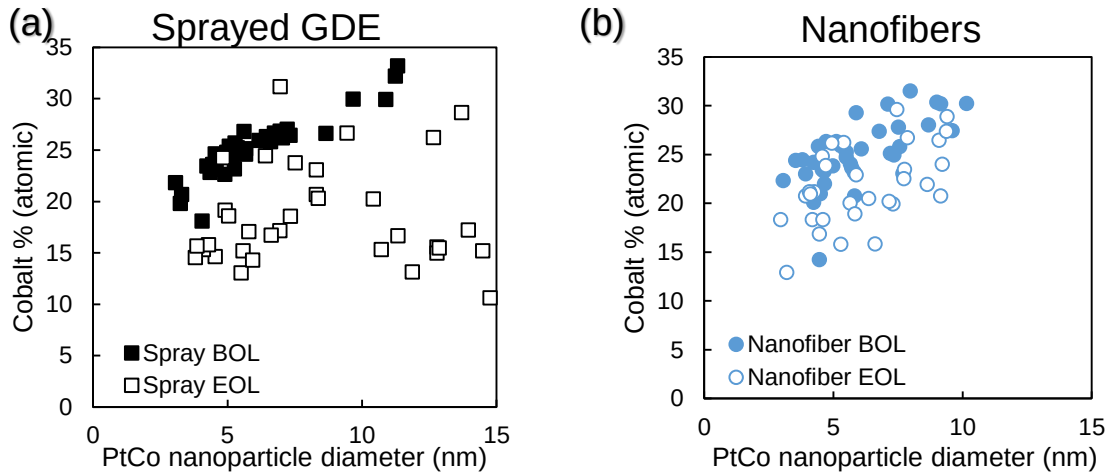

Figure 4.19. Cobalt content of individual nanoparticles with respect to the nanoparticle size for both NTCNA sprayed GDE and electrospun nanofiber electrode MEAs before and after metal dissolution AST.

The cobalt percentage measured in Figure 4.19 is directly linked to the platinum percentage (i.e. the Pt% = 1 – Co%). The average percentage of cobalt retained in a nanoparticle found within the nanofiber electrode is 61% ± 4% while for the sprayed electrode, that average percentage is 49% ± 5%. At EOL, the sprayed electrode showed a higher number of particles that had increased in size (due to Ostwald ripening and/or agglomeration).[37] Thus, the retention of power observed in the nanofiber MEA at EOL is in part due to the retention of cobalt in the PtCo nanoparticles. The increase in nanoparticle diameter in the sprayed electrode is significantly greater than in the nanofiber electrode. When cobalt is retained, the higher intrinsic catalytic activity of the PtCo nanoparticle is maintained[11] and cobalt ions do not leech into the surrounding ionomer which causes a decrease in the ionic conductivity of the binder.[38] This activity retention may be explained by first understanding why PtCo nanoparticles initially have a higher activity than Pt

nanoparticles of the same size. In reference [40], the origin of the enhancement in ORR activity of a PtCo/C catalyst was attributed to the chemical surface structures that arise from the alloying of Pt and Co. The exact reason for the activity enhancement associated with PtCo/C catalysts is still a subject of debate regarding the electronic and geometric structures for Pt-based bimetallic catalysts. However, X-ray photoelectron spectroscopy experiments have been performed to probe the binding energies of the catalyst metal and oxygen; these experiments have determined that PtCo nanoparticles have a more optimal binding energy (compared to Pt) with oxygen to both promote the ORR and release the product (water).[40] This concept is referred to as the Sabatier principle and simply suggests that an ideal catalyst does not bind the reactant too weakly so that the reaction can take place or the product too strongly so that surface-reactant dissociation can take place.[41] As the cobalt content leaches out of the PtCo nanoparticles, the binding energy of the nanoparticles' surface sites becomes more and more "platinum-like", which partially explains the loss in current density observed in the polarization data presented earlier. The growth and agglomeration of particles will decrease the available surface area, further reducing the activity of the electrode. Additionally, the leached cobalt ions can affect the conductivity of the electrode ionomer and membrane.[38] This happens by cobalt cations binding to sulfonic anions, reducing sites for protons to dissociate, reducing the acidity of the surrounding water in the electrode, and therefore reducing the conductivity. With less Co leaching, the ionomer retains conductivity due to the prevention of transition metal poisoning. Figure 4.19 shows that there is a narrower distribution of nanoparticle sizes at EOL in the nanofiber MEA compared to the sprayed GDE. This means there was less growth of nanoparticles due to Ostwald ripening or agglomeration and gives a physical

explanation for why a higher ECSA was observed at EOL in the nanofiber electrode structure. Myers et al. from Argonne National Laboratory showed that after 30,000 square wave voltage cycles in a metal dissolution AST, the mass activity of a sprayed MEA using PtCo/C catalyst dropped by approximately 50% and the particle size increased from ~4 nm to ~14 nm.[42] This is in line with the data from spray MEAs observed in this study (mass activity in NTCNA MEAs dropped from 248 to 144 mA/mg_{Pt} and catalyst particles increased from ~5 to ~15 nm at EOL).

Recovery Protocol: General Motors has developed a protocol which is designed to recover voltage losses after a stress test.[46] This protocol involves setting the voltage to 0.1 V vs. SHE in oversaturated H_2/air feed gases. While this recovery protocol was being performed, the cathode outlet water was collected and sulfate ions were detected. The authors claim that sulfonic acid chain scission after an open circuit stress test adsorb to catalyst sites and are in part responsible for the loss in power after a stress test. The recovery protocol removes these adsorbed sulfate ions which increases the number of available catalyst sites and has been shown to increase mass activity.

The effect of the recovery protocol on fuel cell performance in nanofiber electrode MEAs and sprayed electrode MEAs was determined at Los Alamos National Laboratory (LANL). The maximum power density of a nanofiber electrode MEA using PtCo/C at BOL increased from 836 mW/cm^2 to 1020 mW/cm^2 at 150 kPa absolute after the 4 recovery processes as shown in Figure 4.20. After one recovery protocol, there was minimal improvement in power density.

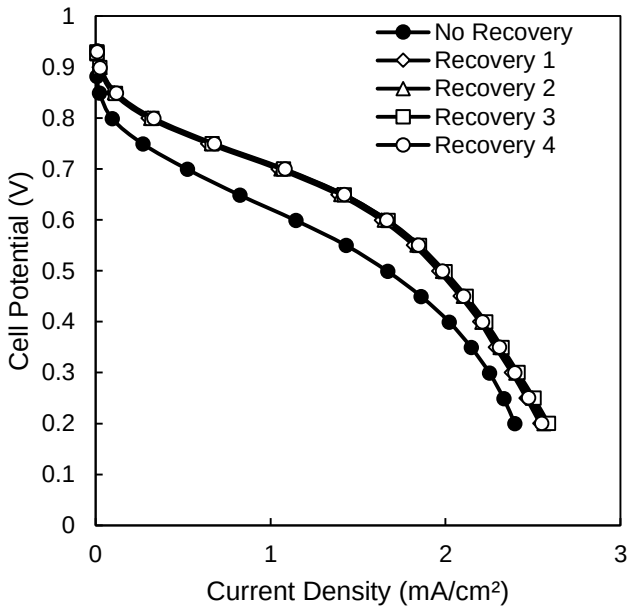

Figure 4.20. Polarization data before and after a given number of recovery protocols for a (PtCo/C)/Nafion/PAA nanofiber electrode MEA. Anode/cathode loading area each 0.1 mg_{Pt}/cm^2. Membrane is Nafion 211. GDLs are Sigracet 29BC. Fuel cell operating conditions are 80 C, 150 kPa absolute, and 1000/3000 sccm H_2/air flow rates measured in a differential flow field at LANL.

In addition to improving power density the mass activity increased from 270 mA/mg_{pt} a maximum of 464 mA/mg_{pt} after 4 recovery cycles (above the 2020 DOE target). According to reference [47], this indicates that there were adsorbed sulfate ions on Pt surfaces even before the MEA was subjected to a stress test. LANL also shows that after 30,000 cycles and the recovery protocol, the mass activity was essentially the same as the BOL mass activity before recovery. This indicates that there were adsorbed sulfate ions on the catalyst sites even initially and that this protocol can help to remove those. The results of the mass activity measurements after 15,000 or 30,000 metal dissolution voltage cycles are shown in Table 4.8.

Table 4.8. Mass activity and GTR at BOL and after either 15,000 or 30,000 metal dissolution voltage cycles with and without recovery measured at LANL.

	Nanofiber Mass Activity (mA/mg_{Pt})	Nanofiber GTR (s/m)	Spray Mass activity (mA/mg_{Pt})	Spray GTR (s/m)
BOL	270	35	N/A	N/A
BOL + 4 Recovery cycles	464	21	431	29
15k voltage cycles	236	35	121	41
15k voltage cycles + 4 Recovery	496	28	231	37
30k voltage cycles	202	37	147	59
30k voltage cycles + 4 Recovery	296	35	189	52

Oxygen Gas Transport Resistance (GTR): Within an electrode, the GTR is the local transport resistance of O_2 to catalyst sites through the ionomer thin film.[44] It is established that high gas transport resistance leads to significant voltage loss in the high current density region of a polarization curve.[44],[45] The resistance of oxygen transport through the electrode is thought to be controlled by Knudsen diffusion (Non-Fickian) as the oxygen diffuses through the Nafion thin-films to catalyst sites.[15] The morphology of the electrode can affect the GTR; NTCNA and LANL measured the GTR for sprayed electrode MEAs and nanofiber electrode MEAs with PtCo/C catalyst. NTCNA observed a sprayed electrode MEA to have a GTR of 52 s/m and a nanofiber electrode MEA to have a GTR of 35 s/m. Since GTR measures oxygen diffusion through the ionomer thin film, this evidence suggests that the way Nafion is dispersed in nanofiber electrodes allows for better access of oxygen to the catalyst sites compared to sprayed electrodes.

The recovery process at LANL improved the GTR for both nanofiber and spray electrode MEAs at BOL and after a metal dissolution AST (see Table 4.9). After 15,000 cycles, the recovery protocol significantly improved both mass activity and GTR, but after 30,000 cycles the effect was less pronounced.

Table 4.9. GTR at BOL and after either 15,000 or 30,000 metal dissolution voltage cycles with and without recovery measured at LANL.

	Nanofiber GTR (s/m)	Spray GTR (s/m)
BOL	35	N/A
BOL + 4 Recovery cycles	21	29
15k voltage cycles	35	41
15k voltage cycles + 4 Recovery cycles	28	37
30k voltage cycles	37	59
30k voltage cycles + 4 Recovery cycles	35	52

After 30,000 metal dissolution cycles, GTR for the nanofiber cathodes was lower than that for a spray at BOL. This indicates that the nanofibers offer both lower BOL resistance to oxygen transport as well as higher retention of gas transport properties.

General Motors published a summary of GTR vs. the product of an MEA's Pt loading and ECSA (known as the "roughness factor"), presented in Figure 4.21, adapted from reference [44]. A PtCo/C/Nafion/PAA nanofiber has a roughness factor of ~45 cm^2_{Pt}/cm^2_{MEA} and a GTR of 35 (before the recovery protocol) and 21 s/m (after the recovery protocol) which is among the lowest values on the curve generated from Kongkandan et al.

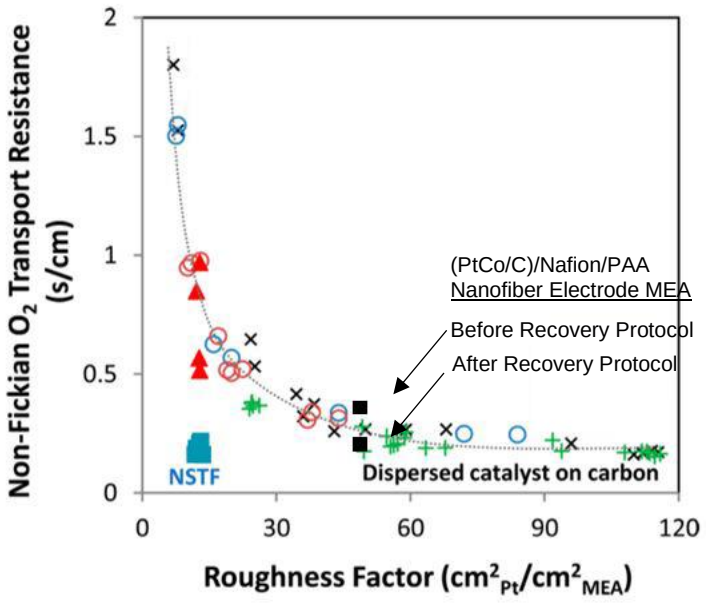

Figure 4.21. Adapted from Reference [44], the O_2 transport resistance as a function of the electrode roughness factor. Black squares represent the GTR and roughness factor of the (PtCo/C)/Nafion/PAA nanofiber electrode MEAs before and after the recovery protocol.

The Effect of RH during Metal Dissolution AST on MEA performance: Metal dissolution accelerated stress tests were performed on a PtCo/C (TKK36F52 catalyst) nanofiber cathode MEA with Nafion/PAA as the binder at 100% RH and 40% RH. The cathode and anode catalyst loading for each MEA was 0.1 mg_{Pt}/cm^2, the membrane was Nafion 211, the GDLs were Sigracet 29BC. The results are shown in Figure 4.22.

The metal dissolution AST performed at 40% RH resulted in EOL performance closer to that of the BOL performance compared to the results when the AST was performed at 100%RH.

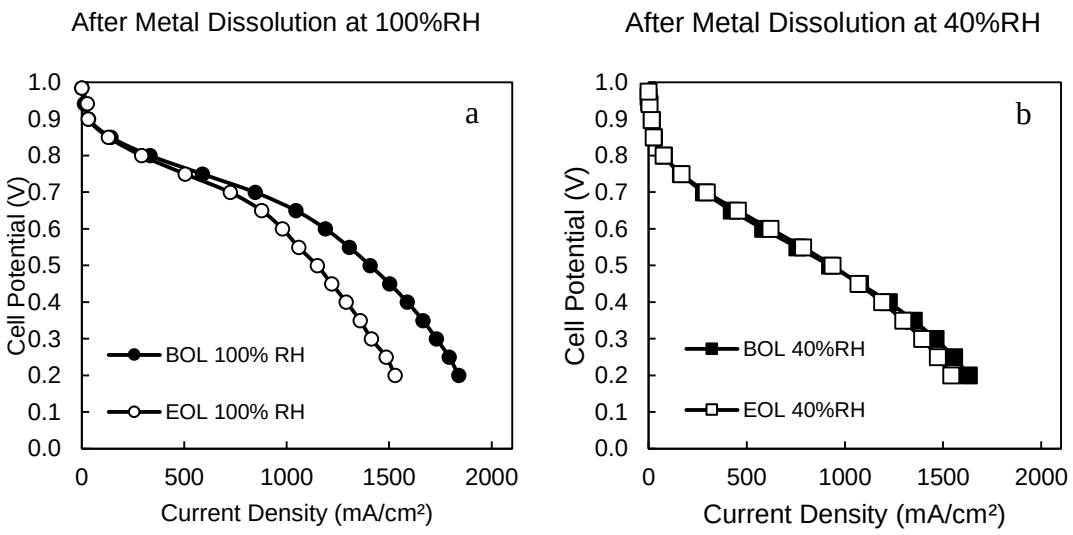

Figure 4.22. BOL and EOL polarization data for a metal dissolution accelerated stress test performed at (a) 100% RH and (b) 40% RH. Polarization conditions are: 80 °C, 200 kPa absolute pressure, and 125/500 sccm H_2/air. Cathode catalyst was PtCo/C and had a loading of 0.1 mg_{Pt}/cm^2 for both MEAs. Membrane was Nafion 211. GDLs are Sigracet 29BC

The metal dissolution AST affects the catalyst by inducing the formation of metal oxides and subsequent dissolution of the metal; this process is hastened by the acidic water in the Nafion channels of the electrode structure.[48] As the relative humidity decreases, the conductivity of the ionomer decreases and there are fewer mobile protons (i.e. less acidity). Fewer mobile protons at low RH conditions during the voltage cycling AST would be expected to result in less dissolution of the metal catalyst sites. This is especially true for the transition metal, cobalt, within the catalyst nanoparticles, as cobalt is soluble in low pH media.[49] The data in Table 4.10 shows that there essentially no change in power at 0.65V after 30,000 cycles at 40% RH within experimental error. The values for EOL after the 100% metal dissolution experiment are also slightly different from the measurements taken at Nissan, within experimental error.

Table 4.10. Power densities for ASTs and polarization curves run at 100%RH or 40%RH

	AST/polarization run at 40% RH	AST/polarization run at 100% RH
BOL Max Power Density (mW/cm²)	489	718
EOL Max Power Density (mW/cm²)	481	588
EOL/BOL Max Power Density x 100	98%	82%
BOL Power Density at 0.65 V (mW/cm²)	276	679
EOL Power Density at 0.65 V (mW/cm²)	296	570
EOL/BOL Power Density at 0.65 V x 100	107%	86%

Carbon Corrosion AST

In addition to the metal dissolution accelerated stress test, the nanofiber MEA was subjected to the United States Department of Energy (DOE) carbon corrosion accelerated stress test which involves using a start-stop potential cycling protocol (triangular wave voltage cycles between 1.0 and 1.5 V vs. SHE at a scan rate 500 mV/s as shown in Figure 4.23).

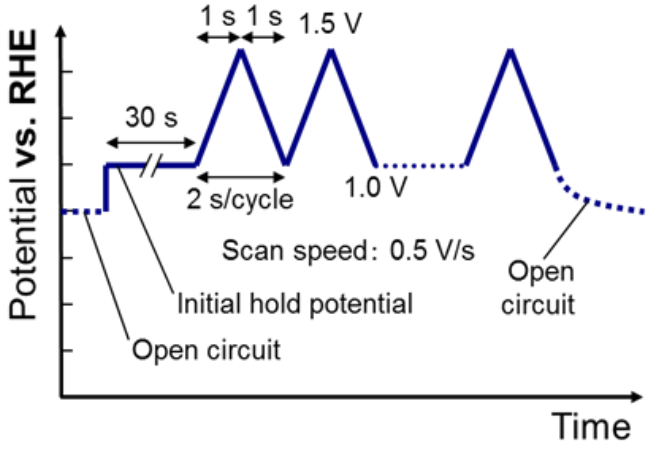

Figure 4.23. Accelerated carbon corrosion durability testing. Conditions during test: 80 °C, H_2/N_2 – 500/500 sccm, 100% RH, 100 kPa absolute.

One of the 2020 DOE durability targets is <20% drop in voltage at 1.2 A/cm^2 after 5,000 voltage cycles from 1.0 V - 1.5 V. As shown in Figure 4.24, after 1000 voltage cycles, the loss in voltage at 1.2 A/cm^2 was 19%. This meets the target for durability, but not after 5000 cycles. The EOL/BOL power densities measured were consistent with the Pt/C data that was collected by Brodt et al.[5] (17% decrease in maximum power density after 1000 voltage cycles).

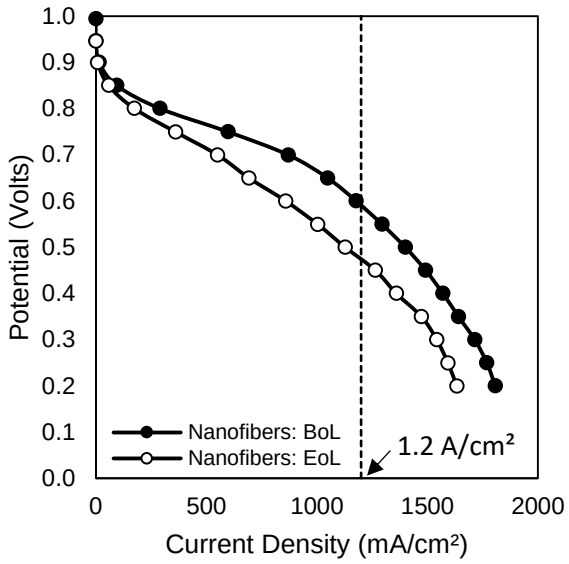

Figure 4.24. H_2/air fuel cell polarization curves before/after a start-stop accelerated stress test (AST). Nanofiber cathode: PtCo/C (TEC36E52), 0.1 $mg_{Pt}/cm^{2,}$ Nafion 211 membrane, Nanofiber anode: 0.1 mg_{Pt}/cm^2 Johnson Matthey Pt/C. GDL: Sigracet 29BC. Fuel Cell Operating Conditions: 80 °C, 200 kPa absolute, 125/500 sccm H_2/air, 100% RH;

4.4 Conclusions

TKK PtCo/C was successfully electrospun into a nanofiber cathode with Nafion/PAA as the binder. This fiber structure was analyzed at Oak Ridge National Lab and it was determined that there is a uniform distribution of Nafion, catalyst particles, and void spaces. The intra-fiber porosity contributed 30% of the overall fiber surface area and the

surface roughness of the fiber contributed another 20%. PtCo/C as a cathode catalyst in nanofiber electrode MEAs significantly improved the power density as compared to a nanofiber MEA with a Pt/C catalyst. A sprayed electrode MEA using PtCo/C with an additional Nafion coating was compared and found to have slightly lower power density compared to nanofibers at BOL, and significantly lower power density after metal dissolution. This behavior was consistent with observations made in previous nanofiber and spray electrode MEAs that used a cathode catalyst of Pt/C.[5] Thus, it appears that the nanofiber cathode architecture will improve the performance of any new cathode catalyst powder, relative to a conventional spray electrode design. The gas transport resistance was measured and both were found to be superior in the nanofibers relative to the spray at both BOL and after a metal dissolution AST. The EOL GTR and mass activity measured at Los Alamos National Laboratory after 4 recovery cycles for a nanofiber cathode was superior to that of a conventional sprayed cathode.

4.5 References

[1] P. Costamagna, S. Srinivasan, *J. Power Sources* **2001**, *102*, 242.

[2] S. Litster, G. McLean, PEM fuel cell electrodes. *J. Power Sources* **2004**, *130*, 61–76.

[3] W. Zhang, P. N. Pintauro, *ChemSusChem* **2011**, *4*, 1753.

[4] M. Brodt, R. Wycisk, P. N. Pintauro, *J. Electrochem. Soc.* **2013**, *160*, F744.

[5] M. Brodt, T. Han, N. Dale, E. Niangar, R. Wycisk, P. Pintauro, *J. Electrochem. Soc.* **2015**, *162*, F84.

[6] M. Brodt, R. Wycisk, N. Dale, P. Pintauro, *J. Electrochem. Soc.* **2016**, *163*, F401.

[7] M. Oezaslan, F. Hasché, P. Strasser, *J. Phys. Chem. Lett.* **2013**, *4*, 3273.

[8] C. Wang, N. M. Markovic, V. R. Stamenkovic, *ACS Catal.* **2012**, *2*, 891.

[9] E. Antolini, J. R. C. Salgado, M. J. Giz, E. R. Gonzalez, *Int. J. Hydrogen Energy*

2005, *30*, 1213.

[10] S. Hidai, M. Kobayashi, H. Niwa, Y. Harada, M. Oshima, Y. Nakamori, T. Aoki, *J. Power Sources* **2011**, *196*, 8340.

[11] P. Yu, M. Pemberton, P. Plasse, *J. Power Sources* **2005**, *144*, 11.

[12] P. Gallo Stampino, C. Cristiani, G. Dotelli, L. Omati, L. Zampori, R. Pelosato, M. Guilizzoni, *Catal. Today* **2009**, *147*, 30.

[13] H. A. Gasteiger, S. S. Kocha, B. Sompalli, F. T. Wagner, Activity benchmarks and requirements for Pt, Pt-alloy, and non-Pt oxygen reduction catalysts for PEMFCs. *Appl. Catal. B Environ.* **2005**, *56*, 9–35.

[14] K. R. Cooper, *Fuel Cell Mag. Scribner Assoc.* **2009**, *1*, 1.

[15] D. R. Baker, C. Wieser, K. C. Neyerlin, M. W. Murphy, *ECS Trans.* **2006**, *3*, 989.

[16] D. R. Baker, D. A. Caulk, K. C. Neyerlin, M. W. Murphy, *J. Electrochem. Soc.* **2009**, *156*, B991.

[17] J. Zhang, L. Paine, *US Appl.* **2011**.

[18] T. Mashio, A. Ohma, S. Yamamoto, K. Shinohara, E. C. S. Transactions, T. E. Society, *ECS Trans.* **2007**, *11*, 529.

[19] K. Sakai, K. Sato, T. Mashio, A. Ohma, K. Tamaguchi, K. Shinohara, *ECS Trans.* **2009**, *25*, 1193.

[20] Y. Fukuyama, T. Shiomi, T. Kotaka, Y. Tabuchi, *Electrochim. Acta* **2014**, *117*, 367.

[21] Fuel Cell Commercialization Conference of Japan, *ECS Trans.* **2010**, *41*, 775.

[22] N. A. Siddique, F. Liu, *Electrochim. Acta* **2010**, *55*, 5357.

[23] E. Antolini, J. R. C. Salgado, E. R. Gonzalez, The stability of Pt–M (M=first row transition metal) alloy catalysts and its effect on the activity in low temperature fuel cells. *J. Power Sources* **2006**, *160*, 957–968.

[24] N. Travitsky, T. Ripenbein, D. Golodnitsky, Y. Rosenberg, L. Burshtein, E. Peled, *J. Power Sources* **2006**, *161*, 782.

[25] Q. He, S. Mukerjee, *Electrochim. Acta* **2010**, *55*, 1709.

[26] R. Lin, T. Zhao, M. Shang, J. Wang, W. Tang, V. E. Guterman, J. Ma, *J. Power Sources* **2015**, *293*, 274.

[27] S. Satyapal, *Hydrogen and Fuel Cells Overview. Department Of Energy. 2018 Annual Merit Review*; 2017.

[28] Y. C. Park, K. Kakinuma, M. Uchida, D. A. Tryk, T. Kamino, H. Uchida, M. Watanabe, *Electrochim. Acta* **2013**, *91*, 195.

[29] S. Arisetty, X. Wang, R. K. Ahluwalia, R. Mukundan, R. Borup, J. Davey, D. Langlois, F. Gambini, O. Polevaya, S. Blanchet, *J. Electrochem. Soc.* **2012**, *159*,

B455.

[30] S. Chen, H. A. Gasteiger, K. Hayakawa, T. Tada, Y. Shao-Horn, Platinum-Alloy Cathode Catalyst Degradation in Proton Exchange Membrane Fuel Cells: Nanometer-Scale Compositional and Morphological Changes. *J. Electrochem. Soc.* **2010**, *157*, A82.

[31] and J. Z. Huamin Zhang, Jianlu Zhang, Jifeng Wu, *PEM Fuel Cell Testing and Diagnosis*; Elsevier Science, 2013.

[32] Y. Liu, M. W. Murphy, D. R. Baker, W. Gu, C. Ji, J. Jorne, H. A. Gasteiger, *J. Electrochem. Soc.* **2009**, *156*, B970.

[33] R. Borup, K. More, A. Weber, *FC135 FC-PAD Fuel Cell Perform. Durab. Consortium. 2018 DOE Fuel Cell Technol. Off. Annu. Merit Rev.* **2018**.

[34] J. Marcinkoski, B. James, C. Houchins, *DOE Hydrog. Fuel Cells Progr. Rec.* **2016**, 1.

[35] Dimitrios Papageorgopoulos, *Fuel Cells R&D Overview. Office of Energy Efficiency and Renewable Energy*; Washington D.C., 2018.

[36] Dimitrios Papageorgopoulos, *Off. ENERGY Effic. Renew. ENERGY*. **2016**, DE-FOA-0001412.

[37] F. T. Wagner, B. Lakshmanan, M. F. Mathias, *J. Phys. Chem. Lett.* **2010**, *1*, 2204.

[38] M. Ledendecker, J. S. Mondschein, O. Kasian, S. Geiger, D. Göhl, M. Schalenbach, A. Zeradjanin, S. Cherevko, R. E. Schaak, K. Mayrhofer, *Angew. Chemie - Int. Ed.* **2017**, *56*, 9767.

[39] E. Antolini, J. R. C. Salgado, E. R. Gonzalez, *J. Power Sources* **2006**, *160*, 957.

[40] Y. Zhao, J. Liu, Y. Zhao, F. Wang, *Phys. Chem. Chem. Phys.* **2014**, *16*, 19298.

[41] G. Rothenberg, *Catalysis: Concepts and Green Applications*; Wiley-VCH, 2008.

[42] D. J. Myers, D. Myers, X. Wang, N. Kariuki, R. Subbaraman, R. Ahluwalia, X. Wang, *U.S. DOE Hydrog. Fuel Cells Progr. Veh. Technol. Progr. Annu. Merit Rev. Peer Eval. Meet. Washingt. D.C.* **2011**, *Project ID*, 1.

[43] R. K. Ahluwalia, X. Wang, J.-K. Peng, N. N. Kariuki, D. J. Myers, S. Rasouli, P. J. Ferreira, Z. Yang, A. Martinez-Bonastre, D. Fongalland, J. Sharman, *J. Electrochem. Soc.* **2018**, *165*, F3316.

[44] A. Kongkanand, M. F. Mathias, *J. Phys. Chem. Lett.* **2016**, *7*, 1127.

[45] A. Ohma, T. Mashio, K. Sato, H. Iden, Y. Ono, K. Sakai, *Electrochim. Acta* **2011**, *56*, 10832.

[46] J. Zhang, B. A. Litteer, F. D. Coms, R. Makharia, *J. Electrochem. Soc.* **2012**, *159*, F287.

[47] J. Zhang, B. A. Litteer, F. D. Coms, R. Makharia, *J. Electrochem. Soc.* **2012**, *159*,

F287.

[48] Atsushi Ohma, Kazuhiko Shinohara, Akihiro Iiyama, Toshihiko Yoshida, and A. Daimaru, *ECS Trans.* **2011**, *41*, 775.

[49] A. S. D. B. D. B. A. S. A. authorA. M. C. L. A. B. E. Triaca, *J. Appl. Electrochem.* **2006**, *36*, 1143.

CHAPTER 5

POLYETHYLENEOXIDE AS A CARRIER FOR PEMFC ELECTRODES

5.1 Introduction

To successfully electrospin nanofiber electrodes with catalyst and ionomer (e.g. Nafion®), a carrier polymer such as poly(acrylic acid) (PAA) is required.[1,2] Nafion forms a micellar dispersion in electrode inks and attempting to electrospin this dispersion will result in only electrosprayed droplets. A. Weber from Lawrence Berkeley National Laboratory and Y. S. Kim Los Alamos National Laboratory have shown that Nafion does not form a true solution in most solvents and instead forms highly solvated micelles due to the differences in main chain and side chain properties.[3,4] The chains of Nafion are not entangled sufficiently for electrospinning [1,2] and require the use of an additional high molecular weight polymer to electrospin. These polymers are referred to as "carrier" polymers because they help to carry Nafion and catalyst particles into a nanofiber structure during the process of electrospinning. To electrospin Nafion or Aquivion ionomer fibers (with no catalyst), the preferred carrier polymer is polyethylene oxide (PEO) because it is effective at low concentrations (<5 wt.%) and it can easily be removed after electrospinning by soaking in hot water.[5] PEO, however, appears to decompose in a cathode ink mixture containing Nafion ionomer and Pt catalyst powder as noted by a significant drop in the viscosity of the ink after mechanical mixing. Thus, PEO was thought to be an ineffective carrier polymer for nanofiber cathodes. For this reason, PAA has been used in most prior cathode fiber studies. PAA, however has drawbacks: (i) it is known from previous slurry electrode studies[6] that the addition of PAA to Nafion lowers the proton conductivity of

the binder and makes the binder more hydrophilic, which promotes electrode flooding, (ii) it has also been shown by Pintauro and coworkers in prior publications that one cannot remove PAA from a fiber mat cathode after electrospinning even after soaking in peroxide and boiling in acid and water[7], and (iii) the long-term stability of PAA in a fuel cell cathode is suspect since hydrocarbon binders are known to be susceptible to oxidation by peroxide and hydroxyl radicals. Despite the presence of PAA carrier polymer, an overall increase in initial power density was observed when utilizing a nanofiber electrode morphology.[1]

Membranes composed of a perfluorosulfonic acid (PFSA) such as Nafion and a carrier polymer have a lower conductivity than that expected from a linear mixing rule. For example, Choi et al. found in 2010 that the conductivity of a 99/1 wt.% PFSA/PEO membrane was 0.036 S/cm compared to 0.055 S/cm without the addition of PEO.[8] However, after boiling in acid and water to remove the PEO carrier polymer, the conductivity returned to 0.054 S/cm. For this reason, it was hypothesized that if the carrier polymer could be removed from electrospun nanofiber cathodes, then power generation would increase due to improved ionic conductivity of the electrode. In the present study, experiments were carried out to replace the PAA carrier electrospun fiber cathodes with PEO.

5.2 Experimental

5.2.1 Ink Preparation

When Nafion/PEO and catalyst (Nafion in acid form) is prepared as an ink, viscosity decreases due presumably to PEO degradation in the presence of catalyst and H^+ (from Nafion). To avoid this degradation, the protons in Nafion were exchanged with

sodium ions (i.e. Nafion in the sodium form was used). The hypothesis was that PEO decomposition in the presence of Pt/C powder was acid-catalyzed. Sodium exchange was accomplished by soaking dry Nafion powder in an aqueous 1.0 M NaCl solution for 24 hours followed by numerous washings with deionized water during filtration, and then polymer drying.

Ink preparation was carried out using the mixing steps previously described with PAA[1,9]: catalyst and water were mixed and sonicated, then Nafion stock solution was added and sonicated. Finally the carrier polymer was added with mechanical mixing overnight. An ink prepared with Na^+ Nafion and PEO did not show any signs of degradation. After several hours, the viscosity was still high and nanofibers were produced during electrospinning. Conditions for successful electrospinning were as follows. Distance from tip to collection drum: 22 cm, applied voltage: 8.16 kV, pump flow rate: 0.75 mL/hour, relative humidity: 20% RH, Temperature: 23 °C. These conditions are significantly different from those required to form nanofibers when using PAA as a carrier (e.g. the distance from the collection drum is more than double and the applied voltage is weaker). Several ink compositions were attempted before finding an appropriate solvent system and ratio of components. The composition of the cathode inks examined and are shown in Table 5.1. Inks 1-4 and 7 only produced spray droplets or a mixture of nanofibers and droplets for a range of applied voltages (1 kV – 12 kV), flow rates (0.25 mL/hr – 1.5 mL/hr) and spin-to-collector distances (4 cm – 22 cm). When sprayed droplets formed, the mat was adhered to the collection drum and was unable to be removed to form free-standing electrode materials.

Table 5.1. Ink composition, dry component weight ratios and the results during electrospinning for the attempts leading up to successful nanofiber formation.

Cathode Inks				
Ink	Ink composition (g)	Dry component mass ratios (Catalyst/Nafion/PEO)	Mixing time for PEO	Result during electrospinning
1	0.20 g Pt/C, 0.80 g water, 0.53 g IPA, 0.37 g stock solution A[1], 0.25 g stock solution C[3]	64/24/12	24 hours	Spray only
2	0.15 g Pt/C, 0.45 g water, 0.20 g n-propanol, 0.11 g dry Nafion Na^+, 0.37 g stock solution D[4]	55/41/4	24 hours	Spray only
3	0.18 g Pt/C, 0.51 g water, 0.19 g n-propanol, 0.36 g stock solution B[2], 0.077 g Stock Solution C[3]	69/28/3	6 hours	Spray with some fibers
4	0.2 g Pt/C, 0.567 g water, 0.567 g n-propanol, 0.615 g stock solution B[2], 0.205 g stock solution C[3]	58/36/6	6 hours	Spray with some fibers.
5	0.19 g Pt/C, 0.63 g water, 0.63 g methanol, 0.70 g stock solution B[2], 0.8 g stock solution D[4]	52/37/11	4 hours	Nanofibers only
6	0.19 g PtCo/C, 0.63 g water, 0.63 g methanol, 0.70 g stock solution B[2], 0.8 g stock solution D[4]	52/37/11	4 hours	Nanofibers only
7	0.19 g PtCo/C, 0.63 g water, 0.63 g methanol, 0.70 g stock solution B[2], 0.8 g stock solution D[4]	52/37/11	24 hours	Spray only.

Stock Solution A: 20% Nafion H^+ in 1:1 water:n-propanol w:w

Stock Solution B: 20% Nafion Na^+ in 1:1 water:n-propanol w:w

Stock Solution C: 10% Polyethylene Oxide (600 kDa MW) in 1:1 water:n-propanol w:w

Stock Solution D: 5% Polyethylene Oxide (600 kDa MW) in 1:1 water:n-propanol w:w

The inks in Table 5.1 show that the time of mixing for the PEO is important as well as the total composition of the fiber. The sodium form of Nafion may be slowing the degradation of PEO in the ink as it mixes, but the "electrospinability" of ink is still time sensitive. After 24 hours, nanofibers cannot be produced as is shown in ink 7 in Table 5.1.

5.2.2 MEA Preparation and Carrier Removal Confirmation via NMR

After the nanofiber mat was electrospun it was annealed at 140 °C for 30 minutes under vacuum. Then, 5 cm^2 MEAs were prepared by hot-pressing a nanofiber cathode and nanofiber anode onto a Nafion 211 membrane. Anodes used in this study were electrospun from either Nafion/PAA or Nafion/PEO inks. Anode inks always used Pt/C catalyst. The composition of the anode nanofiber ink was 65/20/15 (Pt/C)/Nafion/PAA, or 52/37/11 (Pt/C)/Nafion/PEO. MEAs containing Nafion/PEO as a binder underwent a hot water soak in order to remove the PEO carrier polymer. This treatment involved submerging the MEA in 80 °C water for 1 hour. To determine if the PEO was actually removed, an NMR experiment was performed on the soak water used to remove the carrier. First, a reference solution was prepared: a known quantity of 600 kDa molecular weight PEO material (8 mg) was dissolved into 0.4 mL of deuterium oxide (D_2O) with 4 mg of mesitylene as an internal standard. Next, an MEA containing Nafion/PEO nanofiber electrodes was soaked for 1 hour in 3 mL D_2O for 1 hour at 80 °C and then 0.4 mL of this soak water was placed into an NMR tube with 4 mg of mesitylene as an internal standard. Both samples were then analyzed with a 400 MHz Bruker NMR spectrometer. Using the area under the peak of the NMR signal for PEO found in the electrode sample and correlating this to both the area under the mesitylene peak and the peak from the known quantity of PEO, a rough estimate of PEO removed was determined.

NMR spectra are shown in Figure 5.1. This is a qualitative measurement and shows that there is some PEO that has been removed. There are further studies that must be performed to determine the exact amount of PEO that is removed.

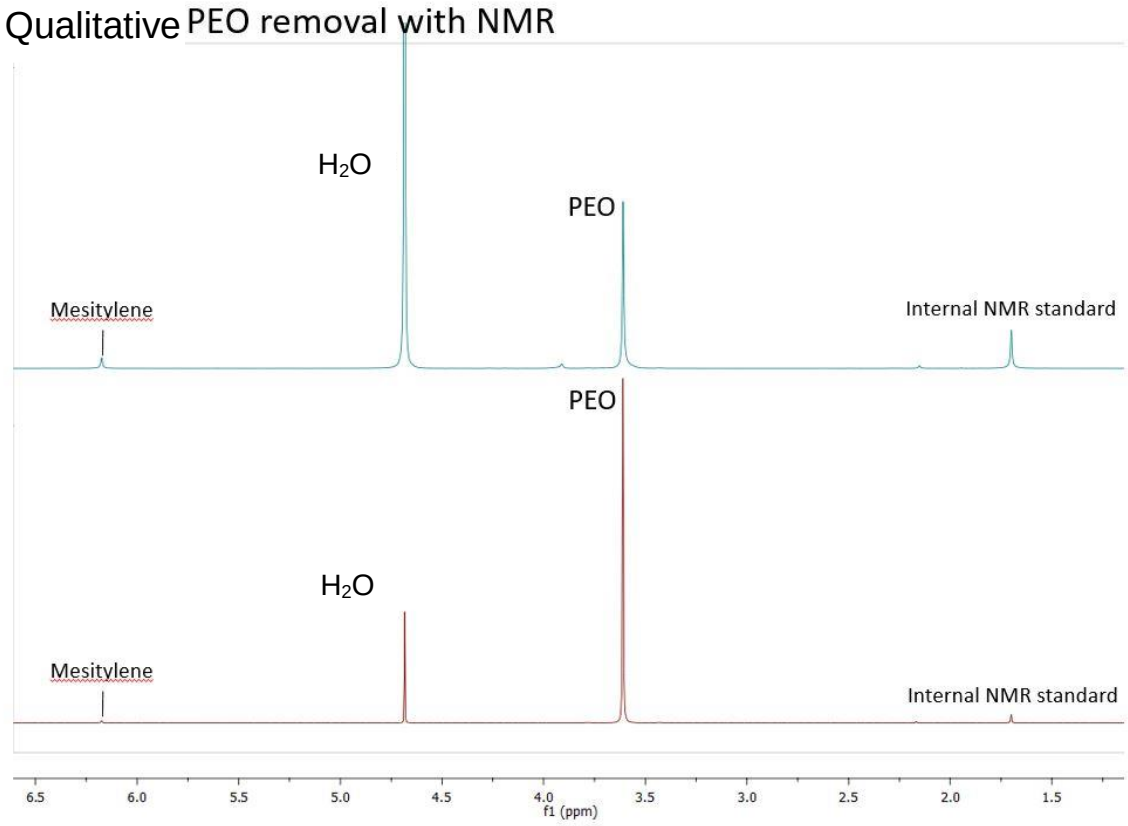

Figure 5.1. NMR results of the electrode soak water after a 1 hour, 80 °C water soak.

To provide additional evidence of PEO removal in a single water wash, a second water (D_2O) soak was performed on the same electrode material for 1 hr at 80 °C. The water from this second soak was then analyzed in the same manner as described above. This time, only a trace amount of PEO was detected. These results are shown in Figure 5.2. This suggests that either a majority of the PEO came out, but this is still not 100% certain because some PEO may be strongly entangled and would not show up in the soak water.

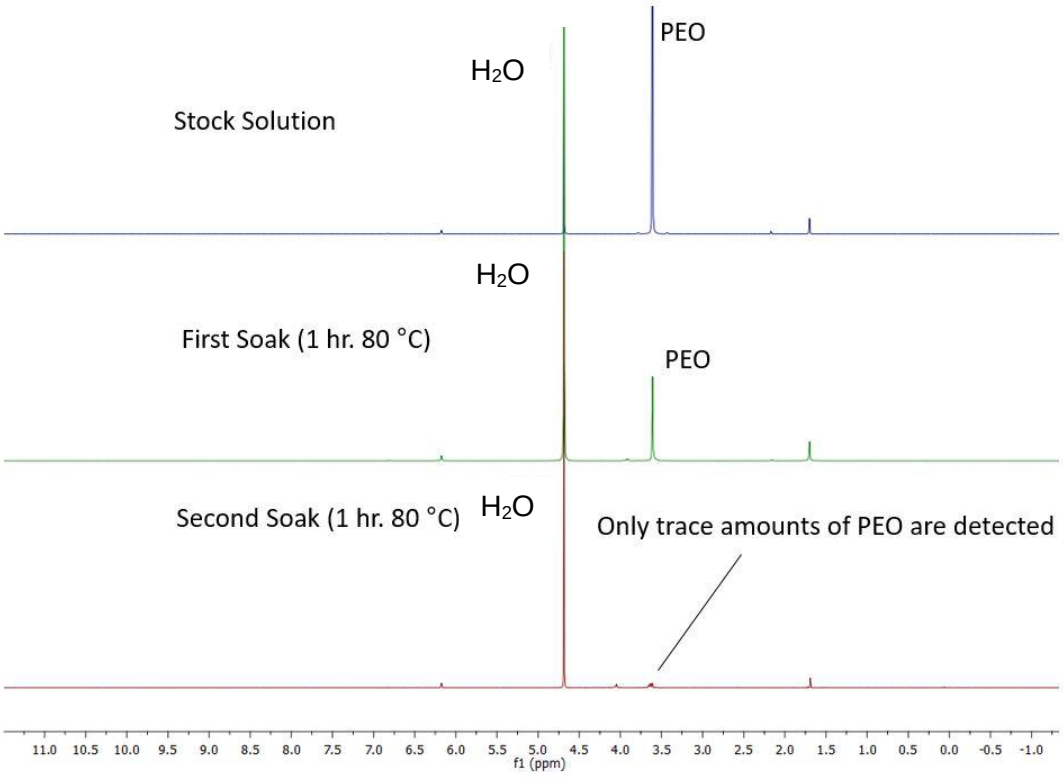

Figure 5.2. NMR results after the first 1 hour soak and a second water soak at 80 °C for 1 hour.

These results suggest that PEO was not trapped in the membrane during the soak. Only a one hour 80 °C water soak was tested with this method. One hour may not be necessary; Ballengee showed that adding PEO to a Nafion membrane reduces its conductivity and that after 5 minutes of 80 °C acid soak and 5 minutes of 80°C water soak, the Nafion/PEO membrane's conductivity was fully recovered.

5.2.3 Electrochemical Characterization and Durability Protocols for MEAs

After the hot water treatment, MEAs were taken out and allowed to dry under vacuum at room temperature for 15 minutes. MEAs were then placed into a Scribner 850e fuel cell test station using a single-serpentine flow channel, with fiberglass reinforced

Teflon gaskets and Sigracet 29BC gas diffusion layers. The torque applied to these cells was 75 inch-pounds. Some MEAs were soaked in 80 C water for 1 hour prior to electrochemical measurements to remove PEO from the electrodes while others did not have the PEO removed. MEAs were then broken-in using the following procedure. The voltage is held for 1 minute at 0.6 V, followed by 1 minute at 0.2 V; this process is repeated until measured current densities stabilize. After MEA break-in, polarization data were collected at 80 °C, 100% RH, 125/500 sccm H_2/air, and 200/200 kPa absolute pressure (anode/cathode). MEAs were also prepared with a slurry cathode where the binder was either neat Nafion or a Nafion/PEO mixture (the same ink composition as the electrospun nanofibers i.e., 52/37/11 wt.% (Pt/C)/Nafion/PEO). Electrochemical analyses included collecting mass activity data and electrochemical surface area. Mass activity was determined by plotting voltage and current collected from 1 A to 0.01 A under pure oxygen at 150 kPa absolute.[10] The current-voltage data were corrected for both hydrogen crossover and high frequency resistance; the mass activity was determined as the current generated at 0.9 V normalized to platinum loading. Electrochemically active surface area (ECSA) was determined by utilizing cyclic voltammetry under H_2/N_2 with 100/100 sccm flow rates on anode/cathode. ECSA was then calculated from the hydrogen desorption area of the cyclic voltammogram between 100 mV and 400 mV after correcting for non-faradaic currents and the loading of Pt used in the electrode of interest.

MEA durability was tested by utilizing the Department of Energy accelerated stress tests (ASTs) which were designed to simulate processes that would naturally occur during the lifetime of a fuel cell electric vehicle. These include starting and stopping the vehicle (a voltage cycling protocol from 1.0 V to 1.5 V which induces carbon corrosion as is shown

in Figure 4.23 from Chapter 4) and accelerating and decelerating the vehicle (a voltage cycling protocol from 0.6 V – 0.95 V which induces metal dissolution as shown in Figure 4.13 from Chapter 4).[11] The carbon corrosion AST was performed for 1,000 voltage cycles which was sufficient to study the differences in durability between MEAs while the metal dissolution AST was performed for 30,000 voltage cycles.

5.2.4 Physical Characterization

Electron microscopy was carried out at both the Vanderbilt Institute of Nanoscale Science and Engineering and Oak Ridge National Laboratory. Microscopy techniques included the use of a Zeiss Merlin scanning electron microscope (SEM) with a 10 kV accelerating voltage at Vanderbilt and a 200kV FEI Talos F200X scanning transmission electron microscope (STEM) with energy dispersive x-ray spectroscopy (EDS) for elemental analysis at Oak Ridge National Laboratory.

All samples for SEM images were gold sputter coated. Samples for STEM imaging were carbon sputter coated. Carbon coating was used to not interfere with the elemental analysis of samples. Both types of sputter coatings were used to increase the conductivity of the sample which inhibits unwanted image artifacts, reduces thermal damage and improves the secondary electron signal required for topographic examination.

Nanofiber samples were prepped for STEM/EDS imaging by first cutting a small rectangle of electrospun mat (2 x 4 mm) and placing into a wet epoxy resin which was then allowed to dry in an oven overnight. These samples were then microtomed using a diamond-tipped blade (cut into sections that were roughly 75 nm thick). These microtomed sections were placed onto TEM grids containing glassy carbon.

5.3 Results and Discussion

5.3.1 Physical Characterization of Nanofibers Spun from Nafion/PEO Inks

As a quick test of the structural integrity of fiber mat cathodes, a mat sample was placed in a beaker containing 80 °C water; after several hours the fiber mat was intact, i.e., after removing water-soluble PEO, the fibers were structurally sound and did not disintegrate. To provide further evidence that the fiber structure is retained after the 1 hour 80 °C water soak, scanning electron microscopy was performed on a section of electrode material before and after water soaking. Figure 5.3 shows SEM images of polymer/particle nanofibers electrospun from an ink containing (Pt/C)/(Nafion Na^+)/PEO before and after the hot water soak. Figure 5.3(a) shows fibers before the soak and Figure 5.3(b) shows the fibers after the soak. The fiber composition before pre-treatment is 52/37/11 weight ratio of catalyst/Nafion/PEO. After the removal of the PEO, the composition of the fiber is 62/38 catalyst/Nafion. The fiber structure is essentailly unchanged and soaking does not structurally damage the fibers. The catalyst used is Johnson Matthey Pt/C, which has a carbon loading of 60%, so the pre-treated fibers have a carbon content that is 37% (62% of 60% of a fiber). Therefore, the I/C ratio is 38 / 37 = 1.03.

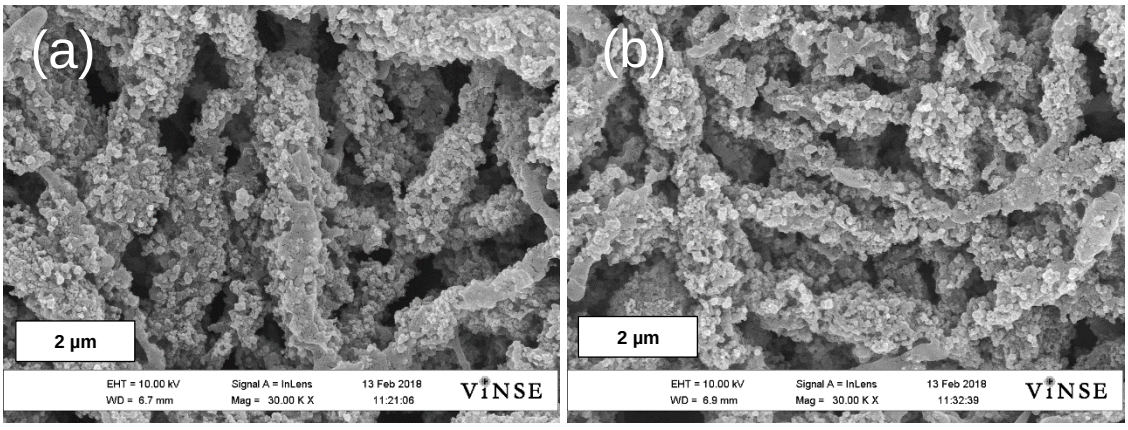

Figure 5.3. SEM analysis of electrospun (Pt/C)/Nafion/PEO fibers (a) before pre-treatment at (30,000x magnification (b) after pre-treatment (30,000x magnification)

The dispersion of catalyst and Nafion in a nanofiber was analyzed by mapping elements Pt and F in nanofiber cross sections using energy dispersive x-ray spectroscopy (EDS). The cross sections used were from microtomed Nafion(H+)/PAA nanofibers and Nafion(Na+)/PEO nanofibers. The results of the Nafion/PAA nanofibers are shown in Figure 5.4. This EDS data is also presented in Figure 4.4 of Chapter 4 of this dissertation and is presented again here for comparative purposes.

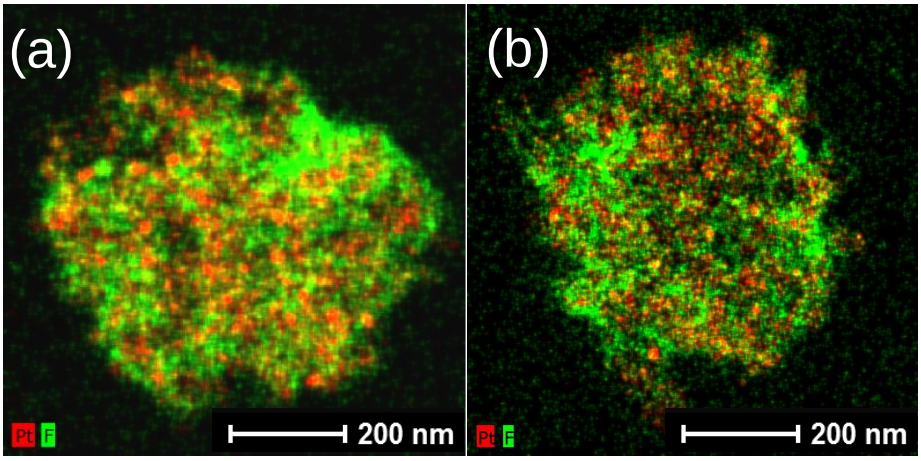

Figure 5.4. Energy Dispersive X-ray Spectroscopy mapping of Nafion/PAA nanofiber cross sections (a) and (b) are two different nanofiber cross sections which show that there is no drastic variation in the distribution within the cross section.

The results of Nafion/PEO nanofiber cross sections after removal by soaking with water are shown in Figure 5.5 (a, b, and c) where Figure 5.5 (c) is an entire electrode cross section. The results show that there is a stark difference between the two types of nanofiber electrode materials. In the Nafion/PEO nanofibers, there is a core-shell structure (more Nafion binder on the nanofiber's surface) which is in contrast to Nafion/PAA fiber cross sections which show a more uniform distribution of Nafion and Pt throughout the fiber diameter. Nanofibers electrospun with PEO show Nafion

enrichment toward the surfaces of the fibers. To quantify the amount of catalyst vs Nafion in each section, the EDS data was analyzed.

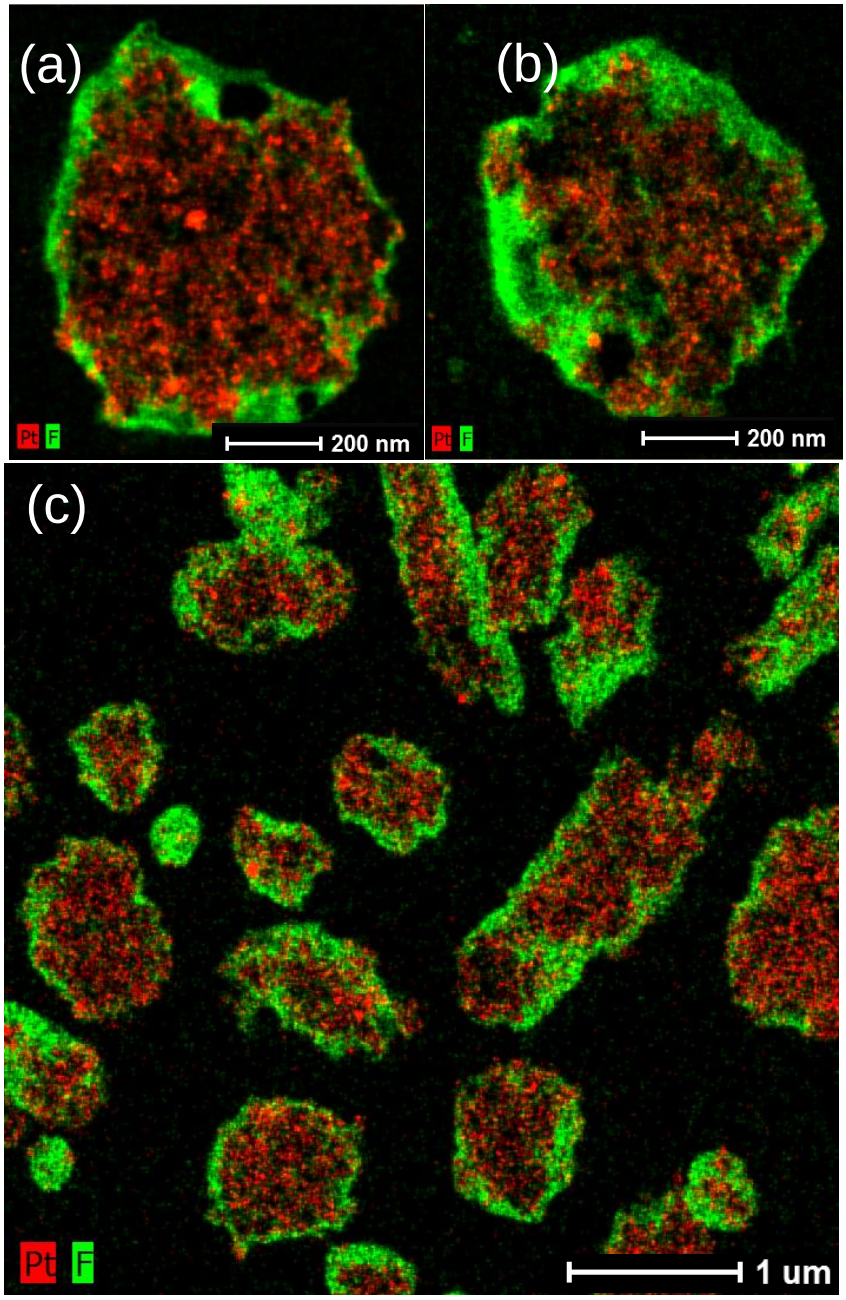

Figure 5.5. EDS mapping of Nafion/PEO nanofibers of (a and b) two fiber cross sections and (c) an electrode cross section.

The I/C ratio of the ink was 1.15 based on the known composition of Pt/C and Nafion added to the ink. The average I/C across five fiber cross sections was found from Pt and F EDS analyses to be 1.07 ± 0.07. This is in good agreement with the I/C calculated from ink composition. The average I/C in the center of the nanofiber (the "core") was 0.46 ± 0.1 and the average I/C in the "shell" was 1.93. Table A.1 shows the detailed percentages measured from the energy dispersive x-ray spectroscopy analysis. There is a significant range of I/C content in the core (between I/C = 0.26 to I/C = 0.73). This indicates that the actual amount of Nafion near catalyst particles varies along the length of the nanofiber. This effect is not understood and tuning the nanofiber to have a more uniform I/C ratio along the length of the fiber may have an effect on performance.

Table 5.1 Pt%, F%, and I/C for the core and entire nanofiber cross section for 5 different cross sectional areas.

Sample #	Section	Pt wt%	F wt%	Measured I/C
1	Core	64%	36%	0.73
	Entire Cross Section	50%	50%	1.32
2	Core	82%	18%	0.28
	Entire Cross Section	58%	42%	0.96
3	Core	64%	36%	0.73
	Entire Cross Section	54%	46%	1.13
4	Core	82%	18%	0.28
	Entire Cross Section	57%	43%	1.01
5	Core	83%	17%	0.26
	Entire Cross Section	59%	41%	0.90

This variation in I/C across the fiber diameter was never seen in Nafion/PAA fibers. As shown in Figure 5.6, where Pt and F EDS signals are decoupled, there is still some Nafion

that is present in the core and still some platinum in the shell. Of note is that the Pt distribution appears to be radially uniform, whereas the Nafion is the component that is non-uniform across the diameter of the fiber. This structure is highly unusual.

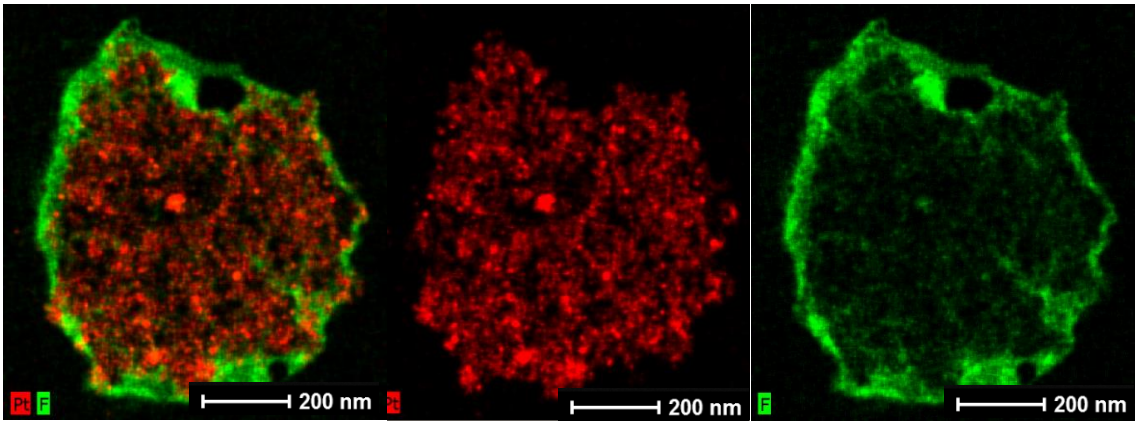

Figure 5.6. EDS maps of a cross sectional image with its Pt and F signals de-coupled to more clearly show the distinct distributions.

SEM images of fiber mats generally confirm the results from the EDS analysis. There are some sections of the fiber that show particles on the outside of the fiber, but upon further inspection, many of the fibers have a smooth coating of polymer on the outside of the fiber-length. This is shown in Figure 5.7. In previous studies, this was thought to be undesirable due to electrical isolation of Pt/C across the fiber. However, in the nanofibers resulting from a Nafion/PEO ink, the catalyst is not isolated, even when fibers do not show particles on their surface.

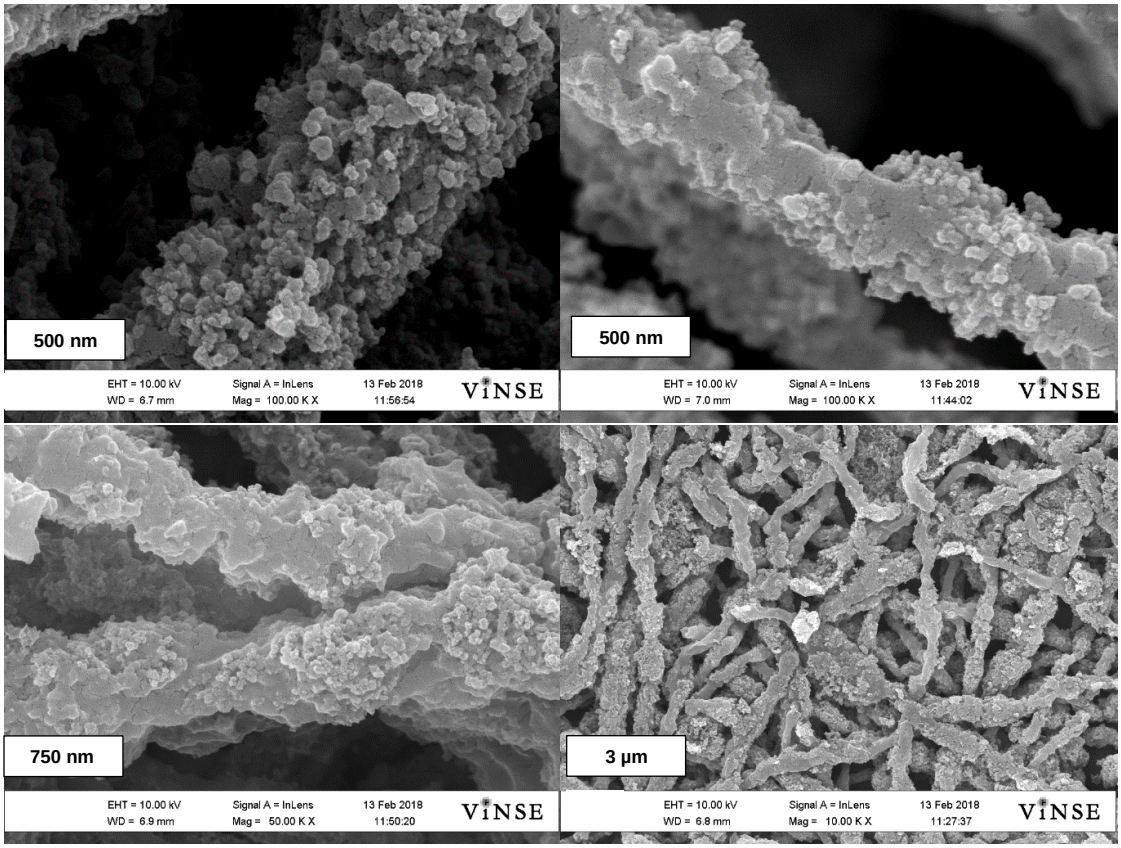

Figure 5.7. SEM images of Nafion(Na+)/PEO nanofibers indicating the coating of polymer on the outside of the fiber.

5.3.2 Initial Performance of Nafion/PEO Electrode MEAs Before/After PEO Removal

Brodt et al. showed that in an MEA with a slurry gas diffusion electrode (GDE), the presence of PAA with Nafion reduces the power generation at all voltages as shown in Figure 5.8 (adapted from reference [2]). Specifically, the H_2/air polarization data with Nafion/PAA appears to show a high ohmic-overpotential (steeper slope in the ohmic region) which is consistent with the notion of reduced ionic conductivity in a Nafion/PAA binder.[6]

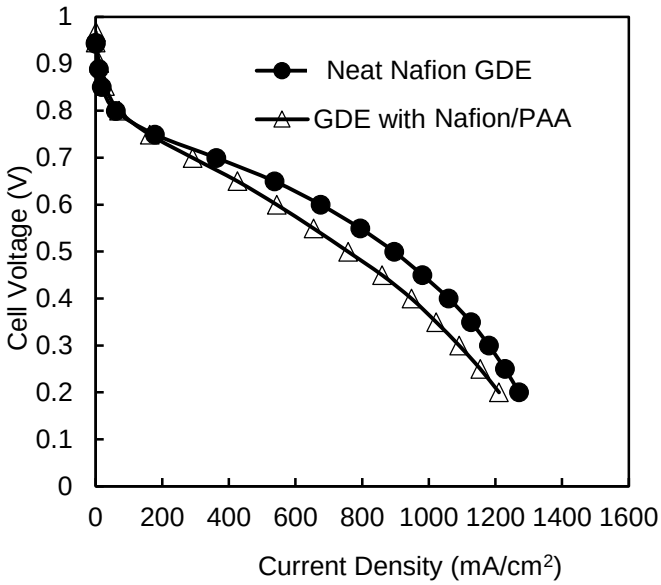

Figure 5.8. Fuel cell polarization curves for 5 cm^2 painted MEAs with TKK-Pt(HSAC) catalyst and a Nafion 211 membrane operated at 80°C with fully humidified H_2 (125 sccm) and air (500 sccm) at ambient pressure. Cathodes and anodes have a Pt loading of 0.10 ± 0.005 mg/cm^2 and are: painted GDE with no PAA and painted GDE with PAA. From reference[2]

To reproduce the result in Figure 5.8 and further investigate the effects of carrier polymers on MEA polarization data, three slurry-cathode MEAs were fabricated and tested. Two carrier polymers were used: polyethylene oxide (PEO) and poly(acrylic acid) (PAA) in addition to a neat Nafion binder MEA. The fuel cell results of these experiments are summarized in Figure 5.9. Each MEA had a neat Nafion anode and a Nafion 211 membrane. The loadings of all electrodes were 0.1 mg_{Pt}/cm^2. The fuel cell operating conditions are 80 °C, 200 kPa absolute, and 125/500 sccm H_2/air. The slurry electrode MEAs with neat Nafion and Nafion/PEO binder (with no hot water soak) worked equally well. Both are better than the MEA with a Nafion/PAA cathode binder (which did not undergo a hot water soak), due presumably to the reduction in ionic conductivity of the binder in the presence of PAA as was seen in references 5 and 6. In these initial

experiments, the cathode fiber mats were not pre-treated in water to remove PEO, nor was there any attempt to exchange Na^+ counter-ions with H^+.

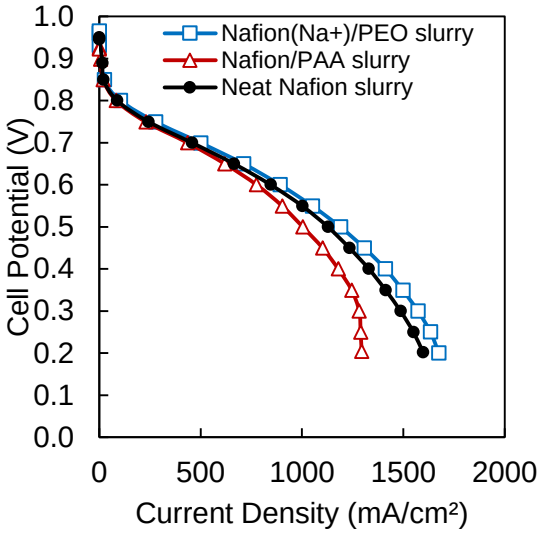

Figure 5.9. Polarization data for painted slurry electrodes with varying cathodes noted in the legend and in all cases, the anode is a neat Nafion pained GDE. (There was no removal of PEO from the MEA.)

The maximum power density attained in the PEO slurry MEA of Figure 5.9 was 594 mW/cm^2 vs. the neat Nafion electrode MEA which was 564 mW/cm^2. The Nafion/PAA electrode slurry MEA produced 502 mW/cm^2, nearly 20% less than the Nafion/PEO electrode MEA. The results from the Nafion/PEO binder slurry show that there is no detrimental effect from this binder on fuel cell performance. It is unclear if the PEO washes out in the product water during the fuel cell operation.

Next, PEO was removed from MEAs with painted/slurry cathodes where the Pt/C catalyst binder was Nafion/PEO. Hydrogen/air fuel cell polarization data were collected before and after a 1.0 hour 80 °C water soak to remove water soluble PEO from the electrode. The purpose of these experiemnts was to determine if PEO removal improved

MEA performance as compared to an MEA with Nafion/PEO and a neat Nafion binder MEA. MEAs were made with Johnson Matthey Pt/C catalyst and Nafion 211 membrane, where the anode and cathode loadings were each 0.1 mg/cm^2. Hot-pressing condtions for attachement of electrodes to the membrane were 140 °C and 4 MPa for 5 minutes.

Fuel cell polariztion data from three MEAs (80 ^{o}C and 100% RH) are presented in Figure 5.10: (i) a control MEA with neat Nafion as the binder for the anode and cathode, (ii) an MEA with Nafion/PEO as the cathode binder and a neat Nafion anode that had no water soak pre-treatment before break-in, and (iii) a hot water soaked MEA with Nafion/PEO as the cathode binder and a neat Nafion anode binder. The fuel cell polarization in Figure 5.10 show that MEAs work equally well before/after a water soak, and after PEO removal the Nafion/PEO binder works equally well as a neat Nafion binder MEA. It is possible that the PEO is decomposing and exiting the binder/MEA during MEA break-in. The MEA with a Nafion/PEO slurry cathode was flipped (so that the neat Nafion anode became the cathode). This MEA was also tested and there was also essentially no difference (<5% max power density and power density at 0.65V).

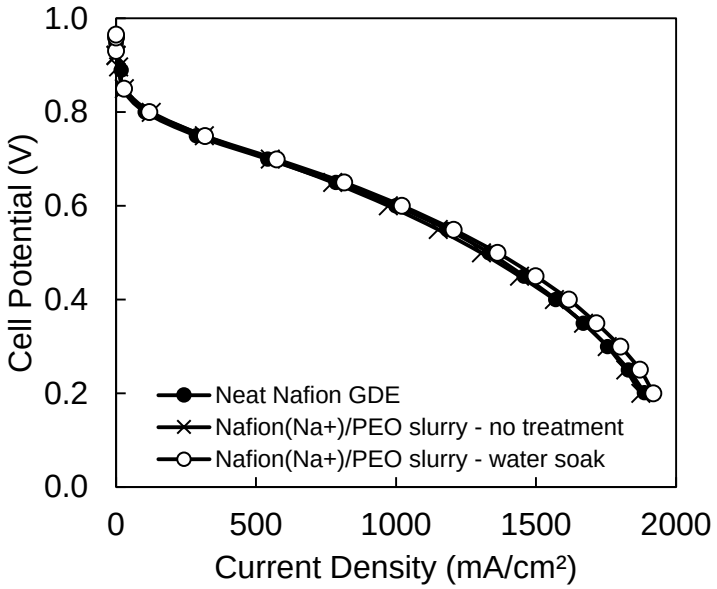

Figure 5.10. Polarization data showing the effect of Nafion/PEO as a binder and either no pre-treatment or a water pre-treatment. Polarization conditions are 100% relative humidity, 80 °C, 200 kPa (absolute), 125/500 sccm H_2/air. All MEAs have a neat Nafion anode binder, a 0.1 mg/cm^2 loading, a Nafion 211 membrane, and Sigracet 29BC gas diffusion layers.

Nanofiber cathode MEAs with Nafion/PEO or Nafion (after PEO removal)

Nanofiber electrode mats made from a Nafion(Na^+)/PEO binder using either a Pt/C (Johnson Matthey on HiSpec 4000 carbon) or a PtCo/C (Tanaka Kikinzoku Kogyo: TKK TEC36E52) catalyst were tested and compared to MEAs with Nafion/PAA cathode and anode binders. After using a standard break-in procedure, polarization data were collected.

In Figure 5.11, the MEAs have a (Pt/C)/Nafion/PAA nanofiber anode. For these MEAs, the cathode fiber mats were not pre-treated in any way to remove PEO, nor was there any attempt to exchange Na^+ counter-ions with H^+ in the Nafion binder. The Nafion nanofiber cathode results show an increase in power density as compared to an MEA with Nafion/PAA using Pt/C and PtCo/C fiber cathodes. The catalyst/binder ratio in both Nafion

nanofiber cathodes was 52/48 on a weight basis, which corresponds to an I/C ratio of 1.15. The ORR mass activity and ECSA are higher for nanofiber cathodes that employ Nafion as the binder.

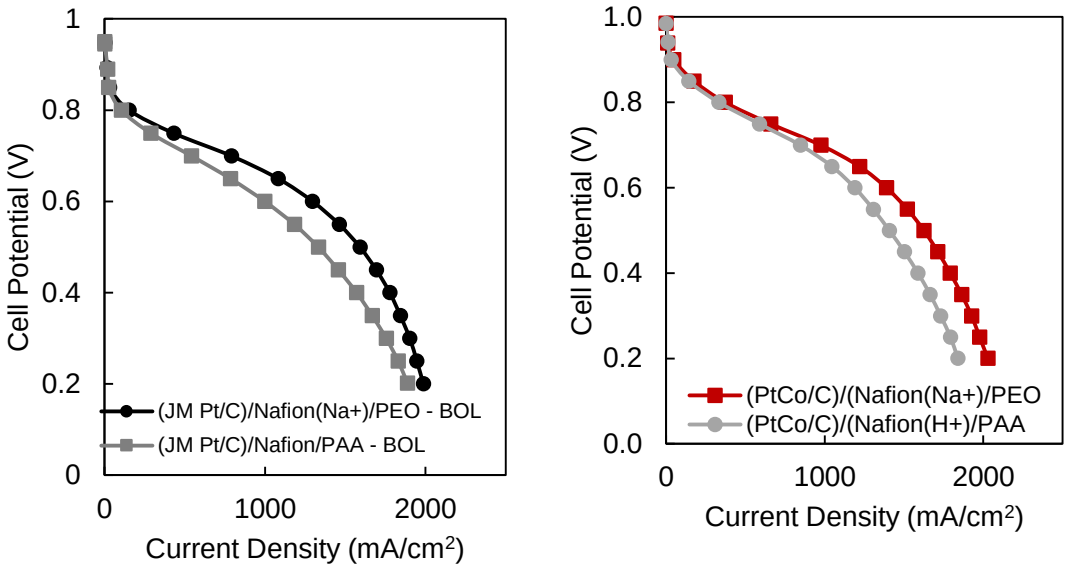

Figure 5.11. Polarization data for (a) Johnson Matthey Pt/C and (b) TKK PtCo/C. The loading of the cathodes are 0.1 mg/cm^2 in both cases. The anode for both MEAs is a nanofiber Johnson Matthey Pt/C anode at 0.1 mg/cm^2. The operating conditions are 80 °C, 200 kPa (absolute), 125/500 sccm H_2/air, and 100% RH.

The improvements in maximum power density and the power density at 0.65 V shown in Table 5.1 were all significantly above the painted slurry electrodes with the same binder composition. A slurry electrode MEA with Nafion/PEO as the binder generated a maximum power density of 590 mW/cm^2 whereas the MEA with a Nafion nanofiber electrode using the same catalyst generated a maximum power of 779 mW/cm^2. While the Nafion/PEO composition in the slurry did not significantly improve/change the polarization data compared to a neat Nafion slurry, the Nafion nanofiber did significantly improve compared to a neat Nafion slurry (40% higher maximum power in a Nafion nanofiber).

Table 5.2 Summary of Power Density, ORR Mass Activity, and electrochemical surface area for nanofiber electrode MEAs with Pt/C and PtCo/C using the Nafion/PAA or Nafion as the cathode fiber binder with a Nafion/PAA nanofiber anode in all cases.

Nanofiber cathode catalyst & binder. (All anodes are Pt/C, Nafion, PAA)	Max Power (mW/cm^2)	Power at 0.65V (mW/cm^2)	Cathode Mass Activity (mA/mg_{Pt})	Cathode ECSA (m^2/g)
PtCo/C Binder: (Nafion (H^+)/PAA)	718	679	298	62
PtCo/C Binder: (Nafion)	840	793	350	69
Pt/C Binder: (Nafion (H^+)/PAA)	650	510	160	59
Pt/C Binder: (Nafion)	779	703	191	67

The power density of an MEA containing a nanofiber Nafion/PEO binder was improved by a water soak pre-treatment of 80 °C for 1 hour before inserting into the fuel cell test station as shown in Figure 5.12. In an MEA containing a (PtCo/C)/Nafion/PEO cathode and a (Pt/C)/Nafion/PAA anode, this pre-treatment improved the power density over an MEA whose cathode and anode were both (PtCo/C)/Nafion/PAA. The power density increase was approximately 15% greater at 0.65 V. There was a difference in behavior between the nanofiber electrode with PEO and a slurry electrode with PEO in that water soaking the slurry electrode did not have a large impact on power density.

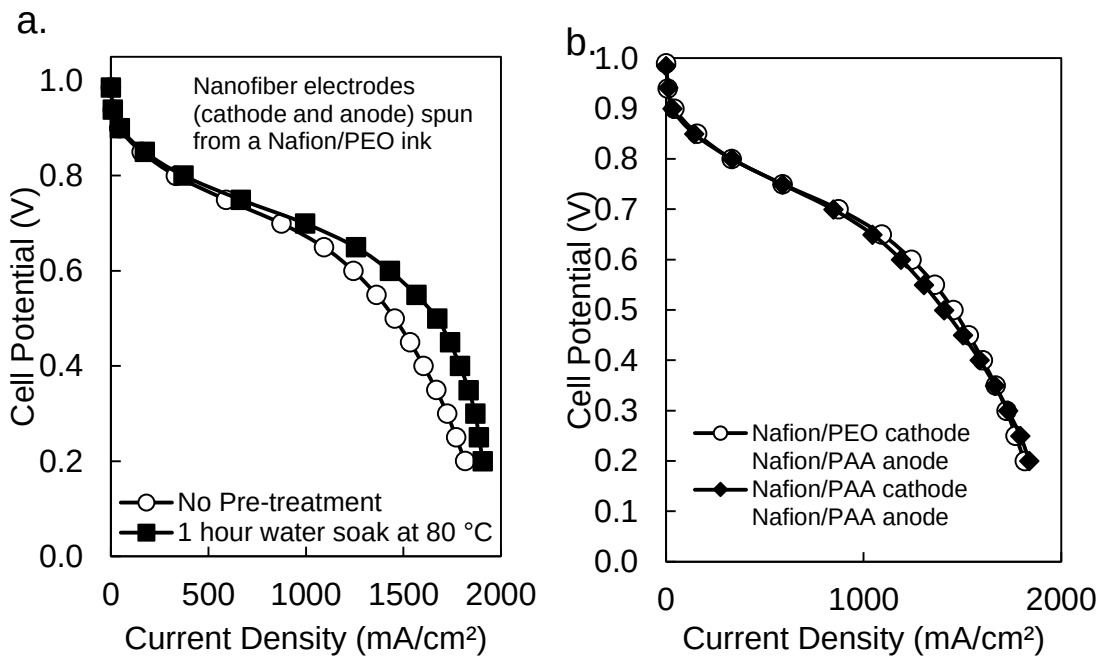

Figure 5.12. (a) Polarization curves for a nanofiber PtCo/C Nafion(Na+)/PEO MEA using a Nafion/PAA-based anode before and after PEO removal. (b) Polarization curves for Nafion/PEO nanofibers vs. Nafion/PAA nanofibers. Cathode/anode loadings are each 0.1 mg/cm^2, with a Nafion 211 membrane. Operating conditions are: 80 °C, 200 kPa absolute pressure, and 125/500 sccm H_2/air.

The results in Figure 5.12(b) show that Nafion/PAA and Nafion/PEO (before removal) behave similarly. Brodt et al.[5] showed that after boiling in water and boiling in hydrogen peroxide, there was no change in the performance of a Nafion/PAA nanofiber cathode MEA. For that reason, Nafion/PEO is preferred since it has been shown to improve power output.

The polarization plots in Figure 5.12(a) shows that the slope in the ohmic region is lower for the nanofiber electrodes that had PEO removed from them compared to Nafion/PAA nanofibers. This result suggests that the ionic resistance of the electrode is lower for Nafion nanofibers without a carrier polymer which is consistent with what Elabd

and Ballengee reported.[5,6] To confirm this, Nissan Technical Center of North America performed EIS experiments to measure the ionic resistance of only the nanofiber electrodes (excluding the contribution of the Nafion 211 membrane or the contact resistance of the membrane+electrode). These experiments were performed on two MEAs: one with a cathode and anode using a Nafion/PAA binder and one MEA with a cathode and anode using Nafion (after PEO was removed). The results showed that the MEA with Nafion/PAA nanofiber electrodes had an ionomer resistance of 140 $m\Omega \cdot cm^2$ whereas the MEA with Nafion nanofiber electrodes had an ionomer resistance of 90 $m\Omega \cdot cm^2$. Henceforth in this dissertation, nanofiber electrode MEAs electrospun from a Nafion/PEO ink after PEO removal will simply be referred to as nanofiber electrodes with a Nafion binder.

Another possible reason for the improvement in power density observed when using an electrode electrospun from a Nafion/PEO ink compared to a Nafion/PAA ink may be reduced catalyst poisoning via sulfonate adsorption as described by Kongkanand et al and Kodama et al.[12,13] who showed that adsorption of the ionomer onto catalyst sites can stiffen the ionomer chain and increase gas transport resistance and inhibit both the conductivity of the ionomer and catalytic activity of the metal. As was shown in the EDS elemental maps for the Nafion binder nanofibers, a majority of the catalyst has reduced contact with Nafion near the center of the fiber (see Figures 5.5 and 5.6).

Nafion nanofiber electrode MEA with Low Pt-loading

An MEA with a total loading of 0.115 mg_{Pt}/cm^2 (0.096 mg_{Pt}/cm^2 for the cathode and 0.019 mg_{Pt}/cm^2 for the anode, as determined by X-ray fluorescence spectroscopy at NTCNA) was fabricated. The anode was made by electrospinning a TKK 20% Pt/C

catalyst with Nafion binder. With the lower Pt content catalyst, a thicker and more uniform anode could be electrospun vs. the use of 40% Pt on carbon. The membrane was Nafion 211 and the gas diffusion layers were Sigracet 29BC. Figure 5.13(a and b) show the effect of three different backpressures at 80 C and 100% RH on this low loading MEA. The effect of backpressure on maximum power is linear for both high (0.2 mg_{Pt}/cm^2 and low (0.115 mg_{Pt}/cm^2) loading (Figure 5.13b) with 10% less power for the MEA with 42.5% less Pt.

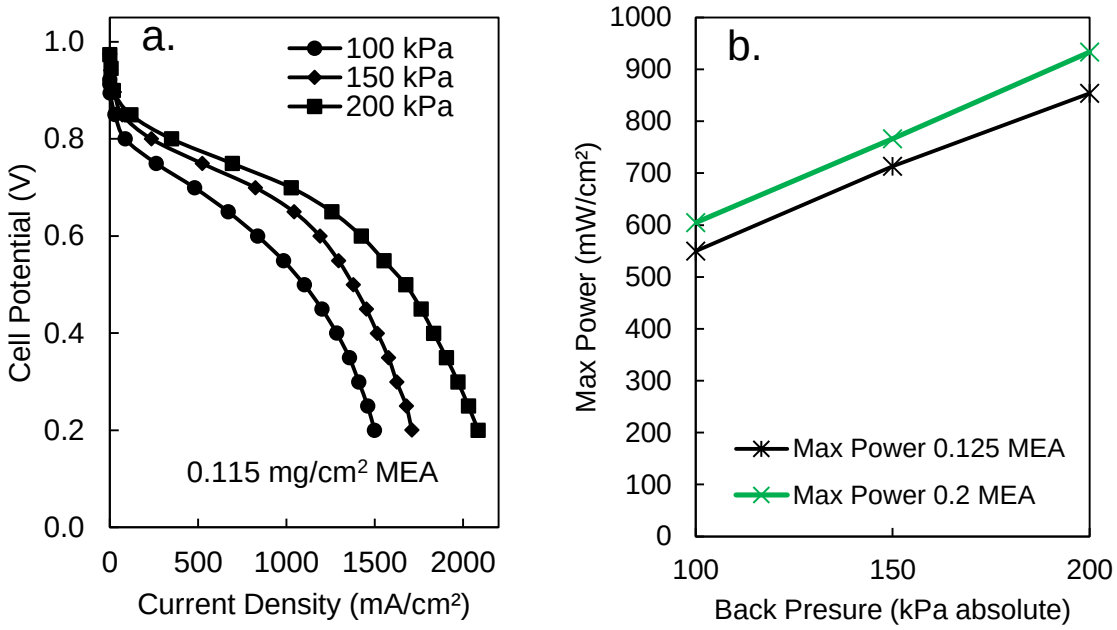

Figure 5.13. Pressure effects for an MEA with 0.115 mg_{Pt}/cm^2 total loading as determined by XRF measurements performed at Nissan Technical Center of North America. (0.96 mg_{Pt}/cm^2 cathode loading and 0.019 mg_{Pt}/cm^2 anode loading). Nafion 211 was the membrane. The cell was fully humidified, at 80°C with 125/500 sccm H_2/air feed gas flow rates.

5.3.3 Accelerated Stress Tests with Nafion nanofiber electrodes

Durability studies with nanofiber cathode MEAs containing Nafion binder (spun from a Nafion/PEO ink) were conducted. After a metal dissolution AST (30,000 square

wave voltage cycles from 0.6 V – 0.95 V vs SHE), the Nafion nanofiber electrode MEA loses a larger percentage of power, vs. a Nafion/PAA binder; but the actual power at both BOL and EOL were higher for a Nafion binder vs. a Nafion/PAA binder as is shown in Figure 5.14 and Table 5.3

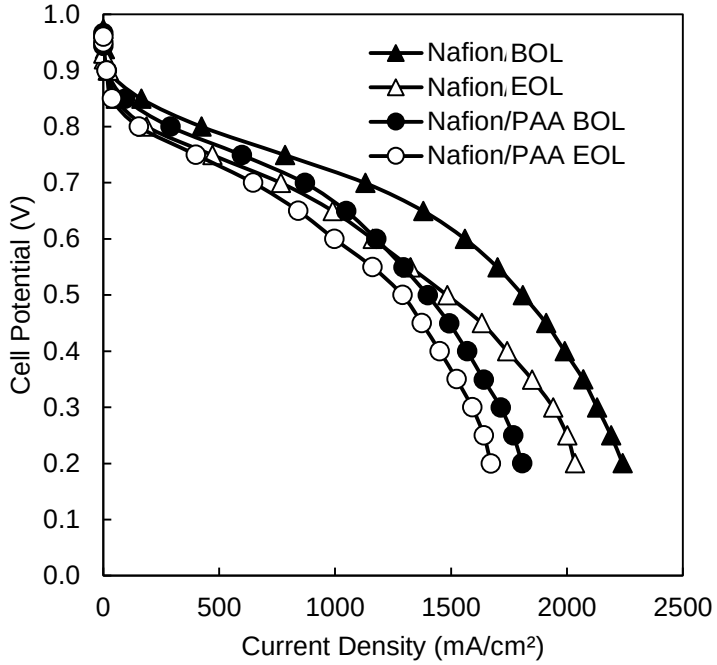

Figure 5.14. Metal Dissolution AST for 30,000 cycles using a TKK PtCo/C catalyst. The loading on both MEAs is 0.1 mg/cm^2 on the cathode and 0.1 mg/cm^2 on the anode. Polarization conditions are: 125/500 sccm H_2/air, 80 °C, 200 kPa absolute.

Table 5.3 Power density comparison between MEAs with cathode/anode binders of either Nafion or Nafion/PAA before and after metal dissolution AST.

Nanofiber electrode binder (for cathode and anode)	**80°C, 100% RH, 200 kPa (abs)**	
	Max Power (mW/cm^2)	**Power at 0.65 V (mW/cm^2)**
Nafion – BOL/EOL	935/741	897/643
Nafion/PAA – BOL/EOL	711/645	679/546

The Nafion binder nanofiber electrode MEA produces more power at BOL than a Nafion/PAA cathode, but it also loses more power after the AST (a 21% drop in maximum power for a Nafion binder vs. a 9% drop for a Nafion/PAA binder).

The better durability for Nafion/PAA nanofibers is due presumably to a decrease in the Nafion binder's ion exchange capacity, a consequence of the presence of PAA. This has been shown by prior membrane experiments with Nafion/PAA which showed a decrease in proton conductivity.[35] With fewer mobile protons in the binder of a Nafion/PAA electrode, the dissolution of catalyst metal is lessened. The nanofiber mat electrospun from a Nafion/PEO ink (which then has the PEO removed) has a higher IEC, more mobile protons, and therefore it is expected that the EOL/BOL power density ratio would be lower.

In addition to the metal dissolution AST, a carbon corrosion AST of was performed using the same voltage cycling protocol shown in Figure 4.16 of Chapter 4. For this experiment, the MEA contained a Johnson Matthey Pt/C nanofiber cathode and nanofiber anode with a Nafion binder. This experiment ran for 1000 cycles. The results are shown in Figure 5.15. The polarization curve for the MEA with a Nafion nanofiber electrode begins and ends above the BOL curve for a Nafion/PAA cathode fiber MEA. The percentage power density loss was greater using a Nafion binder vs. a Nafion/PAA binder. The results show nanofiber cathode MEAs have both improved metal dissolution and carbon corrosion durability. The EOL/BOL maximum power ratio for the MEA using a Nafion binder was 579/804 (i.e., a power density loss of 28%), whereas the same ratio for Nafion/PAA was 533/665 (a 20% loss).

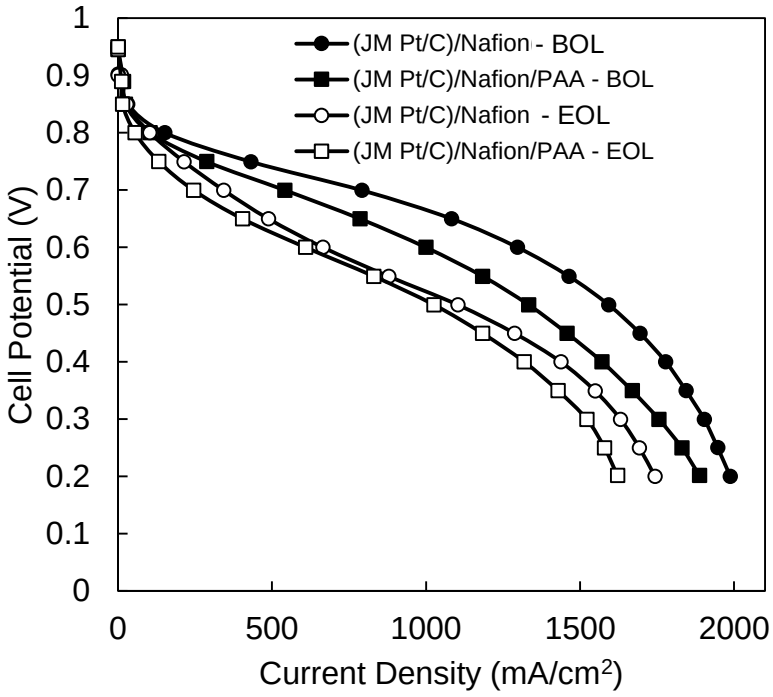

Figure 5.15. Polarization data for nanofiber electrode MEAs at BOL and EOL after a carbon corrosion AST for 1000 cycles using a Johnson Matthey 40% Pt supported on HiSPEC carbon. The loading on both MEAs was 0.1 mg/cm^2 on the cathode and 0.1 mg/cm^2 on the anode. Polarization conditions are: 125/500 sccm H_2/air, 80 °C, 100% RH 200 kPa absolute.

5.3.4 Relative Humidity Effects on MEA Power Output

Several strategies have been examined to improve H_2/air fuel cell power densities at low relative humidity conditions. These include reducing the membrane thickness[14,15] to promote water back diffusion from the cathode to the anode, using more hydrophilic materials in the anode (e.g. silica or low equivalent weight PFSA ionomer binders)[8,16–19], and using asymmetric anode/cathode humidification[20]. These strategies are intended to mitigate unwanted drying in the anode. The results of these experiments have been moderately successful – but still only producing 450 mW/cm^2 at 30% RH with 0.5 mg$_{Pt}$/cm^2, as was achieved by Xin et al. as an example.[21]

The BOL power density of nanofiber cathode MEAs with Nafion/PAA or Nafion/PEO binder (before removal of PEO) with a (Pt/C)/Nafion/PAA nanofiber anode were examined across a range of relative humidities, where the cathode catalyst was TKK PtCo/C. These results are shown in Figure 5.16. Both MEAs have the same catalyst/binder ratio and both have a Pt loading of 0.1 mg/cm^2. The Nafion/PEO nanofiber cathode MEA outperformed the standard Nafion/PAA nanofiber cathode MEA over the entire humidity range. The MEAs with Nafion/PAA as a binder show power densities that are lower with a markedly different RH dependence because: (i) the presence of PAA adversely affects the conductivity of Nafion in the cathode fibers and (ii) the presence of hydrophilic PAA causes some flooding of the cathode at high RH (the optimum power density was achieved at 80% RH). The trend in power density with RH for the Nafion/PEO nanofiber cathode binder (with a Nafion/PAA nanofiber anode) is consistent with prior studies with slurry/sprayed cathodes, i.e., there is a monotonic decrease in power with RH due to less water and a lower proton conductivity in the binder/membrane.[1]

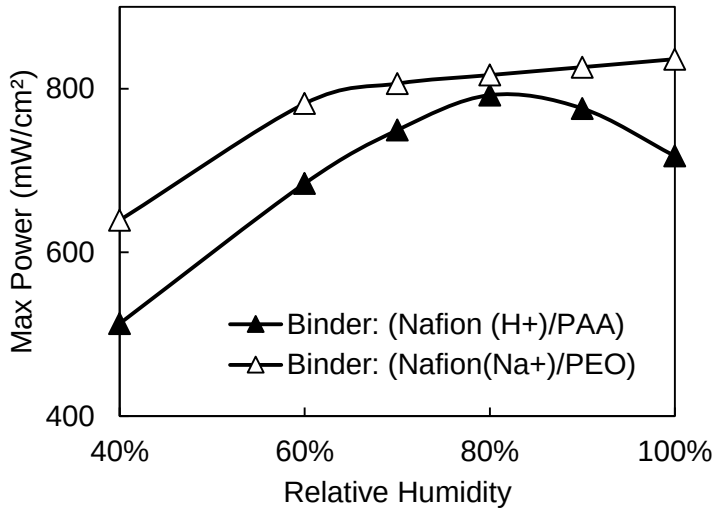

Figure 5.16. Maximum power vs relative humidity for nanofiber electrode MEAs with a PtCo/C catalyst cathode electrode using a binder of either Nafion/PAA or Nafion(Na+)/PEO. Operating conditions are 80 °C, 200 kPa (absolute), 125/500 sccm H_2/air.

Effect of using a spray anode vs a nanofiber anode electrospun from a Nafion/PEO ink

The effect of RH on sprayed electrode MEAs was examined at NTCNA. The results of these experiments are shown in Figure 5.17. When the anode is changed from a spray GDE to a Nafion nanofiber electrode, the power density at low relative humidity improved.

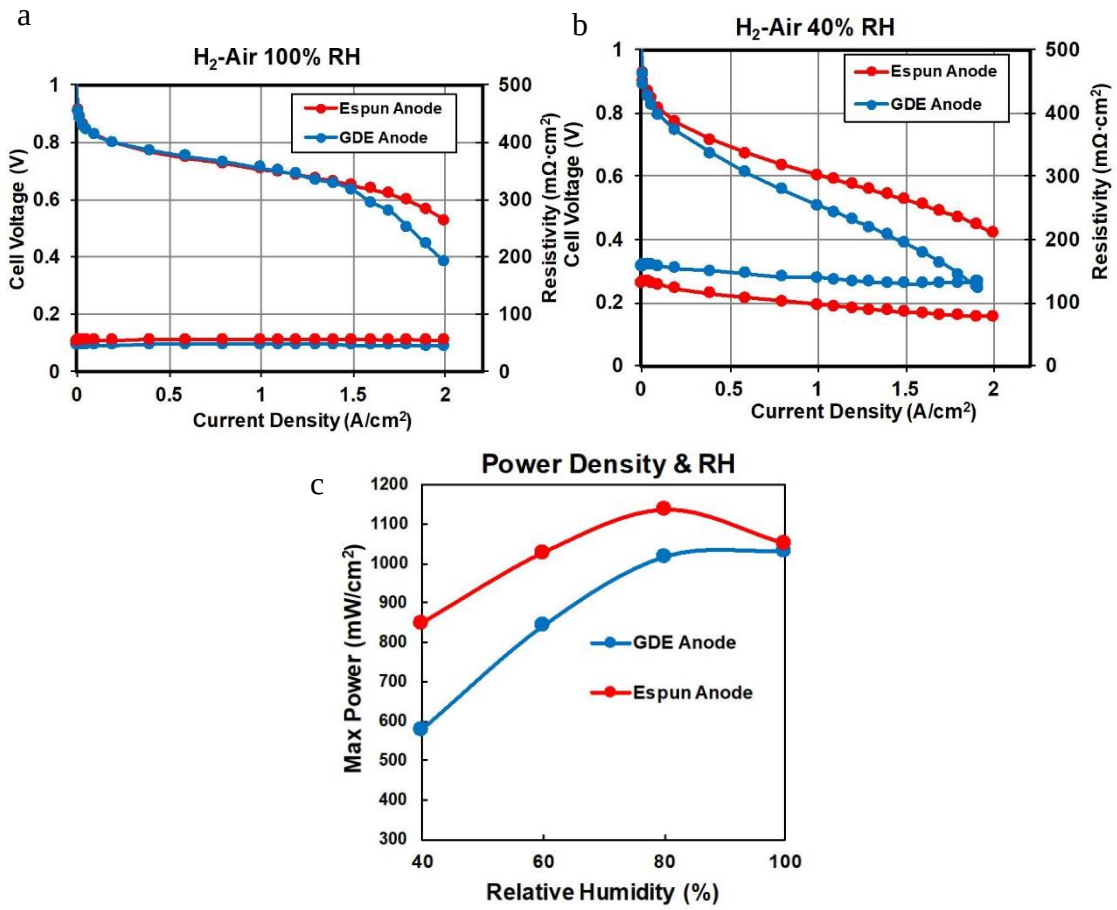

Figure 5.17. (a) Polarization data for showing the effect of changing only the anode, using a Nafion nanofiber cathode at 100% RH and (b) at 40% RH and (c) power density vs RH for 40% RH to 100% RH. In all cases, the cathode catalyst was PtCo/C, the loading was 0.1 mg_{Pt}/cm^2, the membrane was Nafion 211, the diffusion media was Sigracet 29 BC, and the feed gas inlets were parallel flow channels. The operating conditions were 80 °C, 200 kPa absolute pressure, and 4000/8000 sccm H_2/air flow-rates. Experiments were run at NTCNA.

Effect of RH on Nanofiber Electrode MEAs with a Nafion/PAA binder or a Nafion Binder as the Anode

Experiments were conducted to determine the effect of utilizing a Nafion nanofiber at the anode and cathode in an H_2/air fuel cell MEA. In each electrode that was electrospun from a Nafion/PEO ink (for the anode, cathode, or both), the MEA was soaked in hot water as described above. The results indicate that power density varies depending on anode and cathode binders (i.e. if the Nafion binder nanofiber electrode was present in the anode, cathode or both electrodes). Johnson Matthey 40% Pt/C was used as the cathode and anode catalyst. The anode and cathode loadings were each 0.1 mg/cm^2, the membrane was Nafion 211, temperature was 80 °C, the pressure was 200 kPa absolute, and the hydrogen/air flow rates were 125/500 sccm. A summary of the results of the RH tests are shown in Figure 5.18 where max power is plotted against the cell RH.

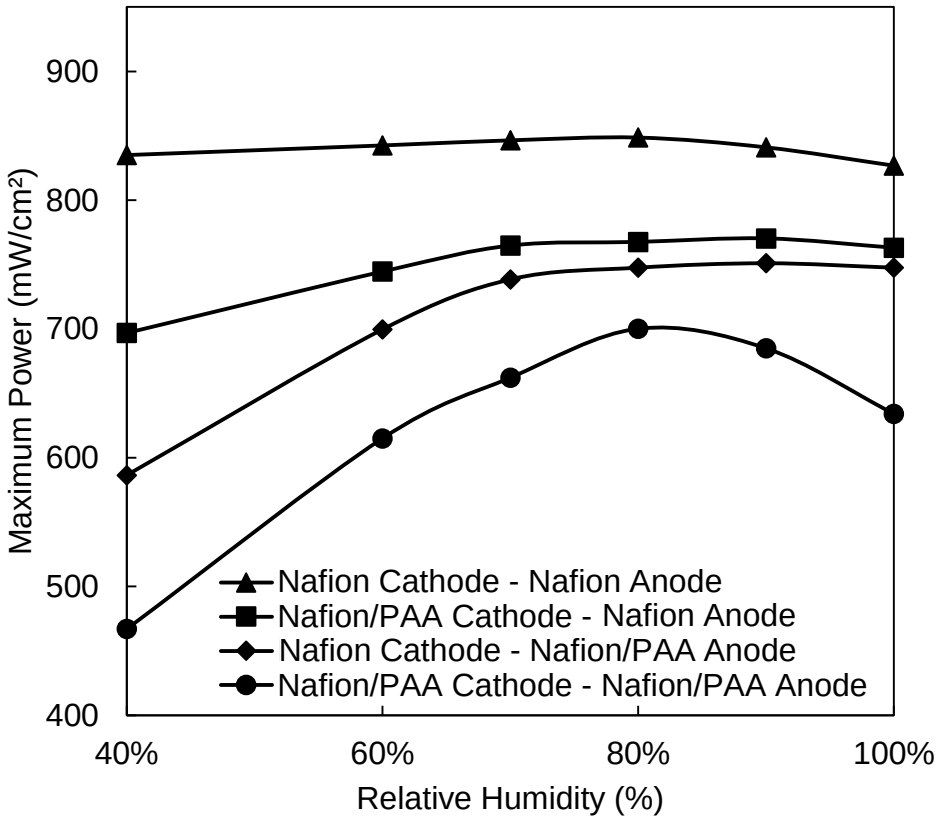

Figure 5.18. Effect of anode/cathode carrier on maximum power density and relative humidity using a Pt/C anode/cathode with a PAA or PEO carrier with Nafion. Cathode and anode are both 0.1 mg_{Pt}/cm^2, membrane is Nafion 211, and GDLs are Sigracet 29 BC. Operating conditions: 80 °C, 200 kPa absolute, 125/500 sccm H_2/air.

These results suggest that the nanofibers electrospun from a Nafion/PEO ink helps hold onto water better at 200 kPa absolute and 80 °C after PEO removal. This is not the first time that the anode composition has been reported to affect the power density of an MEA at both high and low relative humidity. In the literature, Zenyuk and Weber suggest that water management in a PEMFC MEA may be controlled by altering the relative hydrophilicity of the anode compartment.[22] Figure 5.18 suggests that the nanofibers electrospun from a Nafion/PEO ink improve the power density at low RH by decreasing the harmful effects of anode drying (i.e. by holding onto water better in the anode catalyst

layer). The original hypothesis of creating a nanofiber structure with a removable carrier was that the power density may increase due to an increase in the conductivity of the binder. It now appears that a Nafion binder (from a Nafion/PEO ink) has an added benefit of better water retention at low RH.

The results in Figure 5.18 also show that PEO as the anode carrier had a greater impact on power density than having PEO as the cathode carrier. The best result was obtained when PEO was the carrier in the anode and cathode, with a maximum power of 835 mW/cm² at 40% RH and 827 mW/cm² at 100% RH. At 100% RH, the high frequency resistance (HFR) for all MEAs was essentially the same (55-65 mohm-cm²). However, at 40% RH, the HFR for a Nafion/PAA anode/cathode binder MEA was 250 mohm-cm² vs. 70 mohm-cm² when PEO was used as anode/cathode carrier. The effect of PEO on power density was more dramatic at 40% RH due in part to this large difference in HFR. The high frequency resistance (HFR) value is the sum of membrane resistance plus the membrane/electrode contact resistance. As relative humidity decreases from 100% RH to 40% RH, previous studies have shown that the HFR of an MEA increases[23] e.g. the resistance of a slurry electrode MEA with a Nafion binder and a Nafion membrane ranges from 50-90 mΩ·cm² at 100% RH to 175 – 250 mΩ·cm² at low (≤ 40% RH).[24–26]

High power at low relative humidity was also achieved with a Nafion nanofiber anode and cathode using the TKK PtCo/C (TEC36E52) catalyst. These results are shown in Figure 5.19 and Table 5.4.

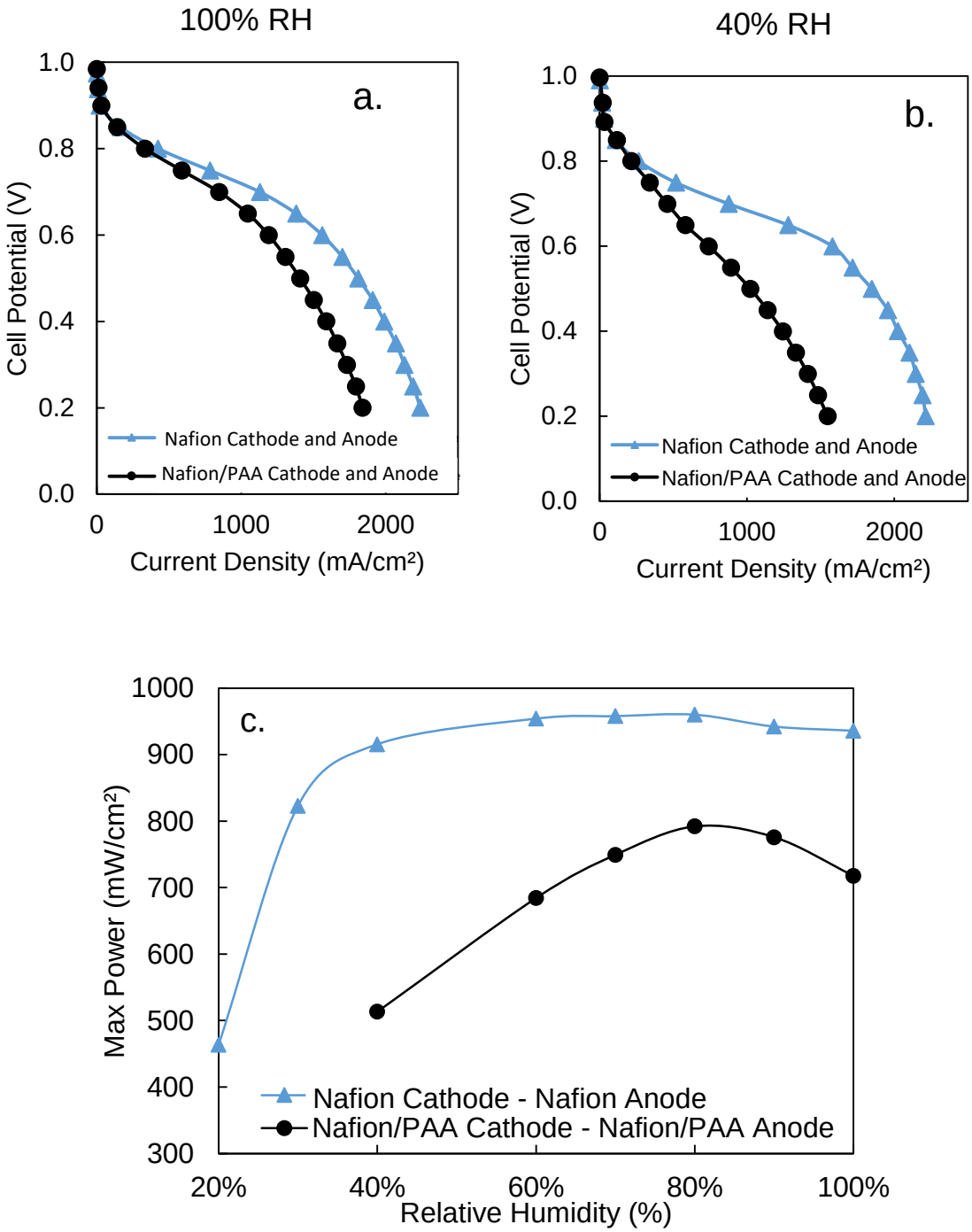

Figure 5.19. (a) Polarization data at 100%RH for PtCo/C with a Nafion binder and Nafion/PAA binder. (b) Polarization data at 40%RH for PtCo/C with a Nafion binder and a Nafion/PAA binder. (c) Maximum Power vs RH for the same MEAs. Fuel cell operating conditions were 80 °C, 200 kPa, 125/500 sccm H_2/air. Cathode/anode loading was 0.1 mg_{Pt}/cm^2. Membrane was Nafion 211. GDLs were Sigracet 29 BC.

Table 5.4 Power and HFR at 100% and 40% RH for MEAs using a PtCo/C cathode catalyst with PEO or PAA as the cathode/anode carriers.

Nanofiber electrodes:	**100% RH**			**40% RH**		
Binders tested:	**Max Power (mW/cm^2)**	**Power at 0.65 (mW/cm^2)**	**HFR ($m\Omega \cdot cm^2$)**	**Max Power (mW/cm^2)**	**Power at 0.65 (mW/cm^2)**	**HFR ($m\Omega \cdot cm^2$)**
Nafion cathode Nafion anode	935	897	61	940	832	71
Nafion/PAA cathode Nafion/PAA anode	718	679	65	513	379	205

In Figure 5.19, the maximum power of the Nafion nanofiber MEA as the anode and cathode binder remains above 900 mW/cm^2 for relative humidities between 40% and 100%. The maximum power density of the (PtCo/C)/Nafion nanofiber electrode MEA was nearly double that of the (PtCo/C)/Nafion/PAA MEA at 40% RH. This effect was also observed with a Pt/C catalyst.

This experiment was repeated for the low platinum loaded MEA (PtCo/C cathode and Pt/C anode) with a total loading of 0.115 mg_{Pt}/cm^2 shown earlier. The effect of RH at 200 kPa and 80 °C is shown in Figure 5.20. The same trend of consistent power density generation across the RH range is observed in the low-loading anode MEA, but shifted down by ~10%. This suggests that the reason the nanofiber electrodes perform better at low RH is independent of the loading that is utilized.

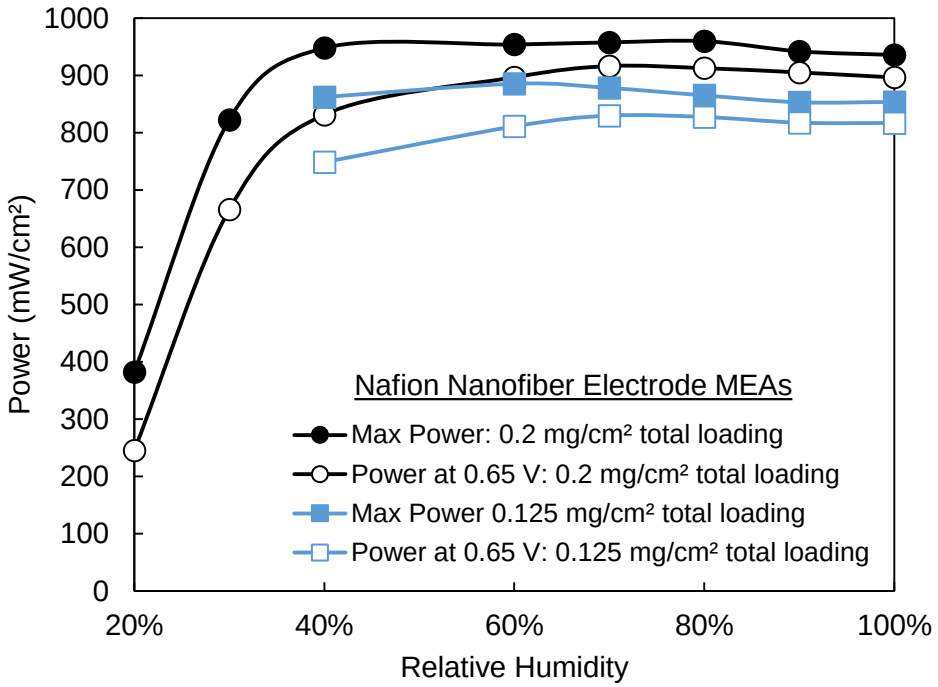

Figure 5.20. Relative humidity effects with 0.2 mg_{Pt}/cm^2 total loading MEA and a 0.115 mg_{Pt}/cm^2 total loading MEA. Membrane was Nafion 211. 80°C, 200 kPa absolute, and 125/500 sccm H_2/air are the feed gas flow rates.

To verify the high power density at low relative humidity with a 0.2 mg_{Pt}/cm^2 loaded MEA with a Nafion binder, a PtCo/C cathode and a Pt/C anode, several samples of 10 cm^2 MEAs were shipped to Nissan Technical Center of North America (NTCNA) where they verified that a Nafion nanofiber electrode MEA outperform a sprayed Nafion electrode MEA at both 100% RH and 40% RH. These results are shown in Figure 5.21. These results are consistent with data collected at Vanderbilt University; the Nafion binder nanofibers produce significantly greater power at 40% RH compared to a Nafion slurry or Nafion sprayed electrode.

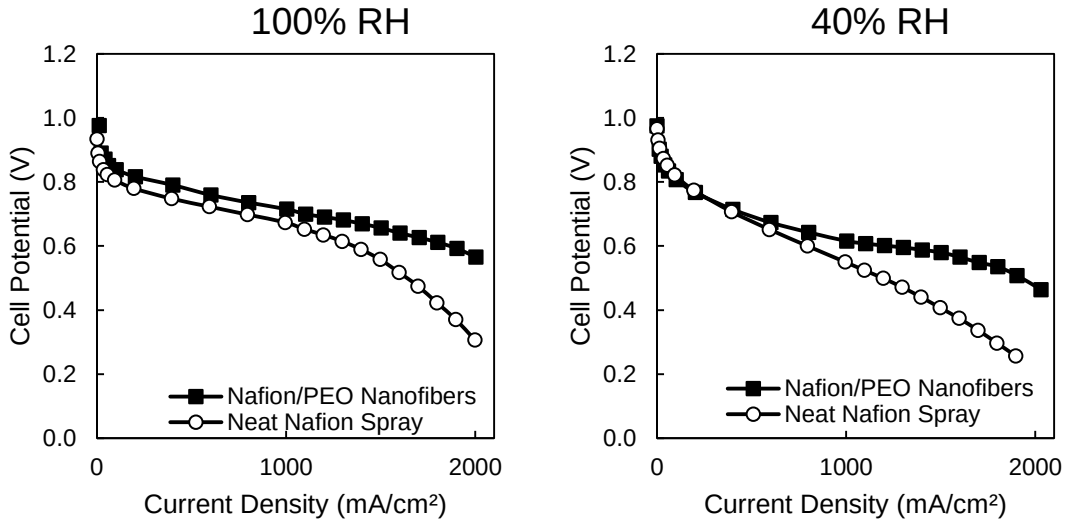

Figure 5.21. Polarization curves for Nafion nanofibers vs Nafion spray. MEAs are both 10 cm^2. Cathode catalysts were PtCo/C, the loading was 0.1 mg_{Pt}/cm^2, the membrane was Nafion 211, the diffusion media was Sigracet 29 BC, and the feed gas inlets were parallel flow channels. The operating conditions were 80 °C, 200 kPa absolute pressure, and 4000/8000 sccm H_2/air flow-rates. Experiments were run at NTCNA.

MEAs were also sent to Los Alamos National Laboratory (LANL) for additional testing. The RH results from Vanderbilt, NTCNA, and LANL are summarized in Figure 5.22. There is a slight downward trend with RH in both the LANL and Nissan test station that is attributed to the high gas flow rates used by these groups. The high frequency resistance (HFR) measured by electrochemical impedance spectroscopy (EIS) for both the Nafion nanofibers and a Nissan sprayed electrode is presented in Table 5.5. The decrease in the HFR suggests that the Nafion binder nanofiber electrodes are helping the membrane retain more water at low relative humidities.

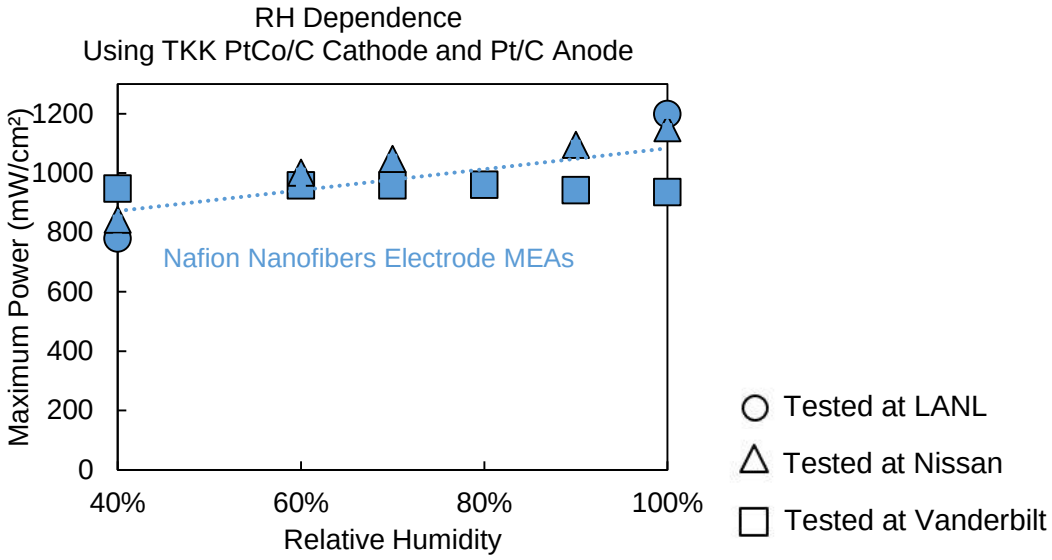

Figure 5.22. Max Power generated from Nafion nanofiber electrode MEAs tested at three independent laboratories. All MEAs have a 0.1 mg/cm^2 cathode catalyst loading and a Nafion 211 membrane. Test conditions for Vanderbilt are: 80 °C, 200 kPa absolute, and 125/500 sccm H_2/air. Test conditions for NTCNA are: 80 °C, 200 kPa absolute, and 4000/8000 sccm H_2/air. Test conditions for LANL are: 80 °C, 200 kPa absolute, and 500/2000 sccm H_2/air.

Table 5.2 High frequency resistance of a Nafion nanofiber electrode MEAs vs a slurry baseline as measured by Nissan, Vanderbilt, and Los Alamos National Lab.

	HFR (mΩ·cm²)			
	Nafion Nanofibers		Nissan Spray	
	100% RH	40% RH	100% RH	40% RH
Vanderbilt	60	77	N/A	N/A
NTCNA	56	95	47	208
LANL	58	74	N/A	N/A

Fully Electrospun MEA with 725 PFSA and PEO carrier: A fully electrospun nanofiber MEA was created using PEO as the electrode carrier for both the cathode and anode. The membrane was a dual fiber electrospun nanofiber composite film with a composition of 80/20 (725 EW perfluorosulfonic acid)/PVDF with a final thickness of ~20 μm. The

cathode was electrospun from an ink that contained PtCo/C, Nafion, and PEO. The anode was electrospun from an ink that contained Pt/C, 725 EW PFSA, and PEO.

This MEA was different in three primary ways compared to the MEAs tested in the previous sections of this chapter: (1) The composition of the membrane was different (made from reinforced 725EW PFSA ionomer) (2) The membrane was thinner than the standard Nafion 211 membrane. Finally, (3) the ionomer in the anode binder was 725 EW PFSA. The motivation to utilize a lower equivalent weight ionomer in the binder and membrane was because it has been shown to perform better at low relative humidity.[29] In addition, a thinner membrane (20 microns) was chosen to increase the back-diffusion of water from the cathode to the anode which should improve the fuel cell power generation at low RH.[30]

Polarization data compared to Nafion nanofibers is shown in Figure 5.23a, and the high current density at 20% RH is shown in Figure 5.23b. The performance of this MEA at varying RH is shown in Figure 5.23c.

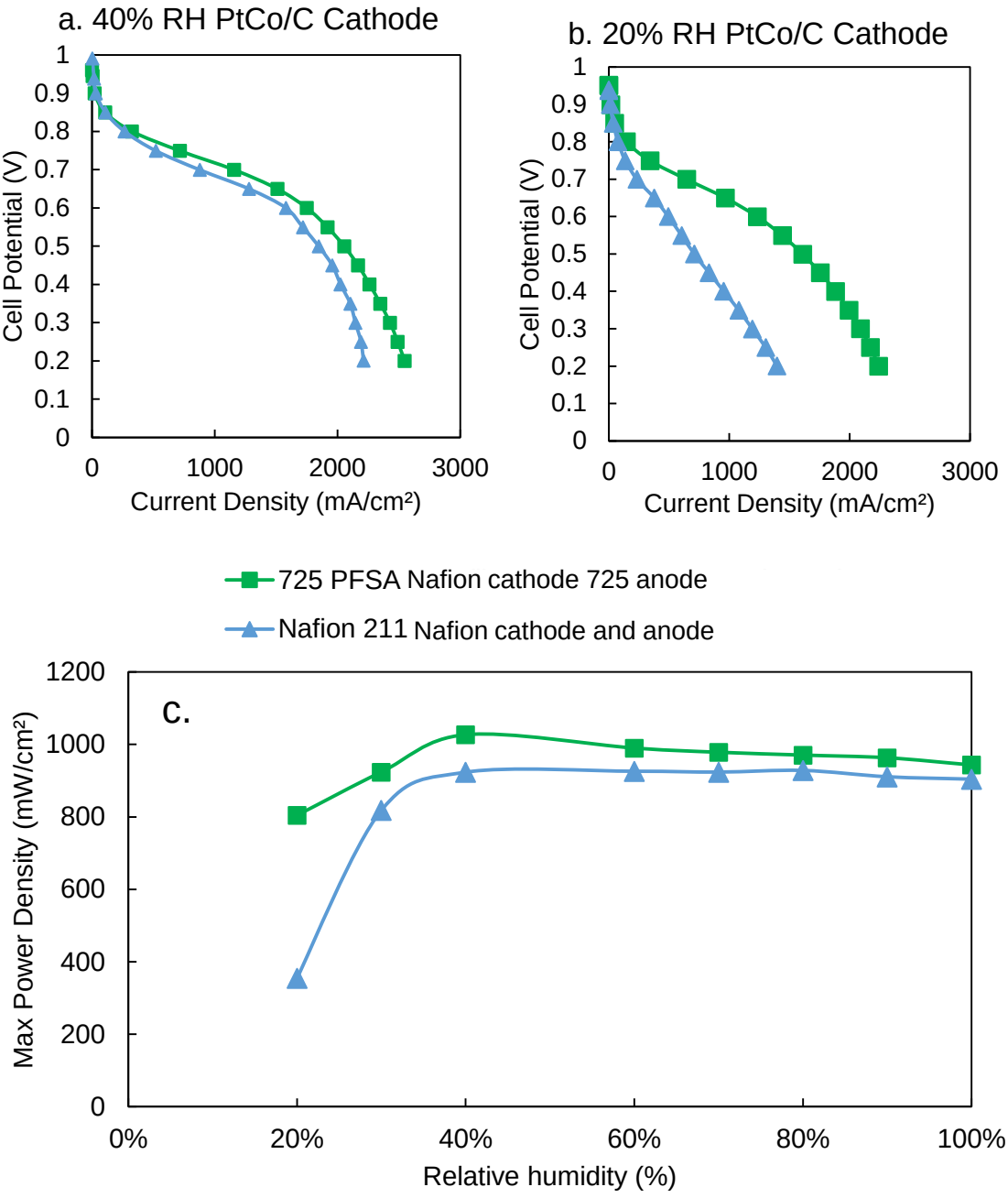

Figure 5.23. Power vs RH for a fully electrospun MEA containing Nafion as the cathode binder, 725 EW PFSA as the membrane and anode ionomer. Operating conditions are 200 kPa (abs), 125/500 sccm H_2/air, 80 °C PtCo/C. Cathode: anode/cathode loading: 0.1 mg/cm² ± 0.005. Square symbols represent the fully electrospun MEA with a 725 EW PFSA anode binder and Nafion cathode binder with an 80/20 725EW PFSA/ PVDF 20 micron membrane. Triangular symbols represent the Nafion binder nanofiber electrode MEA with a Nafion 211 membrane.

This MEA produced over 800 mW/cm^2 at 20% RH, and over 1000 mW/cm^2 at 40% RH. More work must be done to reproduce these results and to determine a number of factors including SEM images of the electrode, STEM cross sectional images of the electrode material with 725 PFSA to see if there is still a core/shell structure, determine the optimal ratios of 725 PFSA to catalyst in the electrode, and to alter the membrane thickness (i.e. create a thinner membrane).

RH dependence after a metal dissolution AST

After a metal dissolution voltage cycling AST at 100% RH, the power density remains invariant with RH, just as before the AST. This is shown in Figure 5.24 for both the maximum power and the power at 0.65 V. As expected, the power density at 0.65 V is less than maximum power and the power at EOL is less than the power at BOL.

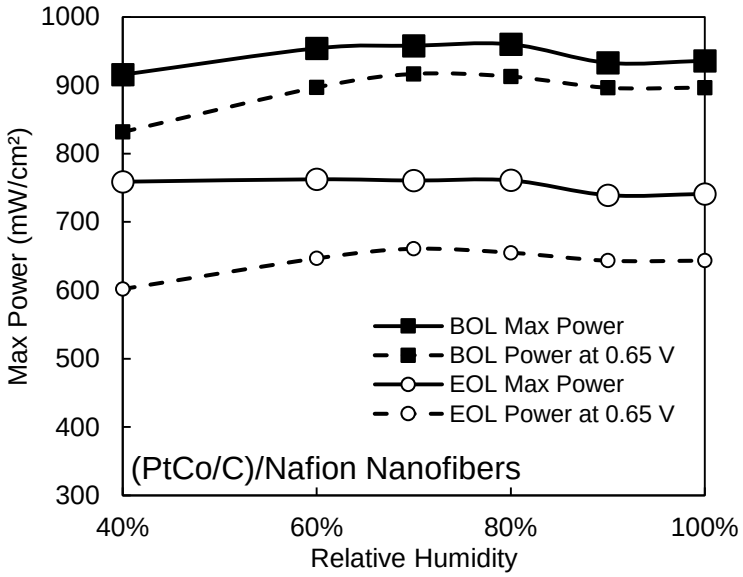

Figure 5.24. Maximum Power vs RH for a (PtCo/C)/Nafion nanofiber cathode MEA before and after a metal dissolution AST Experiment: square wave potential cycle between 0.60 V and 0.95 V for 30,000 cycles. Operating conditions: 80 °C, 200 kPa, 125/500 sccm. AST was run at 80 °C, 100% RH in H_2/N_2 at 100/100 sccm.

ORR kinetics at low RH: The kinetics of the oxygen reduction reaction (ORR) at a Pt/C cathode in a fuel cell MEA are slower as the relative humidity (RH) of the cell is decreased; an empirical model has been developed to fit the Tafel slope for the oxygen reduction reaction kinetic data as a function of RH.[31,32]

$$Tafel\ Slope = \frac{2.303RT}{\alpha_o n_{\alpha o} F} \quad \text{(Equation 5.1)}$$

$$Transfer\ coefficient:$$
$$\alpha_o = (0.0011552RH + 0.000139)T \quad \text{(Equation 5.2)}$$

Where R is the ideal gas constant (8.314 J/mol·K), T is temperature (K), α_o is the transfer coefficient, the $n_{\alpha o}$ is the number of electrons in the reaction, and F is Faraday's constant (96485 C/mol). The Tafel slope of a slurry cathode with Pt/C catalyst and neat Nafion binder at various values of RH was determined at Vanderbilt University by collecting current/voltage data with pure oxygen at unit activity O_2 and plotting the potential and the current on a semi-log plot. The temperature of the experiment was 80 °C. To maintain unit activity O_2 (100 kPa oxygen pressure), the total pressure was changed to match the vapor pressure of water, e.g., at 100% RH and 80 °C, the vapor pressure of water is 47 kPa, so the total pressure was set at 147 kPa. Table 5.6 shows the vapor pressure of water at different RH values and the corresponding back pressure that was applied in a Tafel Slope experiment. The relative humidity for the anode and cathode was the same for each Tafel slope determination and the gas flow rates were fixed at 100/100 sccm H_2/O_2. Measured currents were corrected for the hydrogen crossover current, where crossover was measured

in a separate linear sweep voltammetry experiment at each RH (total pressure) condition using H_2 at the anode and N_2 at the cathode where the two cases are humidified and with back pressure according to Table 5.6. Measured voltages were corrected by first measuring the high frequency resistance (HFR) in an EIS experiment at a given relative humidity and then using the HFR values to correct the voltage for ohmic overpotential at a given current (where the overpotential was found by multiplying the HFR and current).

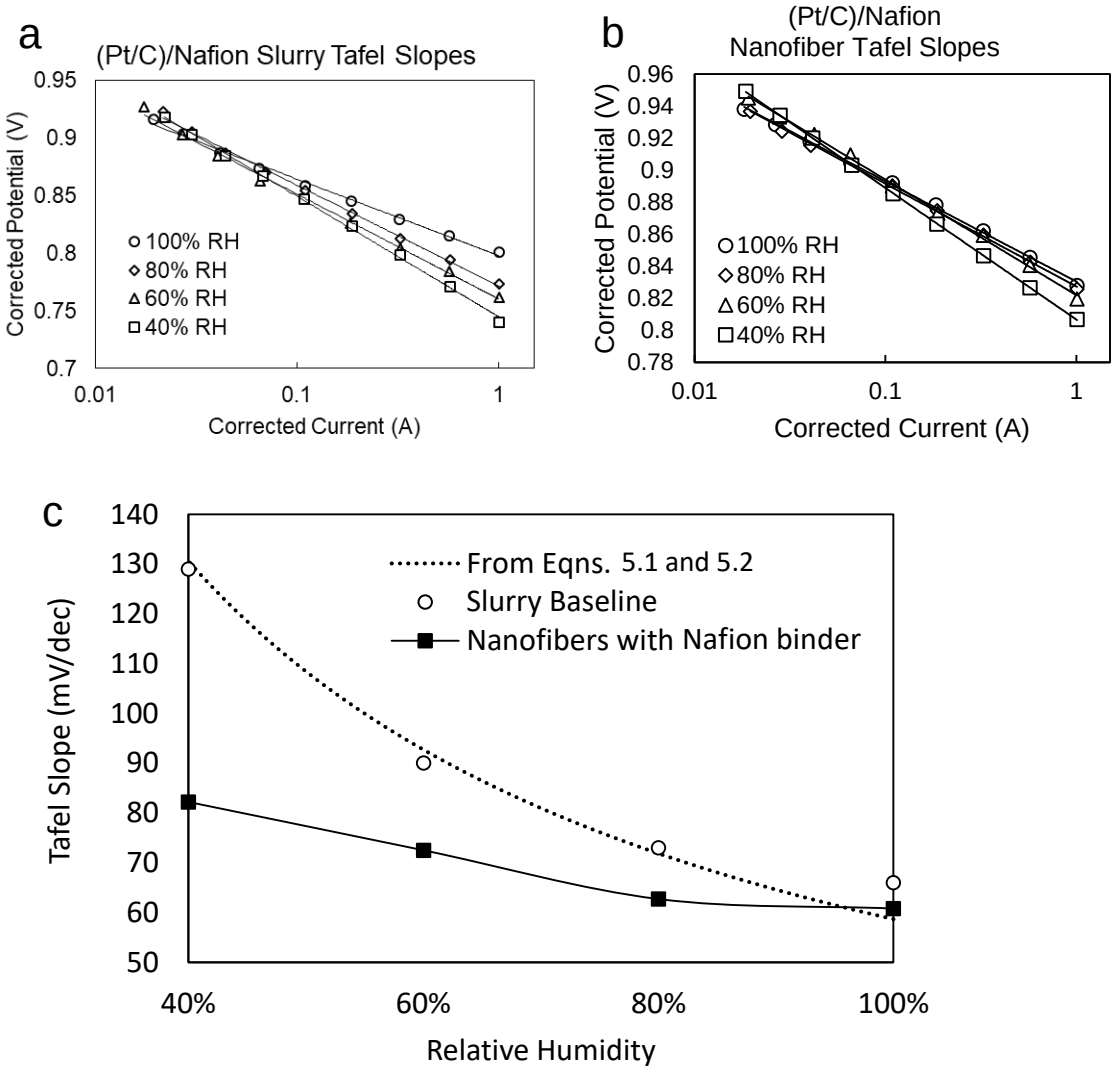

Figure 5.25. (a) Measured ORR Tafel slopes collected at unit activity O_2 for a painted slurry electrode MEA and (b) ORR Tafel slopes for a nanofiber electrode MEA with a Nafion binder spun from a Nafion/PEO ink. (c) Tafel slopes of a baseline slurry MEA, a

nanofiber MEA and the predicted values plotted against relative humidity. ORR data was collected at 80 C, 100/100 sccm H_2/O_2, and the pressures given in Table 5.6.

Table 5.6 vapor pressure of water at different relative humidity and the corresponding back pressure applied during the measurement of the Tafel slope

RH	Water vapor pressure (kPa)	Back pressure applied (kPa)
100%	47	147
80%	38	138
60%	28	128
40%	19	119

For the Tafel slope experiments, 5 cm² MEAs were used, where the cathode and anode catalyst loading was 0.1 mg_{Pt}/cm^2, the membrane was Nafion 211, the GDLs were Sigracet 29BC, and the gasket material was silicon reinforced Teflon. Current-voltage Tafel plots for the baseline slurry cathode MEA and a nanofiber MEA with a Nafion binder (fibers prepared from a Nafion/PEO ink) at four different relative humidities are shown in Figures 5.25a and 5.25b, respectively. A comparison of the resulting Tafel slopes as a function of RH and a comparison of the measured data with those predicted from Equations 5.1 and 5.2 are shown in Figure 5.25c. There are two important conclusions from this study: (1) The ORR Tafel slopes from the slurry cathode MEA match those predicted from the correlations developed in reference [33] for the relative humidities between 40% and 100% and (2) the Nafion nanofiber electrodes exhibited a lower Tafel slope, indicating faster ORR kinetics. The implication is that the Nafion fiber cathode retains water better at lower RH. This hypothesis is explored further in the next section.

Pore Size Distribution in Nanofiber Electrodes: Using scanning transmission electron microscopy, the cross sections of both a Nafion/PAA nanofiber and a Nafion nanofiber were analyzed for porosity. In total, 8 cross sections were analyzed for each type of

nanofiber (16 total images were analyzed). An example of each type of nanofiber cross section is provided in Figure 5.26. Porosity was determined using ImageJ and binarizing the image to return void-space or solid space. From these areas, void-space porosity was calculated. These images were collected at Oak Ridge National Laboratory (ORNL) using the FEI Talos scanning transmission electron microscope. The overall measured porosity for the Nafion/PAA nanofibers was 29% ± 1% while the overall porosity of the Nafion nanofibers was 31% ± 1%. Therefore, there was essentially the same overall porosity for the two fiber types. This result is in agreement with the STEM 3D reconstruction analysis of the Nafion/PAA tomography images which suggested that 30% of the surface area is due to internal porosity (as previously discussed in Figure 4.3 of Chapter 4 of this dissertation). The catalyst/binder composition for each fiber was 55% catalyst 45% binder for the Nafion/PAA fibers (I/C = 1.08) and 52% catalyst, 48% binder for the Nafion fibers (I/C = 1.15). If all of the PEO is removed, the resultant composition is 62% catalyst and 38% binder. The ratio of the Nafion/PAA was 2/1 whereas the ratio of the Nafion/PEO was 3.5/1. The catalyst used in each case was PtCo/C.

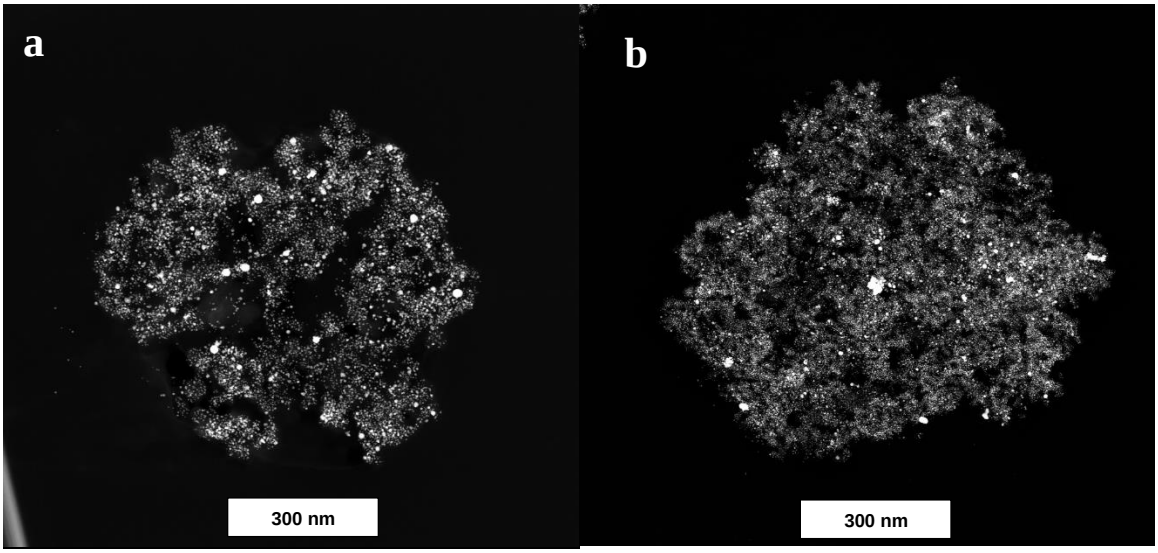

Figure 5.26. STEM imaging of nanofiber cross sections that generated the porosity data with a PtCo/C catalyst for (a) a Nafion/PAA nanofiber and (b) a Nafion binder nanofiber.

The size of pores in digitized STEM fiber cross sections was estimated using ImageJ software. The resulting pore-size distributions are plotted in Figure 5.27(a). The results show that the Nafion cathode nanofibers prepared from a Nafion/PEO ink contain smaller pores, on average, than the Nafion/PAA cathode nanofibers. A portion of the pores in both fibers could be small enough for water condensation where the maximum (critical) pore size for water condensation was estimated from the Kelvin Equation[34],

$$\ln \frac{p}{p_0} = \frac{2\gamma V_{\mathrm{m}}}{rRT}$$

(Equation 5.3)

In Equation 5.3, γ is the surface tension of water at 80 °C (0.0626 N/m), V_m is the partial molar volume of water at 80 °C (0.0185 L/mol), R is the ideal gas constant 8314.4 (L Pa K^{-1} mol^{-1}), r is radius (m), and T is the temperature of interest in Kelvin 353 (80 °C). A plot of critical pore size for water condensation vs. pressure at 80 °C, from Equation 5.3 is shown in Figure 5.27(b). According to this analysis, water will condense in pores smaller than 1.2 nm in dimeter at 200 kPa pressure.

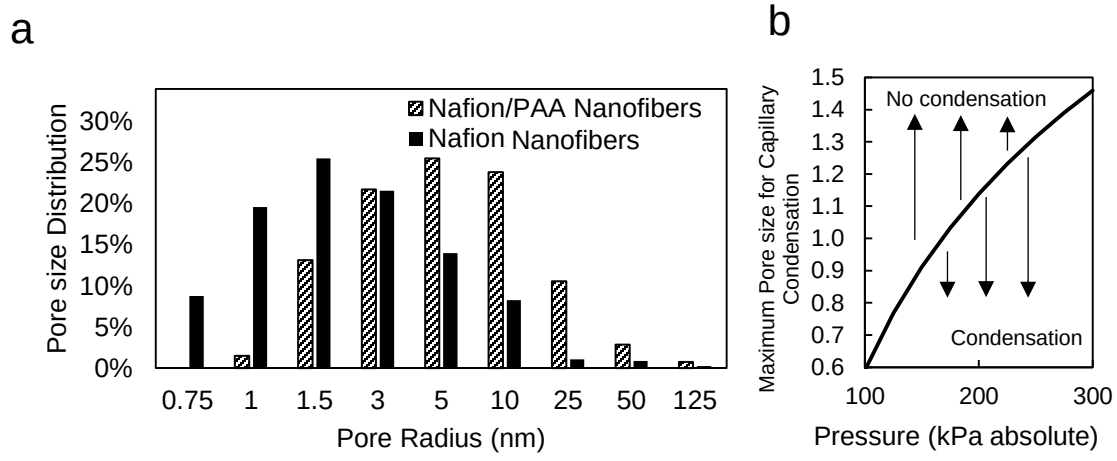

Figure 5.27. (a) Pore size distribution for a Nafion/PAA nanofiber and a Nafion nanofiber. (b) The maximum pore size to condense water via capillary condensation at 80 C according to the Kelvin equation.

As shown in Figure 5.27a, at 200 kPa absolute, ~25% of the pores within the carrier-free Nafion nanofiber cathode and are sufficiently small to condense water whereas water will condense in only 5% of the pores in a Nafion/PAA cathode fiber. This analysis provides one possible explanation as to why nanofiber MEAs with Nafion binder (electrospun from Nafion/PEO inks) have high power and fast ORR kinetics at low RH; they simply hold water via capillary condensation at low RH. This analysis assumes that the size distribution of pores in dry fibers (under vacuum) is the same as that in a hydrated fiber mat electrode. This may be the case because catalyst particles in a fiber (at a very high concentration of 50-70 wt.%) will act as physical cross-linkers and minimize/limit Nafion swelling. Additionally, the Kelvin equation assumes that the surface tension of water is equivalent to that of bulk water which may not be the case in pores where there may be interactions of water with sulfonic acid sites of Nafion. For these reasons, this analysis is a first approximation and more experiments are necessary to further explore the capillary condensation effect in electrospun fibers.

Figure 5.28a confirms this behavior; there is a significant drop in current density at any given voltage comparing 100 kPa to 200 kPa absolute pressure at 40% RH. This dramatic difference is not seen at 100% RH in Figure 5.28b where there is ample water to provide hydration to keep the ionomer conductive. The hypothesis is as follows: power density is improved at low relative humidity in Nafion nanofibers because these nanofibers are holding onto water better than Nafion/PAA due to capillary condensation. This capillary condensation depends on the pressure being elevated according to the Kelvin equation. At ambient pressure, the predicted pore size for capillary condensation is ~0.6 nm; this value is smaller than the measured pore sizes in the Nafion nanofiber cross section.

Based on this analysis, the current generation at low RH should be significantly worse at ambient pressure conditions (where minimal capillary condensation can occur). As is observed in Figure 5.28a, there is a larger difference between 100 kPa and 200 kPa at 40% RH due (presumably) to the increased condensation of water and improved Ohmic region.

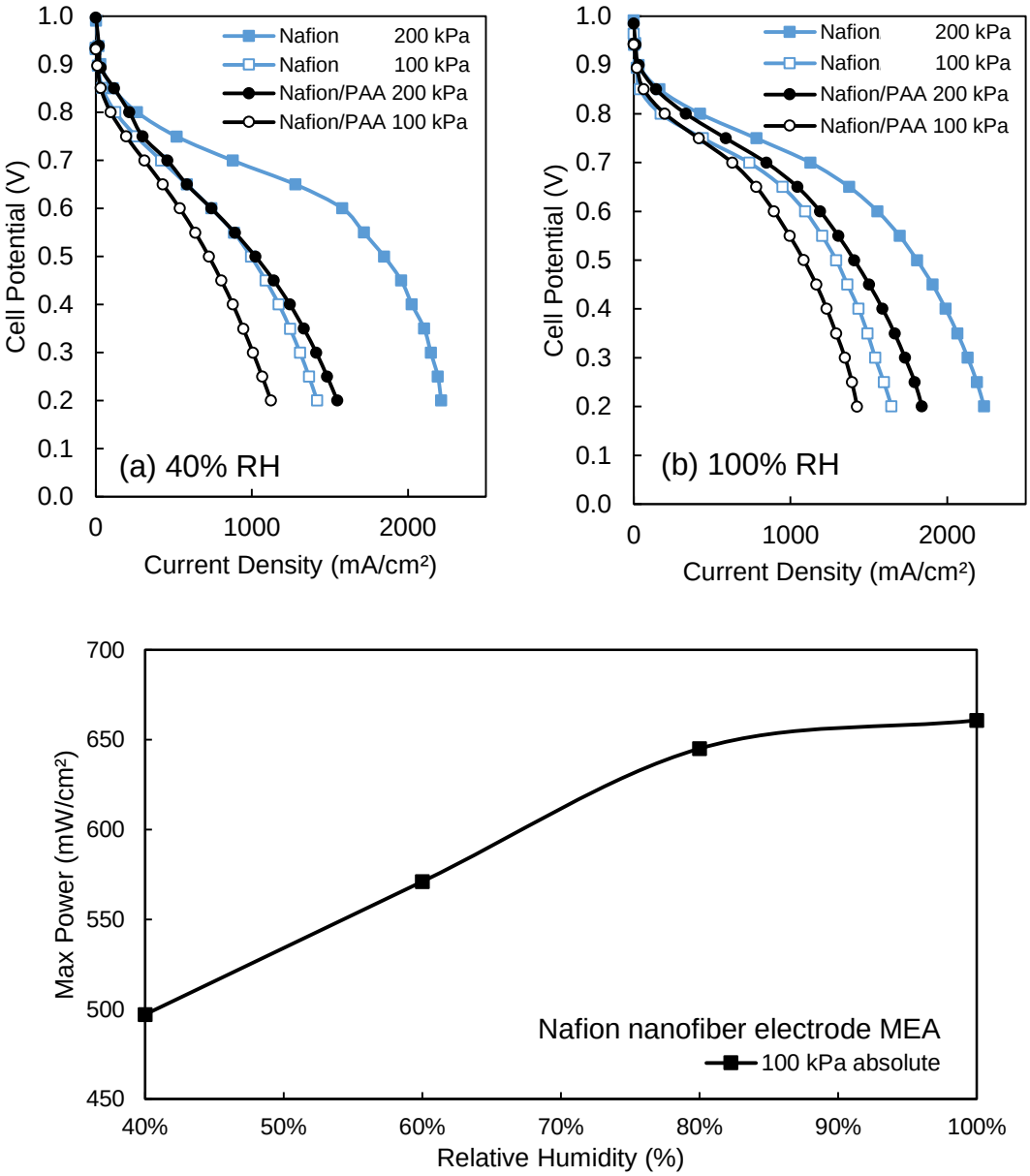

Figure 5.28 (a) Polarization data showing pressure effects at 40%RH, (b) Polarization data showing pressure effects at 100%RH for Nafion/PAA nanofibers and Nafion nanofibers. (c) Max power vs RH at ambient pressure for a PtCo/C cathode catalyst and a Nafion binder at both the anode and cathode for 100 kPa (ambient) pressure and 200 kPa pressure. For

all parts: anode/cathode catalyst loading is 0.1 mg/cm^2, operating conditions are 125/500 sccm H_2/air, 80 °C.

Finally, there is a stark difference in the measured MEA HFR at 40% for 100 kPa and 200 kPa back pressure. At 40% RH, the Nafion MEA under ambient pressure (100 kPa) exhibits an HFR of 161 mΩ·cm^2 whereas under 200 kPa pressure, the same MEA exhibits 71 mΩ·cm^2. That is to say the HFR decreases by more than half when increasing pressure from 100 kPa to 200 kPa at 40% RH whereas MEAs with Nafion/PAA do not show a change in HFR for 100 kPa and 200 kPa. This indicates that the MEA is significantly more hydrated at 200 kPa compared to 100 kPa.

5.4 Conclusions

A new electrospinning ink was used to prepare Pt/C and PtCo/C fiber electrodes where the spinning solution contained Nafion and polyethylene oxide as the carrier. The carrier polymer for these nanofiber electrode was successfully removed. This was proven using NMR to directly observe PEO in an electrode soak water after 1 hour at 80 °C. Slurries made from Nafion/PEO inks did not drastically improve power density over neat Nafion slurries, but there was an improvement in MEA power when PEO was removed from nanofibers. The resulting nanofibers exhibited a drastically different radial distribution of Nafion and catalyst as compared to a Nafion/PAA nanofiber with an enrichment of Nafion toward the outer fiber surface. There was an improvement in power density with Nafion binder nanofiber electrode MEAs as compared to Nafion/PAA nanofiber electrode MEAs. The best performing MEAs used as Nafion nanofiber electrodes obtained from a Nafion/PEO ink at both the anode and the cathode. Nanofiber electrodes with Nafion also showed lower ionomer resistance compared to Nafion/PAA nanofiber electrode MEAs.

The Nafion binder nanofibers electrode MEA showed faster ORR kinetics at low RH compared to a slurry electrode MEA due presumably to better water retention. STEM imaging also shows a smaller average pore size in the interior of the Nafion nanofiber compared to a Nafion/PAA nanofiber. The pore sizes measured in vacuum appear to be small enough for capillary condensation of water at elevated pressures.

5.5 References

[1] W. Zhang, P. N. Pintauro, *ChemSusChem* **2011**, *4*, 1753.

[2] M. Brodt, R. Wycisk, P. N. Pintauro, *J. Electrochem. Soc.* **2013**, *160*, F744.

[3] A. Kusoglu, A. Z. Weber, *Chem. Rev.* **2017**, *117*, 987.

[4] C. Welch, A. Labouriau, R. Hjelm, B. Orler, C. Johnston, Y. S. Kim, *ACS Macro Lett.* **2012**, *1*, 1403.

[5] Ballengee, Electrospun nanofiber composite proton exchange membranes, Vanderbilt University, 2013.

[6] H. Chen, J. D. Snyder, Y. A. Elabd, *Macromolecules* **2008**, *41*, 128.

[7] M. W. Brodt, ELECTROSPUN NANOFIBER ELECTRODES FOR HYDROGEN/AIR PROTON EXCHANGE MEMBRANE FUEL CELLS, Vanderbilt University, 2015.

[8] J. Choi, K. M. Lee, R. Wycisk, P. N. Pintauro, P. T. Mather, *J. Mater. Chem.* **2010**, *20*, 6282.

[9] M. Brodt, T. Han, N. Dale, E. Niangar, R. Wycisk, P. Pintauro, *J. Electrochem. Soc.* **2014**, *162*, F84.

[10] H. A. Gasteiger, S. S. Kocha, B. Sompalli, F. T. Wagner, Activity benchmarks and requirements for Pt, Pt-alloy, and non-Pt oxygen reduction catalysts for PEMFCs. *Appl. Catal. B Environ.* **2005**, *56*, 9–35.

[11] U.S. Department of Energy, *Annu. Prog. Rep.* **2014**.

[12] A. Kongkanand, M. F. Mathias, *J. Phys. Chem. Lett.* **2016**, *7*, 1127.

[13] R. Kensaku Kodama, Akihiro Shinohara, Naoki Hasegawa, Kazuma Shinozaki, Y. M. Jinnouchi, Takahisa Suzuki, Tatsuya Hatanaka, *ECS Trans.* **2013**, *58*, 363.

[14] M. C. B. Kienitz, J. Kolde, S. Priester, C. Baczkowski, *Trans. E C S Soc. Electrochem.* **2011**, *41*, 1521.

[15] X. Zhu, H. Zhang, Y. Zhang, Y. Liang, X. Wang, **2006**, 14240.

[16] R. Wycisk, P. N. Pintauro, J. W. Park, *Curr. Opin. Chem. Eng.* **2014**, *4*, 71.

[17] I. Ezzell, R. Bobby, L. Jackson, P. William, Low Equivalent Weight Sulfonic Fluoropolymers **1987**.

[18] C. Laberty-Robert, K. Vallé, F. Pereira, C. Sanchez, *Chem. Soc. Rev.* **2011**, *40*, 961.

[19] L. Dos Santos, M. Maréchal, A. Guillermo, S. Lyonnard, S. Moldovan, O. Ersen, O. Sel, H. Perrot, C. Laberty-Robert, *Adv. Funct. Mater.* **2016**, *26*, 594.

[20] M. M. Saleh, T. Okajima, M. Hayase, F. Kitamura, T. Ohsaka, *J. Power Sources* **2007**, *164*, 503.

[21] L. Xin, F. Yang, J. Xie, Z. Yang, N. N. Kariuki, D. J. Myers, J.-K. Peng, X. Wang, R. K. Ahluwalia, K. Yu, P. J. Ferreira, A. M. Bonastre, D. Fongalland, J. Sharman, *J. Electrochem. Soc.* **2017**, *164*, F674.

[22] D. Spernjak, R. Mukundan, R. L. Borup, L. G. Connolly, B. I. Zackin, V. De Andrade, M. Wojcik, D. Y. Parkinson, D. L. Jacobson, D. S. Hussey, K. L. More, T. Chan, A. Z. Weber, I. V Zenyuk, *Appl. Energy Mater.* **2018**.

[23] J. Zhang, Y. Tang, C. Song, Z. Xia, H. Li, H. Wang, J. Zhang, *Electrochim. Acta* **2008**, *53*, 5315.

[24] Y. Liu, M. W. Murphy, D. R. Baker, W. Gu, C. Ji, J. Jorne, H. A. Gasteiger, *J. Electrochem. Soc.* **2009**, *156*, B970.

[25] J. Mishler, Y. Wang, R. Lujan, R. Mukundan, R. L. Borup, *J. Electrochem. Soc.* **2013**, *160*, F514.

[26] T. Soboleva, K. Malek, Z. Xie, T. Navessin, S. Holdcroft, *ACS Appl. Mater. Interfaces* **2011**, *3*, 1827.

[27] R. Makharia, M. F. Mathias, D. R. Baker, *J. Electrochem. Soc.* **2005**, *152*, A970.

[28] M. C. Lefebvre, *Electrochem. Solid-State Lett.* **1999**, *2*, 259.

[29] P. Xiao, J. Li, H. Tang, Z. Wang, M. Pan, *J. Memb. Sci.* **2013**, *442*, 65.

[30] M. Breitwieser, T. Bayer, A. Büchler, R. Zengerle, S. M. Lyth, S. Thiele, *J. Power Sources* **2017**, *351*, 145.

[31] J. Zhang, C. Song, J. Zhang, R. Baker, L. Zhang, *J. Electroanal. Chem.* **2013**, *688*, 130.

[32] C. Song, J. Zhang, *PEM Fuel Cell Electrocatal. Catal. Layers Fundam. Appl.* **2008**, 89.

[33] H. Xu, Y. Song, H. R. Kunz, J. M. Fenton, *J. Electrochem. Soc.* **2005**, *152*, A1828.

[34] Sir William Thomson, *Philos. Mag.* **1871**, *4*, 448.

CHAPTER 6

RELATING THE STRUCTURE OF NAFION/PVDF-BASED ELECTRODE MEAS TO THEIR INCREASED DURABILITY

6.1 Introduction

Durability is an important consideration in the design of new materials and structures for proton exchange membrane fuel cell membrane electrode assemblies (MEAs). The methods of characterizing durability include electrochemical analyses[1–3], morphological observations[2,4,5], elemental analysis[6], and atomic structure analysis[7]. Factors that influence degradation include the type of catalyst used, the support material of the catalyst, and the ionomer/interfacial contact.[8] Durability has improved in recent years by utilizing a number of strategies including modifying/altering the catalyst support material[9], eliminating the carbon support[10], using a nanofiber cathode structure[11–13], and incorporating a highly hydrophobic component to the electrode binder.[14] Each of these strategies has improved the retention of beginning of life (BOL) power density at the end of life (EOL). In previous work, Pintauro and coworkers showed that adding polyvinylidene fluoride (PVDF) to a traditional slurry or nanofiber electrode drastically improved the durability of the electrodes during a carbon corrosion accelerated stress test.[14]

The purpose of the present investigation is to more clearly explain the improved durability of membrane electrode assemblies (MEAs) with binders containing PVDF. Previous studies regarding the structure of catalyst layers after a carbon corrosion voltage cycling accelerated stress test (AST) have focused on catalyst coarsening/agglomeration, loss of hydrophobic character, generation of carbon-oxygen moieties, a decrease in

electrical conductivity of the catalyst support, a decrease in graphitic content, decrease in the size of large electrode pores, and a decrease in overall catalyst layer thickness.[15–18] Uchida et al. described PEMFC catalyst layers as having two distinctive pore size distributions – primary pores with a diameter smaller than 0.1 μm and secondary pores larger than 0.1 μm.[19] Pore size decrease resulting from catalyst layer collapse after a carbon corrosion AST refers to secondary pores. This phenomenon is addressed in the current study on a series of nanofiber and slurry cathode MEAs which contain either neat Nafion, Nafion/PAA, or Nafion/PVDF as the cathode catalyst binder.

One method of electrode analysis is to image a cathode structure before and after the carbon corrosion accelerated stress test protocols as defined by the U.S. Department of Energy.[20] In the present study, SEM and TEM images are related to polarization data, electrochemically active surface area (ECSA), and mass activity to demonstrate the impact of PVDF on retaining the cathode structure and performance after a carbon corrosion voltage cycling accelerated stress test (AST).

6.2 Experimental

6.2.1 MEA Preparation and Degradation

MEAs were used from the previously published study by Brodt et al.[14] All cathodes were prepared by Brodt using Johnson Matthey Pt-supported on HiSPEC 4000 carbon. Nanofiber inks contained a solids content (catalyst and binder) of 15wt.%. Slurry inks contained solids content of 5wt.%. The dry components of the ink for each MEA are given in Table 1. For inks containing PVDF, the solvent system was either dimethylformamide (DMF)/acetone or DMF/tetrahydrofuran (THF)/acetone. Otherwise, the ink solvent system was alcohol/water. Catalyst and high-boiling solvent (either DMF or water) were combined

and the mixture was sonicated for 30 minutes. Then additional solvent and the polymer components were added and sonicated again for 1 hour. Finally, the ink was allowed to mix overnight using a mechanical stirrer. Inks intended for electrospinning were drawn into a 3 mL syringe, capped with a 22 gauge metal needle, and placed into a syringe pump as part of the electrospinning apparatus (described previously.[11,14,21]) The electrospinning conditions for inks prepared with PVDF require an environment of high relative humidity (50%-70% RH at ambient temperature), a needle-to-collector distance of 10 cm, a syringe pump flow rate of 1.0 mL/hr and a voltage bias in the range of 12–15 kV. Once electrospun, the free-standing nanofiber electrode material was cut into 5 cm^2 pieces and hot-pressed onto a Nafion 211 membrane to form the final MEA for testing. The anode for all MEAs was an electrospun nanofiber electrode with Nafion/PAA binder with a composition of 64/24/12 wt.% (Pt/C)/Nafion/PAA, corresponding to an ionomer to carbon ratio of 1.16. Cathodes with PVDF contained 70% catalyst content corresponding to an ionomer to carbon ratio of 0.88. The cathode and anode catalyst loading was always 0.1 mg_{Pt}/cm^2.

Table 6.1. Membrane electrode assemblies prepared for characterization (two of each was prepared to analyze the beginning of life (BOL) structure and end of life (EOL) structure).

MEA	**Dry Cathode Composition (weight %)**	**Cathode Type**	**Ink solvents**
1. BOL 2. EOL	70 catalyst / 30 PVDF	nanofiber	DMF/acetone
3. BOL 4. EOL	70 catalyst / 10 Nafion / 20 PVDF	nanofiber	DMF/THF/acetone
5. BOL 6. EOL	70 catalyst / 15 Nafion / 15 PVDF	nanofiber	DMF/THF/acetone
7. BOL 8. EOL	70 catalyst / 24 Nafion / 6 PVDF	nanofiber	DMF/THF/acetone
9. BOL 10. EOL	64 catalyst / 24 Nafion / 12 PAA	nanofiber	Alcohol/water
11. BOL 12. EOL	70 catalyst /15 Nafion / 15 PVDF	slurry	DMF/THF/acetone
13. BOL	64 catalyst / 24 Nafion / 12 PAA	slurry	Alcohol/water

14. EOL			
15. BOL 16. EOL	70 catalyst / 30 Nafion	slurry	Alcohol/water

6.2.2 Electrochemical Characterization

After fabrication, each 5 cm² MEA was individually tested in a Scribner Associates Inc. 850e single cell test station using a test fixture with a single serpentine flow channel. MEAs were conditioned at 80 °C and ambient pressure by alternating potentiostatic and galvanostatic holds for two minutes each at 150 mA/cm^2 and 0.2 V. This was performed until steady state was reached (~3 hours). The MEA is now considered to be at beginning of life (BOL) (i.e. after conditioning and before the AST). At this point, polarization data were collected at ambient pressure, 80 °C, and with fully humidified hydrogen and air streams with flow rates of 125 sccm and 500 sccm, respectively. Cathode mass activity was obtained at 150 kPa$_{abs}$, 80 °C, 100 sccm H_2 and O_2 using a current-controlled scan from high to low current (1.0 A to 0.01 A at four points/decade for a total of 8 points). Mass activities were determined as current normalized to mass (from a loading of 0.1 mg$_{Pt}$/cm^2) at 0.9 V by plotting the IR-free voltage (corrected from a separate HFR measurement) against hydrogen-crossover corrected current densities.[22] Electrochemical surface area was obtained from the area corresponding to hydrogen adsorption from a cyclic voltammogram, where the fuel cell was operating at 30 °C and 100% RH, with a nitrogen-purged cathode and a hydrogen-feed of 100 sccm at the anode.[23]

After collecting all BOL data, MEAs underwent a carbon corrosion accelerated stress test (AST). As originally outlined by the fuel cell commercialization conference of Japan[24] and the United States Department of Energy[25], the voltage at the cathode was cycled

between 1.0 and 1.5 V at a scan rate of 500 mV/s with a triangular voltage wave for 1,000 cycles. This number of cycles was chosen because it was sufficient to determine a difference between the types of electrodes used. The operating conditions during the AST were 80 °C, ambient pressure, 100% RH, and feed-gases were 125 standard cubic centimeters per minute (sccm) hydrogen at the anode and 250 sccm nitrogen at the cathode. The voltage cycling was performed by an external potentiostat (Gamry Instruments Reference 3000). For the duration of the AST, as the carbon supported is oxidized into carbon dioxide as shown in Reaction 6.1, this emitted CO_2 was monitored from the cathode outlet using an infrared CO_2 detector from CO_2 Meter Inc. (Model No. CM-0152).

$$C + 2H_2O \rightarrow CO_2 + 4H^+ + 4e^- \qquad \text{Reaction 6.1}$$

6.2.3 Electron Microscopy Characterization

The series of membrane electrode assemblies (MEAs) shown in Table 1 were characterized at BOL and EOL for cathode catalyst layer (CL) thinning, and changes in pore-size distribution. Samples were prepared for analysis by diamond-knife ultramicrotomy. For each sample, an approximately 100 micron cross section of MEA was imaged using a Hitachi S4800 scanning electron microscope (SEM) with an yttrium aluminum garnet (YAG) scintillator detector for backscatter electrons (BSE). Across this section of MEA, three 10,000 x magnification images were taken of the CL to obtain a representative average thickness and to measure variation in thickness along the length of the CL. Each of these images was analyzed for thickness using FIJI ImageJ software by taking 15 measurements per image for a total of 45 separate measurements to obtain a statistically significant CL thickness. This process was performed for both BOL and EOL MEAs.

Scanning transmission electron microscopy (STEM) was performed using an FEI Talos F200X to obtain high resolution images of the cathode at BOL and EOL for porosity determinations. Porosity measurements are made by using FIJI ImageJ, to obtain a distribution of pore-size in a cathode cross section. The images were first binarized such that each pixel returns either a signal of black or white. In each case, white pixels corresponded to solid particles (either platinum, carbon, Nafion, or PVDF) and black pixels corresponded to void-space. The void space areas were summed up using a "classic watershed" algorithm which is designed to mark boundaries of regions that are segmented based on pixel intensity.[26]

6.3 Results and Discussion

6.3.1 Characterization of Catalyst Layer Thinning

A decrease in the thickness of a cathode catalyst layer (CL) after carbon corrosion voltage cycling indicates several types of damage, including loss of carbon as CO_2, collapse of pores, and platinum agglomeration.[27] These changes affect the electrochemical performance of the cell by reducing ECSA (increasing activation overpotential) and inhibiting access of oxygen to catalyst sites (increasing cathode hydrophilicity, flooding, and mass transport overpotential).[28] Measuring the CL thickness of each MEA in Table 1, provides a deeper understanding of how PVDF binder affects cathode durability. Figure 1 shows the beginning of life and end of life thicknesses of four representative MEAs. Figure 1 (a) and (b) show back-scatter electron (BSE) SEM cross sections of a conventional slurry electrode with neat Nafion which exhibits a >50% decrease in thickness which is consistent with previously published data.[27,29] Watanabe and coworkers noted that corrosion resulted in catalyst layer thickness reduction of 53% accompanied by Pt

detachment from the carbon black support when using a triangular voltage wave AST.[30] Caqué et al. showed that thinning of the cathode catalyst layer in a fuel cell MEA is accompanied by Pt agglomeration, reduction in electrical conductivity due to an increase in carbon-oxygen moieties, and membrane failure near the thinnest portions of the catalyst layer.[27]

Figure 1 (c) and (d) show BSE SEMs of a slurry cathode with a binder of 1:1 Nafion:PVDF. In these images, there is no statistically significant change in the CL thickness. Given that the same type of carbon was used in both slurry electrodes, the retention of the original catalyst layer thickness is unexpected. Figure 1 (e) and (f) show BSE SEMs of a nanofiber cathode MEA with no PVDF, (a standard Nafion/PAA) binder as described in works by Pintauro and coworkers.[11,21] This electrode also shows significant thinning >50%. Figure (g) and (h) show BSE SEMs of a nanofiber electrode with a binder of 1:1 Nafion:PVDF. As was seen in the slurry electrode of the same composition, there was no change in the thickness of the CL. Therefore, MEAs with cathode binders that contain 50% PVDF or more show essentially no thickness change regardless of cathode morphology (e.g. nanofiber or slurry). This coincides well with the enhanced power density retention and lowered CO_2 emission of both nanofiber and slurry cathode MEAs with PVDF as shown by Brodt et al.[14]

Upon closer inspection, the back-scatter electron SEM images (in which a brighter signal corresponds to denser material) show that the distribution of platinum in electrodes that contain Nafion/PVDF is no less uniform at EOL, as compared to BOL. This is not the case in the neat Nafion CL indicating Pt agglomeration previously reported by Dubau et al.[27] Thus, retention of electrode thickness coincides with less Pt agglomeration.

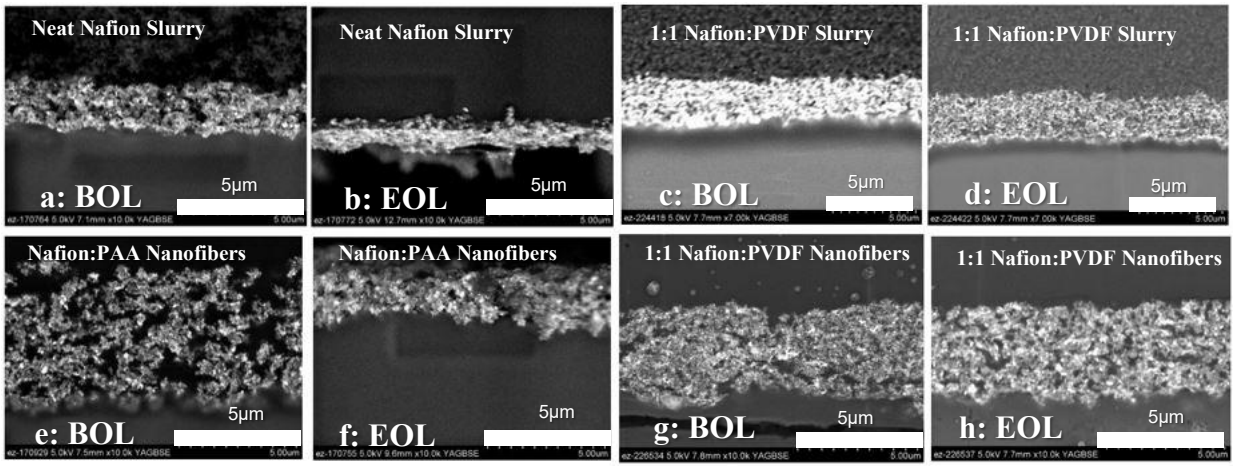

Figure 6.1 Representative cross-sectional back-scatter SEM images of cathode catalyst layers in an MEA: (a) BOL neat Nafion slurry, (b) EOL neat Nafion slurry, (c) BOL 1:1 Nafion:PVDF slurry, (d) EOL 1:1 Nafion:PVDF slurry (e) BOL Nafion:PAA Nanofibers (0% PVDF) (f) EOL Nafion:PAA Nanofibers (0% PVDF) (g) BOL 1:1 Nafion:PVDF Nanofibers, and (h) EOL 1:1 Nafion:PVDF Nanofibers.

The results of measurements made on nanofiber electrodes containing varying amounts of PVDF are shown in Figure 2 and are overlapped with data showing the carbon loss as determined from CO_2 emission in the air exhaust as was measured by Brodt et al.[14]

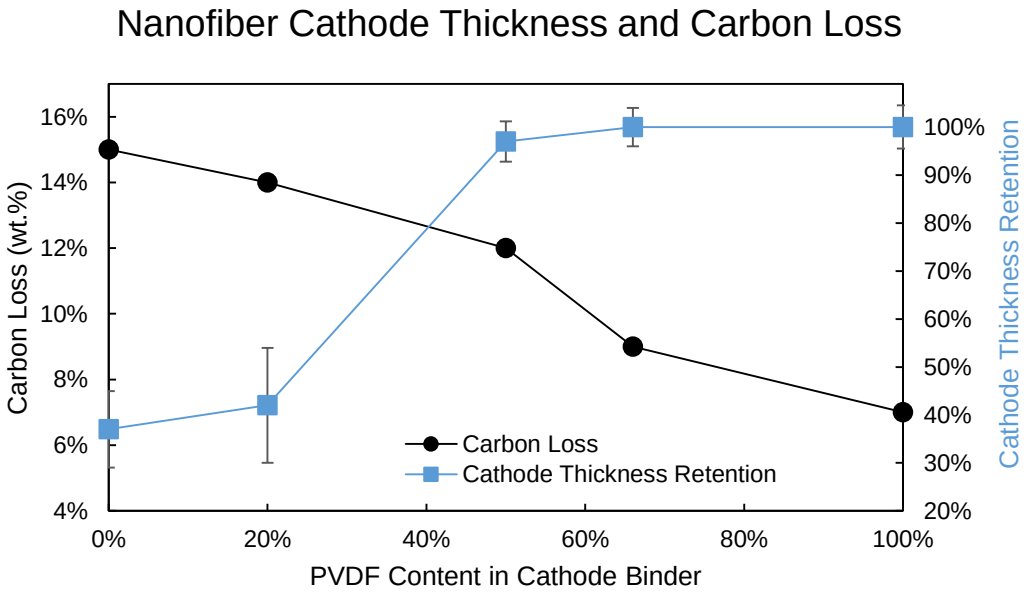

Figure 6.2 Nanofiber electrode carbon loss and retention of cathode thickness as a function of PVDF content. Carbon loss data obtained from Brodt et al.[14]

Each cathode thickness data point in Figure 2 represents 45 distinct measurements in three different areal sections of the cathode CL for each MEA. These large data sets result in a statistically significant thickness measurement after the AST. The observed trends correlate well: there is a greater retention of cathode thickness when there is less carbon loss. This is logical, as a certain amount of the thinning that takes place is due to carbon oxidizing to CO_2 as per Reaction 6.1. The results in Figure 2 show that there is not a direct quantitative correlation between CO_2 generation and thinning. For example, at 50% PVDF content in the cathode binder, a significant amount of carbon is lost as CO_2 (12 wt.%), but thickness does not change. Since carbon from the catalyst support is being lost, the lack of thinning suggests that the PVDF helps to maintain the structural integrity of the CL. This is not seen at lower contents of PVDF which suggests that an optimal amount of PVDF exists to maintain CL thickness. The uncertainty in the CL thickness at low PVDF contents was due to non-uniform thinning. The error bars in Figure 2 were determined by multiplying the standard error (standard deviation/sample size) with the z-value for 95% confidence followed by normalizing to the mean of the thicknesses for each cathode. The statistical significance of the measured CL thicknesses was evaluated using analysis of variance (ANOVA). In this evaluation, the variance of the total measurements was compared to the variance within each MEA CL dataset and to the variance between each MEA CL dataset ($p < 0.01$).

While there is qualitative consistency between the CO_2 generation and catalyst layer thinning observations, fuel cell power loss is greater in painted slurry electrodes relative to nanofiber electrodes of the same Nafion/PVDF composition at both BOL and EOL.[14] Other groups such as Castanheira et al. have been able to mitigate the effects of catalyst

layer thinning through the use of completely graphitic carbon supports[31] or by completely eliminating the carbon support as is the case with the 3M's nanostructured thin film (NSTF) electrodes.[32] Castanheira et al. also observed that the use of a completely graphitic carbon support reduces the degree of agglomeration of the Pt nanocrystals in comparison to a high surface area carbon black support which contains fewer graphitic domains. While graphitized carbon supports retain a greater degree of total electrode surface area after aging, they often have lower ECSA due to hydrophobic surfaces that result in non-optimal Pt distribution.[33] This is in contrast to using a Nafion/PVDF binder with a nanofiber electrode morphology which does not reduce the electrochemically active surface area at BOL as was shown by Brodt et al.[14] Depending on the PVDF content, nanofiber electrodes with this binder lose 20-35% of initial ECSA after a carbon corrosion AST which is a similar loss in ECSA to fully graphitic carbon support and much lower than a traditional high surface area carbon support which can lose up to 80% of its original ECSA.[31]

6.3.2 Porosity Collapse

Porosity measurements from STEM images indicate that there is a much higher retention of porosity in both slurry and nanofiber cathodes containing PVDF after an AST as compared to those with a neat Nafion binder. Figure 3 shows the BOL and EOL STEM images of a Neat Nafion slurry cathode, a 1/1 Nafion/PVDF slurry cathode and a nanofiber cathode with 1/1 Nafion/PVDF binder. Next to each set of images is a histogram which details the pore area calculated from each image. The mean pore areas for the neat Nafion slurry cathode at BOL and EOL are 1180 nm² and 85 nm² respectively. The mean pore areas for the 1/1 Nafion/PVDF slurry electrode are 835 nm² and 779 nm² at BOL and EOL. The mean pore areas for the 1/1 Nafion/PVDF nanofiber electrode are 950 nm² and 1025

nm² at BOL and EOL. Additionally, the average pore size is larger for the nanofiber electrode compared to the slurry electrode of the same composition which explains the differences in performance seen at EOL between these two electrodes – larger pores (i.e. secondary pores as described by Uchida et al.)[30] act as channels that allow for oxygen access and better water removal. Retention of CL porosity, or in this case an increase in CL porosity, is associated with improved MEA mass transport properties.[34],[33]

The slight increase in porosity observed for the nanofiber electrode is consistent with the observations of carbon loss and thickness retention. This is also consistent with the observed polarization data at EOL shown in Figure 6.4. This polarization data clearly shows that the neat Nafion slurry cathode MEA exhibits a sharper decline in current density at low voltages (below 0.35 V) whereas no such decline is observed in the nanofiber electrode MEA with PVDF. This indicates a difference in EOL mass transport properties and suggests that the neat Nafion slurry cathode MEA has a flooding issue whereas the Nafion/PVDF nanofiber cathode does not.

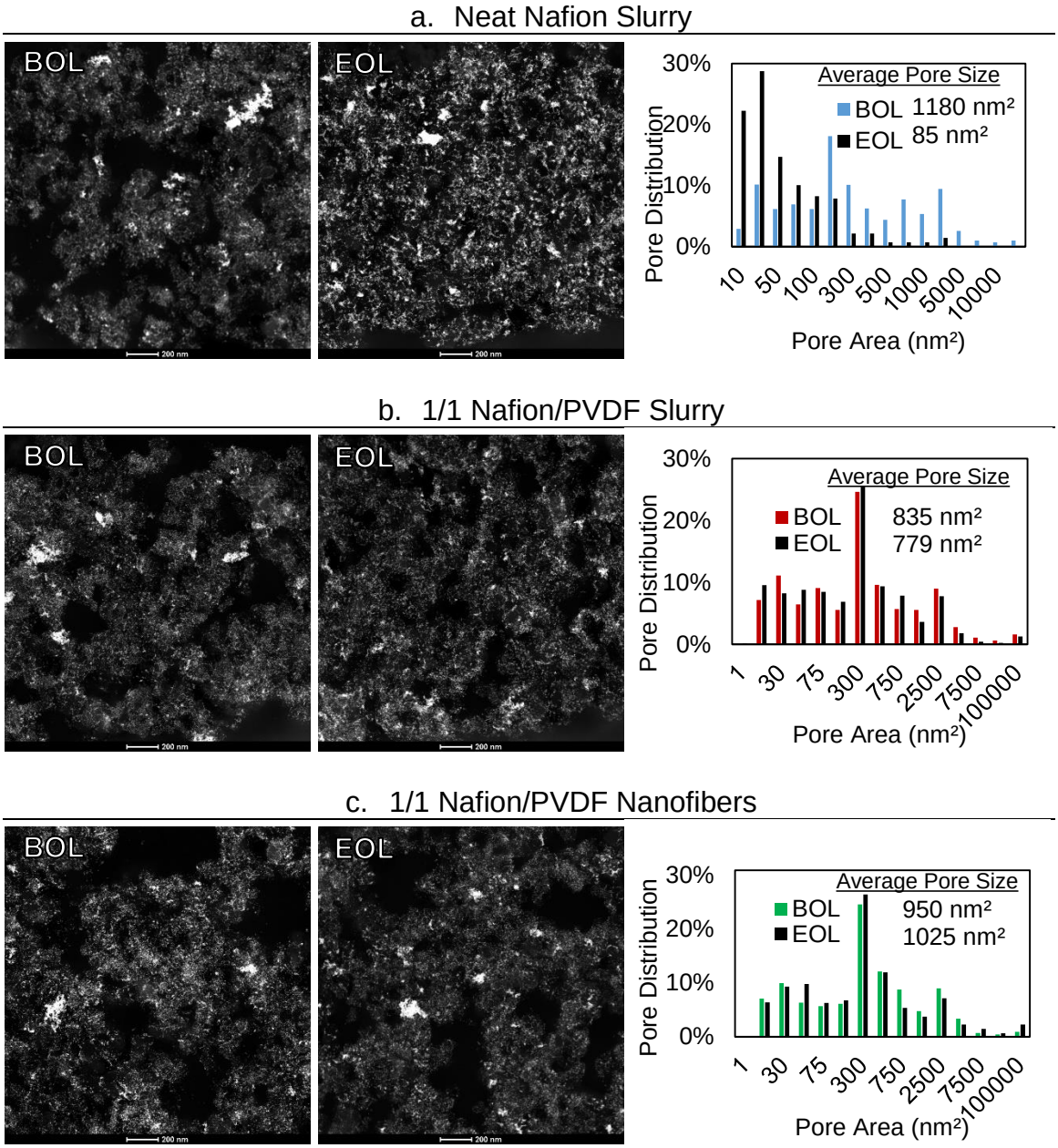

Figure 6.3. STEM imaging analysis of pore area distribution for the BOL and EOL (1000 carbon corrosion voltage cycles) accompanied by a BOL/EOL histogram of pore area distribution for (a) neat Nafion slurry electrode, (b) 1/1 Nafion/PVDF slurry electrode and (c) 1/1 Nafion/PVDF nanofiber electrode.

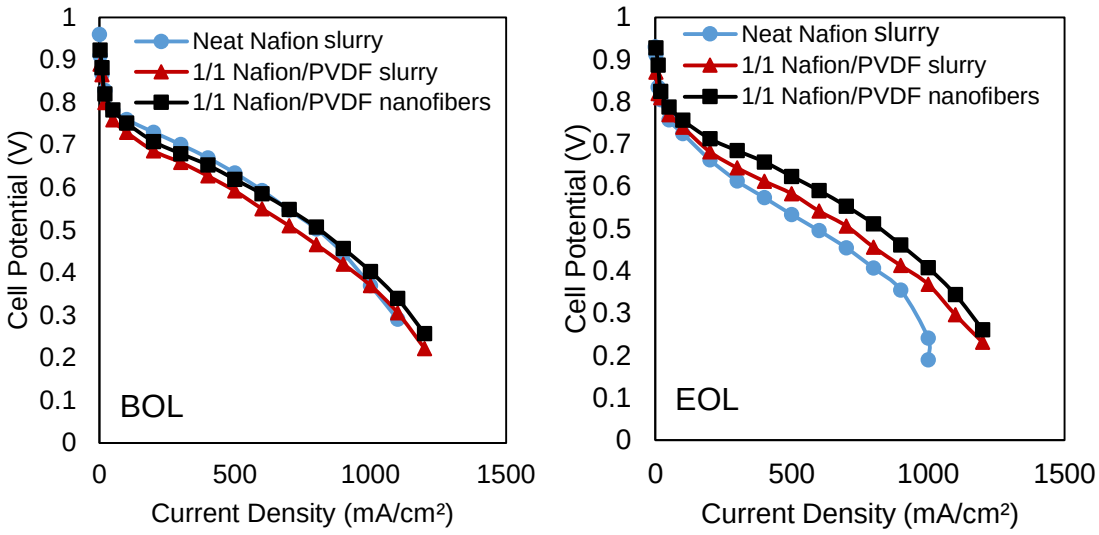

Figure 6.4. Polarization data for neat Nafion electrode, 1/1 Nafion/PVDF slurry electrode, and 1/1 Nafion/PVDF nanofiber electrode MEAs at BOL and EOL where EOL is 1000 carbon corrosion voltage cycles from 1.0 V – 1.5 V at 500 mV/s in a triangular wave. All MEAs have a loading of 0.1 mg/cm^2 Pt at the anode and cathode, a Nafion 211 membrane, and a Sigracet 29BC gas diffusion layer. The operating conditions are 80 C, ambient pressure, and 125/500 sccm H_2/air feed gas flow rates.

6.4 Conclusions

The addition of PVDF to the binder of either a conventional slurry cathode or a nanofiber cathode MEA improves durability after a carbon corrosion voltage cycling accelerated stress test. After 1000 voltage cycles, MEAs with nanofiber cathodes containing PVDF retain more of their original thickness and a higher degree of their original porosity, as compared to a slurry cathode of the same composition or a slurry cathode containing neat Nafion. Regardless of morphology, for a cathode with a binder of 1:1 Nafion:PVDF, there is essentially no decrease in cathode thickness after the carbon corrosion AST. Thickness correlates well with the loss of carbon after the carbon corrosion AST for both a slurry and a nanofiber electrode with PVDF. The loss of ECSA, mass activity, and power at EOL for the slurry cathode containing PVDF relative to a nanofiber cathode with the same binder is explained by the loss in porosity of both cathodes. In summation, the presence of PVDF

in a nanofiber aids in the retention of carbon and provides structural support to retain cathode thickness and prevent collapse of porosity which help to retain ECSA after carbon corrosion.

6.5 References

[1] T. Yoda, H. Uchida, M. Watanabe, *Electrochim. Acta* **2007**, *52*, 5997.

[2] A. S. Aricò, A. Stassi, E. Modica, R. Ornelas, I. Gatto, E. Passalacqua, V. Antonucci, *J. Power Sources* **2008**, *178*, 525.

[3] J. Xie, D. L. Wood, D. M. Wayne, T. A. Zawodzinski, P. Atanassov, R. L. Borup, *J. Electrochem. Soc.* **2005**, *152*, A104.

[4] P. Yu, M. Pemberton, P. Plasse, *J. Power Sources* **2005**, *144*, 11.

[5] K. Matsuoka, S. Sakamoto, K. Nakato, A. Hamada, Y. Itoh, *J. Power Sources* **2008**, *179*, 560.

[6] K. H. Kangasniemi, D. A. Condit, T. D. Jarvi, *J. Electrochem. Soc.* **2004**, *151*, E125.

[7] H. Yoshida, T. Kinumoto, Y. Iriyama, Y. Uchimoto, Z. Ogumi, *ECS Trans.* **2007**, *11(1)*, 1321.

[8] S. Zhang, X. Z. Yuan, J. N. C. Hin, H. Wang, J. Wu, K. A. Friedrich, M. Schulze, *J. Power Sources* **2009**, *194*, 588.

[9] M. U. Kento Takahashi, Ryo Koda, Katsuyoshi Kakinuma, *J. Electrochem. Soc.* **2017**, *164*, F235.

[10] M. K. Debe, A. K. Schmoeckel, G. D. Vernstrom, R. Atanasoski, *J. Power Sources* **2006**, *161*, 1002.

[11] W. Zhang, P. N. Pintauro, *ChemSusChem* **2011**, *4*, 1753.

[12] M. Brodt, T. Han, N. Dale, E. Niangar, R. Wycisk, P. Pintauro, *J. Electrochem. Soc.* **2015**, *162*, F84.

[13] M. Brodt, R. Wycisk, P. N. Pintauro, *J. Electrochem. Soc.* **2013**, *160*, F744.

[14] M. Brodt, R. Wycisk, N. Dale, P. Pintauro, *J. Electrochem. Soc.* **2016**, *163*, F401.

[15] R. Joseph Fairweather, Bo Li, Rangachary Mukundan, James Fenton, Borup, *ECS Trans.* **2010**, *33*, 433.

[16] N. Macauley, D. D. Papadias, J. Fairweather, D. Spernjak, D. Langlois, R.

Ahluwalia, K. L. More, R. Mukundan, R. L. Borup, *J. Electrochem. Soc.* **2018**, *165*, F3148.

[17] B. T. Sneed, D. A. Cullen, K. S. Reeves, O. E. Dyck, D. A. Langlois, R. Mukundan, R. L. Borup, K. L. More, *ACS Appl. Mater. Interfaces* **2017**, *9*, 29839.

[18] J. Wang, G. Yin, Y. Shao, S. Zhang, Z. Wang, Y. Gao, *J. Power Sources* **2007**, *171*, 331.

[19] M. Uchida, *J. Electrochem. Soc.* **1995**, *142*, 4143.

[20] N. T. Stetson, R. C. Bowman, *DOE Hydrog. Fuel Cells Progr. Rec. 16020* **2009**.

[21] M. Brodt, T. Han, N. Dale, E. Niangar, R. Wycisk, P. Pintauro, *J. Electrochem. Soc.* **2014**, *162*, F84.

[22] H. A. Gasteiger, S. S. Kocha, B. Sompalli, F. T. Wagner, Activity benchmarks and requirements for Pt, Pt-alloy, and non-Pt oxygen reduction catalysts for PEMFCs. *Appl. Catal. B Environ.* **2005**, *56*, 9–35.

[23] and J. Z. Huamin Zhang, Jianlu Zhang, Jifeng Wu, *PEM Fuel Cell Testing and Diagnosis*; Elsevier Science, 2013.

[24] Atsushi Ohma, Kazuhiko Shinohara, Akihiro Iiyama, Toshihiko Yoshida, and A. Daimaru, *ECS Trans.* **2011**, *41*, 775.

[25] U.S. Department of Energy, *Annu. Prog. Rep.* **2014**.

[26] P. Soille, L. M. Vincent, **1990**, 240.

[27] L. Dubau, L. Castanheira, M. Chatenet, F. Maillard, J. Dillet, G. Maranzana, S. Abbou, O. Lottin, G. De Moor, A. El Kaddouri, C. Bas, L. Flandin, E. Rossinot, N. Caqué, *Int. J. Hydrogen Energy* **2014**, *39*.

[28] K. G. G. R. M. D. T. F. Fuller, In *Handbook of Fuel Cells*; 2010; p. 6.

[29] T. Abe, H. Shima, K. Watanabe, Y. Ito, *J. Electrochem. Soc.* **2004**, *151*, A101.

[30] Y. C. Park, K. Kakinuma, M. Uchida, D. A. Tryk, T. Kamino, H. Uchida, M. Watanabe, *Electrochim. Acta* **2013**, *91*, 195.

[31] L. Castanheira, W. O. Silva, F. H. B. Lima, A. Crisci, L. Dubau, F. Maillard, *ACS Catal.* **2015**, *5*, 2184.

[32] A. Kongkanand, Z. Liu, I. Dutta, F. T. Wagner, *J. Electrochem. Soc.* **2011**, *158*, B1286.

[33] J. C. Meier, C. Galeano, I. Katsounaros, J. Witte, H. J. Bongard, A. A. Topalov, C. Baldizzone, S. Mezzavilla, F. Sch??th, K. J. J. Mayrhofer, *Beilstein J. Nanotechnol.*

2014, *5*, 44.

[34] A. . Schulenburg, H.; Schwanitz, B.; Linse, N.; Scherer, G. G.; Wokaun, I. Krbanjevic, J.; Grothausmann, R.; Manke, *J. Phys. Chem. C* **2011**, *115*, 14236.

CHAPTER 7

SULFONATED SILICA NETWORK AS A HIGH IEC-BINDER

7.1 Introduction

H_2/air fuel cell electrodes typically contain an ionically conductive binder to maintain low ionic resistance for the transport of protons to/from the catalyst sites at the anode and cathode.[1] This is generally accomplished by utilizing a polymeric ionomer such as a perfluorosulfonic acid (PFSA).[2,3] The ionic conductivity of PFSA polymers are highly dependent on the relative humidity and range from 0.01 S/cm to greater than 0.1 S/cm.[4] While the PFSA ionomers are widely used in fuel cells due to the superacidity of their side-chains, these polymers can face several issues including degradation[5], poor retention of conductivity at low RH and high temperature[6], excessive in-plane swelling leading to mechanical failure during the operation of a fuel cell,[7] and the synthesis of PFSAs is damaging to the environment. In addition to their manufacturing process being environmentally harmful, the degradation products of PFSAs may also be dangerous to both humans and the environment. For these reasons, alternatives to PFSAs are being examined. The most mature technology competing with PFSA polymers include sulfonated hydrocarbon polymers. The proton conductivity of a sulfonated hydrocarbon polymer such as poly(4-phenoxybenzoyl1,4-phenylene) or Sulfonated poly(etheretherketone) range from 10^{-6} at low relative humidity to 10^{-2} S/cm at high relative humidity, making these types of polymers generally less conductive than PFSAs at all humidities. In addition to this, hydrocarbon-based proton exchange polymers may be very brittle in the anhydrous state which can intermittently occur in a fuel cell operation, and the chemical durability is suspect. A more recent advancement as an alternative to PFSA is to utilize a sulfonated

silicate precursor to generate a hybrid organic/inorganic ionically conductive network through the use of a sol-gel reaction.[8,9] The conductivity measured by Maneeratana et al. was 101 mS/cm at 120 °C and 80% RH which is comparable to Nafion under the same conditions.

While there have been several papers published about the use of sulfonated silica in a membrane[8–10], there is also one reference of the use of sulfonated silica in a fuel cell electrode.[11] These authors utilized a similar scheme to membrane fabrication and incorporated TEOS and a sulfonated precursor in an electrode ink. The sulfonated precursor used in this study was 3-(trihydroxysilyl)-1-propanesulfonic acid (TPS). This organosilane sulfonated precursor was hygroscopic and did not contain a phenyl group which helped to promote hydration of the catalyst layer. The electrochemical analysis of this electrode in an MEA was only provided in H_2/O_2 at 80 °C, 170 kPa absolute between 20% RH and 100% RH, with a Nafion 212 membrane and a cathode loading of 0.34 mg_{Pt}/cm^2. At these conditions, the maximum power densities reported were ~300 mW/cm^2. The durability of the slurry-based sulfonated silica electrode binder was not provided.

In this chapter, the preparation of nanofiber fuel cell cathodes with a sol-gel reaction taking place during the electrospinning process is described. The fuel cell electrodes contained a hybrid organic-inorganic sulfonated silicate network. In the present study, the sol-gel reaction occurred in polyvinylidene fluoride (PVDF) nanofibers to provide mechanical and chemical stability to the electrode mat.

7.2 Experimental

Nanofiber cathodes were prepared with Pt/C catalyst and a polyvinylidene fluoride binder (PVDF), with/without a highly conductive sulfonated silica inorganic network created from tetraethyl orthosilicate (TEOS) and (4-chlorosulfonylphenyl)ethyltrichlorosilane (CSPTC). The total inorganic content (sulfonated silica network resulting from the sol-gel reaction of TEOS and CSPTC) was held constant at 23 wt.%. The TEOS/CSPTC mass ratio was either 1/1 or 1/2, giving a theoretical electrode ion exchange capacity (IEC) of 0.75 mmol/g or 0.97 mmol/g. In an electrode that contains 23 wt.% Nafion, the effective IEC is (23% · 0.909 mmol/g) = IEC of 0.21 mmol/g. These IEC values are smaller than the pure ionomer IEC because they are based on the total electrode weight, including the mass of the catalyst and PVDF. (E.g. neat Nafion has an IEC of 0.909 mmol/g, and a 1/2 TEOS/CSPTC network has an IEC of 4.2 mmol/g).

Two primary types of nanofiber cathode inks were prepared and are distinguished by their components: (1) (Pt/C)/PVDF and (2) (Pt/C)/PVDF/(CSPTC/TEOS). All inks contained the same type of catalyst, Johnson Matthey HiSPEC 40% Pt/C. Each ink was prepared by dispersing the carbon supported catalyst in dimethyl formamide (DMF) followed by mechanical mixing with a magnetic stir bar and sonication. All sonication steps lasted 30 minutes in an ice bath using a Fisher Scientific FS20D sonication bath. A stock solution of 10% PVDF (1:1 wt. ratio DMF:acetone) was added and mechanically mixed overnight. For type 2 inks, TEOS and CSPTC were added after the catalyst and PVDF ink components were mechanically mixed overnight. Once the TEOS and CSPTC were added, the dispersion was magnetically stirred at 70 °C for 1 hour, and then directly electrospun. One drop of H_2SO_4 was added to ensure that the ink was acidic to create the

desired network. The hydrolysis reaction begins as soon as the TEOS and CSPTC are added to the ink, during the 70 °C stirring, and during the electrospinning process. Anodes for this study were all 65/23/12 – (Pt/C)/Nafion/PAA nanofibers prepared as previously discussed in this dissertation in Chapters 4, and 5.

For electrospinning sol-gel fibers, electrode inks were drawn into a 3 mL syringe with a 22 gauge metal needle tip. The electrospinning conditions for the electrode inks are provided in Table 7.1.

Table 7.1 Electrospinning conditions for two types of electrode materials.

	Electrode Type 1	Electrode Type 2
Solution Components	(Pt/C)/PVDF	(Pt/C)/PVDF/(CSPTC/TEOS)
Electrode Composition	65/35	65/12/23
Voltage (kV)	12	10
Ink flow rate (mL/h)	1	0.75
Spinneret to collector distance (cm)	8	10
Relative Humidity (%)	75%	70%

Nanofiber mats were imaged using electron probe microscopy, which was carried out at Vanderbilt Institute of Nanoscale Science and Engineering using a Zeiss Merlin scanning electron microscope (SEM) with a 10 kV accelerating voltage. Samples were gold sputter coated to increase their conductivity and inhibit unwanted image artifacts.

Membrane electrode assemblies (MEAs) were prepared from the materials electrospun using conditions in Table 7.1. Mats were cut into 5 cm^2 squares and hot pressed with a Nafion 211 membrane at 140 °C and 4 MPa, for 5 minutes. MEAs were used with Sigracet 29BC gas diffusion layers (GDLs). The final MEAs were tested in a Scribner 850e fuel cell test station where.

After collecting BOL polarization data, MEAs underwent a carbon corrosion accelerated stress test (AST). As outlined by the United States Department of Energy, the voltage at the cathode was cycled between 1.0 and 1.5 V at a scan rate of 500 mV/s with a triangular wave for 1000 cycles. The operating conditions during the AST were 80 °C, ambient pressure, 100% RH and H_2/N_2 gas flow rates of 125/500 sccm. The voltage cycling was performed using a potentiostat (Gamry Instruments Reference 3000).

7.3 Results and Discussion

7.3.1 Ion Exchange Capacity of the Sulfonated Silica Network/Sulfonated Precursor

The structure of the starting compounds used to prepare the sulfonated silicate network are shown in Figure 7.1. The sulfonated silicate network that forms from these compounds is 3-dimensional; the chlorine groups leave the CSPTC and the ethyl groups leave the TEOS. Then the silicon atom in the CSPTC then bonds to an oxygen in the TEOS, or TEOS precursors can bond to each other. This propagates until the network is formed. The exact structure of the network is not easily depicted.

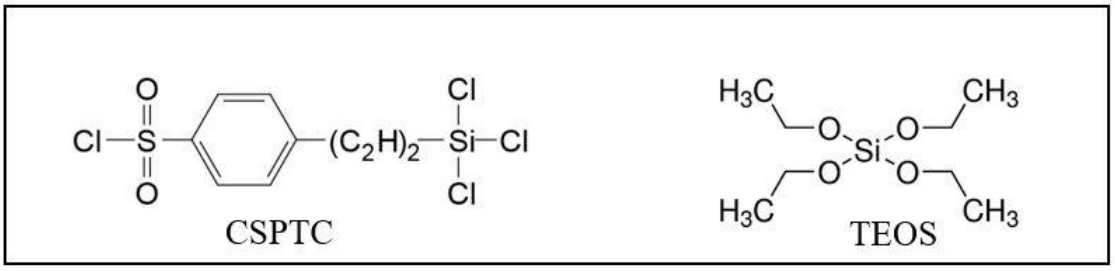

Figure 7.1 Structure of [2-(4-Chlorosulfonylphenyl)ethyl]trichlorosilane (CSPTC) and tetraethyl orthosilicate (TEOS).

To calculate a theoretical ion exchange capacity (IEC) of the inorganic binder of the electrode, the moles of the sulfonic acid sites and the mass of the total inorganic network were determined using Equations 7.1 and 7.2. IEC values from these equations

are upper bounds assuming the sol-gel reactions (hydrolysis and condensation) proceed to completion.

$$\text{Hybrid Network Mass} = \left(m_{TEOS} \cdot \left(\frac{m_{TEOS,After\ Hydrolysis}}{M_{TEOS,Before\ Hydrolysis}} \right) + m_{CSPTC} \cdot \left(\frac{m_{CSPTC,After\ Hydrolysis}}{M_{CSPTC,Before\ Hydrolysis}} \right) \right) \quad (7.1)$$

Where "m" is the mass of either TEOS or CSPTC (grams), and "M" is the molecular weight of the component either before or after hydrolysis (grams/mole). This results in the total mass of the sulfonated silicate network. To determine the IEC of the network, Equation 2 is used.

$$\text{IEC} = \frac{\frac{m_{CSPTC}}{M_{CSPTC,After\ Hydrolysis}}}{(Hybrid\ Network\ Mass)} \quad (7.2)$$

The ion exchange capacity is equal to the moles of sulfonic acid groups per mass of total inorganic network; this value is dependent on the CSPTC content relative to that of TEOS after the sol-gel reaction has taken place. As the mass ratio of initially added CSPTC relative to TEOS increases, both the sulfonic acid sites and the total mass of the inorganic network after the hydrolysis and condensation reactions increase. For this reason, the IEC does not increase linearly with the amount of CSPTC added.

7.3.2 Physical Characterization of Electrospun PVDF Fibers with Sol-Gel Sulfonated Silica

Top-down SEM images of the electrospun nanofibers composed of Pt/C, PVDF, and sulfonated silica network are shown in Figure 7.2a (1/1 TEOS/CSPTC) and 7.2b (1/2 TEOS/CSPTC). The fiber structure was not significantly different between the two ratios. In both cases, the total sulfonated silica network content was held constant at 23%.

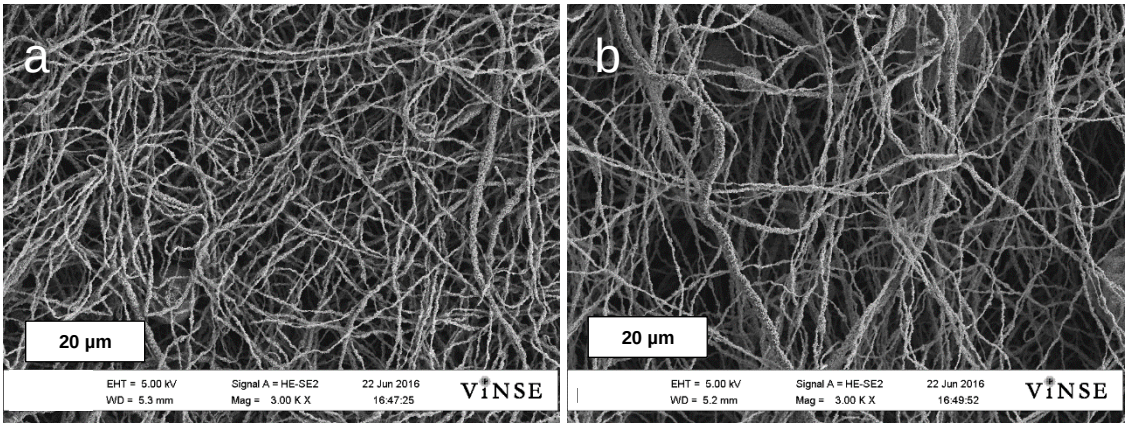

Figure 7.2. Scanning Electron Micrographs of Pt/C, PVDF nanofibers with (a) 1/1 TEOS/CSPTC and (b) 1/2 TEOS/CSPTC.

7.3.3 Electrochemical Analysis

Polarization data were collected for three MEAs: a baseline (Pt/C)/PVDF nanofiber cathode MEA, and two MEAs containing Pt/C, PVDF, and a hybrid organic/inorganic sulfonated silica network, where the sulfonated silica network had either a 1/1 or a 1/2 TEOS/CSPTC ratio. The results of these experiments are shown in Figure 7.3 and in Table 7.2 Fuel cell polarization data were collected at either 100% RH or 40% RH for the H_2 and air feed gasses, where the cell temperature was 80 °C, the back pressure was 200 kPa, and the gas flow rates were 125/500 sccm H_2/air.

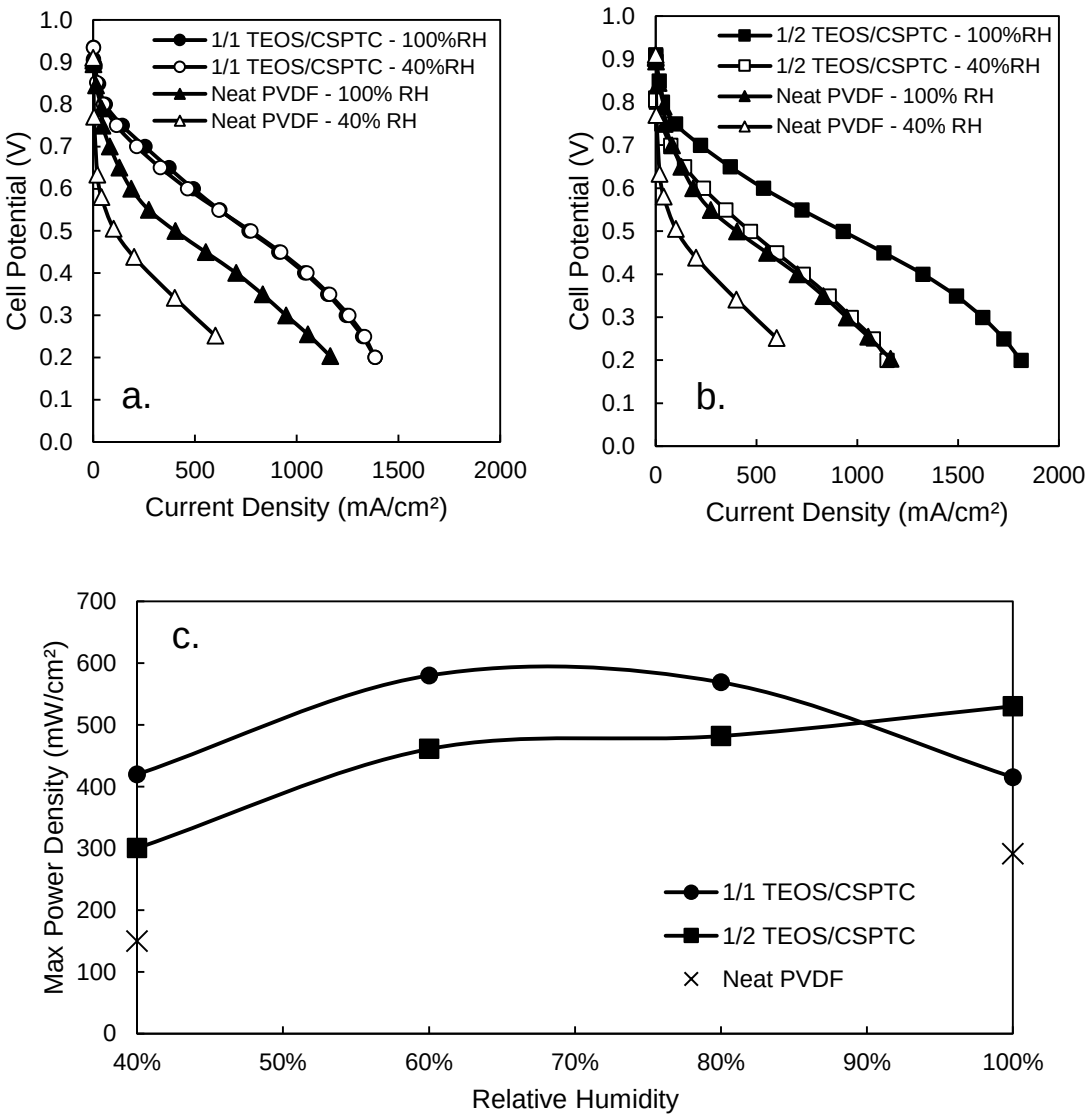

Figure 7.3. (a) Polarization data for 1/1 TEOS/CSPTC ratio nanofiber electrode MEAs using Pt/C and PVDF as well as a neat PVDF baseline and (b) 1/2 TEOS/CSPTC ratio nanofiber electrode MEAs using Pt/C and PVDF as well as a neat PVDF baseline. (c) Maximum power density for each MEA from 40% to 100% relative humidity. Operating conditions were: 200 kPa absolute, 80 °C, 125/500 sccm H_2/air. All MEAs had a cathode/anode catalyst loading of 0.1 mg/cm^2, a Nafion 211 membrane, and Sigracet 29BC gas diffusion layers.

The polarization data from the neat PVDF nanofiber cathode MEA is in good agreement with previously published neat PVDF nanofiber data from Brodt et al.[12] Power is low at 100% RH and 40% RH with a neat PVDF binder due to lack of proton

conductivity. The sol-gel nanofiber cathode MEA produced significantly more power compared to the neat PVDF electrode MEA. At full humidification, the MEA with the higher CSPTC content (1/2 TEOS/CSPTC) produced 27% more power as compared to the 1/1 TEOS/CSPTC ratio. However, at 40% RH, the MEA containing 1/1 TEOS/CSPTC produced 39% higher maximum power.

Table 7.2 IEC, and power density at for Nanofiber electrodes at 0.1 mg/cm^2, using a Nafion 211 membrane, with 29 BC GDLs. Operating conditions for power densities: 80 °C, 125/500 sccm, 200 kPa.

	Calculated IEC of electrode (mmol/g)	100% RH Power at Max (mW/cm²)	40% RH Power at Max (mW/cm²)
Neat PVDF	0.00	291	151
1/1 TEOS/CSPTC	0.75	415	420
1/2 TEOS/CSPTC	0.97	530	300

A related observation was made by Dos Santos et al.[13] Above a certain percentage of total inorganic content in a sol-gel membrane, the measured IEC decreased and swelling increased. Their results suggest that above a certain inorganic content and with a sufficiently high CSPTC content, there may be some loss of material due to precipitation of sol-gel silica particles and/or particle leaching.

Given that the electrodes in this dissertation utilized a 23% total inorganic network content, a similar phenomenon to that overserved by Dos Santos et al. may be occurring. Too much sulfonated silica may cause precipitation of individual particles which could leach over time, causing the conductivity to decrease and power to drop.

7.3.4 Electrode Polarization after a Carbon Corrosion Accelerated Stress Test

MEAs made with nanofiber cathodes using neat PVDF, and PVDF/sulfonated silica networks underwent the DOE carbon corrosion AST for 1000 cycles to compare BOL and EOL power density. Polarization data at beginning of life (BOL) and end of life (EOL) are plotted in Figure 7.4. and summarized in Table 7.3. The results of the neat PVDF nanofiber electrodes are consistent with that published by Brodt et al.[12] in that the power at EOL is slightly higher than the power at BOL. The EOL power density of the nanofibers with the sulfonated silica network is strongly dependent on the relative amount of CSPTC to TEOS. The nanofiber electrode MEA with 1/1 TEOS/CSPTC lost only 12% of its max power at 100% RH and lost only 5% of its max power at 40% RH (suggesting that the electrode had become more hydrophilic after the carbon corrosion AST in a similar fashion to what was previously reported by Brodt et al.)[12] However, the MEA with the higher CSPTC content lost much more power (44% loss at 100% RH and 58% loss at 40%RH).

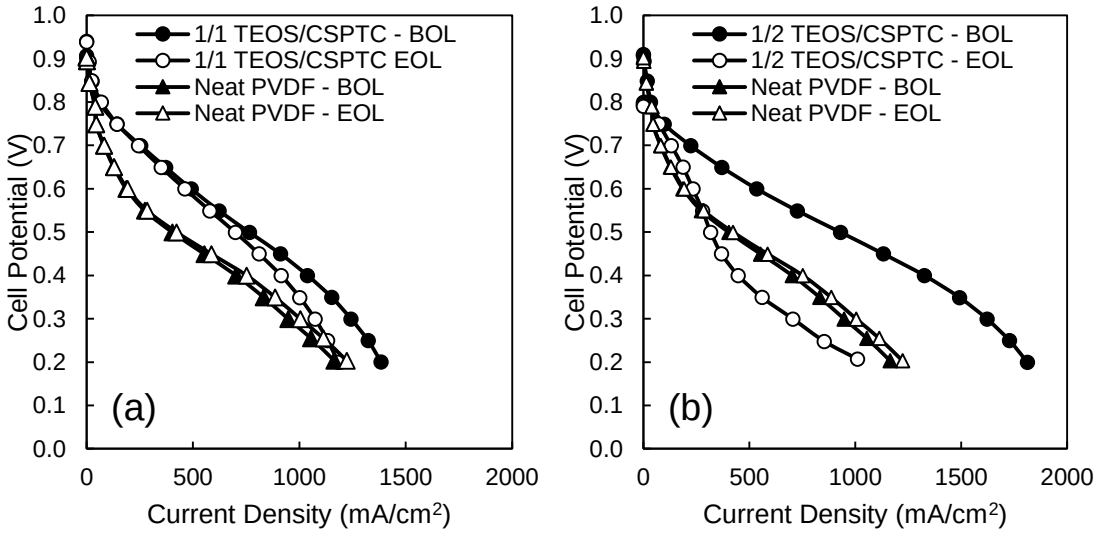

Figure 7.4. Polarization data at BOL and after 1,000 voltage cycles (EOL) from 1.0 V to 1.5V vs SHE following the DOE protocol for nanofiber electrodes with neat PVDF and (a) PVDF/(1/1 TEOS/CSPTC) and (b) PVDF/(1/2 TEOS/CSPTC). Operating conditions: 80

°C, 200 kPa, 125/500 sccm H_2/air. Anode/cathode loadings: 0.1 mg_{Pt}/cm^2, Nafion 211, and Sigracet 29BC GDLs.

The lower EOL power density of the electrode containing a higher amount of CSPTC could be a result of it being more hydrophilic (as Brodt et al. observed[12], the more hydrophilic electrodes had lower EOL power density relative to BOL).

Table 7.3. Power density at BOL and after 1,000 carbon corrosion cycles (1.0 V – 1.5 V) where the AST was performed at 100% RH.

	1/1 TEOS/CSPTC		1/2 TEOS/CSPTC		Neat PVDF	
	100% RH	40% RH	100% RH	40% RH	100% RH	40% RH
BOL Max (mW/cm^2)	415	420	530	300	291	151
EOL Max (mW/cm^2)	365	397	295	127	310	132
EOL/BOL	88%	95%	56%	42%	107%	87%

7.4 Conclusion

A hybrid organic/inorganic network of sulfonated silica was created in nanofiber electrodes containing Pt/C and polyvinylidene fluoride. This was accomplished through the use of a sol-gel reaction before, during, and after particle/polymer electrospinning. The resulting nanofiber electrode mat had a high theoretical ion-exchange capacity without the use of a PFSA or a hydrocarbon ionomer. H_2/air fuel cell MEAs with such cathodes produced higher power at low RH as compared to a baseline nanofiber cathode MEA with neat PVDF as the binder. The power density at low RH was also higher than that obtained from previously published spray electrodes containing a sulfonated silica network.[14] Increasing the amount of sulfonated silica precursor (CSPTC) relative to unsulfonated silica precursor (TEOS) significantly decreased the power density at low relative humidity

and decreased the EOL power density after 1000 carbon corrosion voltage cycles. The total content of inorganic silica network was held constant at 23 wt.% in this study; previously presented results suggest that when the inorganic network content is greater than 15 wt.% there is a decrease in measured IEC and increase in swelling due to leaching of highly charged silica particles and/or incomplete sol-gel reaction. This may be the case in the electrodes and more work should be done using a total sulfonated silica network content of 15 wt.% or less. More work can be also done to increase the power density at low RH by examining different ratios of sulfonated silica and TEOS. Additionally, precursors should be examined that do not contain a phenyl group (such as 3-(trihydroxysilyl)-1-propanesulfonic acid), since aromatic (hydrocarbon) sulfonates are prone to chemical degradation during fuel cell operation.

References

[1] D. R. Baker, D. A. Caulk, K. C. Neyerlin, M. W. Murphy, *J. Electrochem. Soc.* **2009**, *156*, B991.
[2] E. A. Ticianelli, C. R. Derouin, L. Alamos, L. Alamos, T. Gemini, **2018**.
[3] J. Peron, Z. Shi, S. Holdcroft, *Energy Environ. Sci.* **2011**, *4*, 1575.
[4] J. Fimrite, B. Carnes, H. Struchtrup, N. Djilali, *J. Electrochem. Soc.* **2005**, *152*, A1815.
[5] J. Healy, C. Hayden, T. Xie, K. Olson, R. Waldo, M. Brundage, H. Gasteiger, J. Abbott, *Fuel Cells* **2005**, *5*, 302.
[6] M. K. Epping, J. P. Kopasz, *Fuel Cells* **2009**, *9*, 356.
[7] S. Subianto, M. Pica, M. Casciola, P. Cojocaru, L. Merlo, G. Hards, D. J. Jones, *J. Power Sources* **2013**, *233*, 216.
[8] C. Laberty-Robert, K. Vallé, F. Pereira, C. Sanchez, *Chem. Soc. Rev.* **2011**, *40*, 961.
[9] V. Maneeratana, J. D. Bass, T. Azaïs, A. Patissier, K. Vallé, M. Maréchal, G. Gebel, C. Laberty-Robert, C. Sanchez, *Adv. Funct. Mater.* **2013**, *23*, 2872.
[10] L. Dos Santos, M. Maréchal, A. Guillermo, S. Lyonnard, S. Moldovan, O. Ersen, O. Sel, H. Perrot, C. Laberty-Robert, *Adv. Funct. Mater.* **2016**, *26*, 594.
[11] J. I. Eastcott, E. B. Easton, *J. Power Sources* **2014**, *245*, 487.
[12] M. Brodt, R. Wycisk, N. Dale, P. Pintauro, *J. Electrochem. Soc.* **2016**, *163*, F401.

[13] R. W. and P. N. P. Leslie Dos Santos, Devon Powers, In *21st International Conference on Solid State Ionics*; Padua, Italy, 2017; pp. 1–20.
[14] J. I. E. E. Bradley Easton, Sulfonated Silica-based electrode materials useful in fuel cells **2014**, 1–13.

CHAPTER 8

SUMMARY

1. Nafion/PVDF was used as a binder for electrospun nanofiber cathodes containing PGM-free catalysts provided by Pajarito Powder LLC for proton exchange membrane fuel cells (PEMFC). Ink composition and preparation techniques were identified to successfully prepare membrane-electrode-assemblies (MEAs) that contained either:
    a. Neat Nafion sprayed cathodes with 70% catalyst and 30% binder at 3.0 mg/cm^2 loading with a Nafion 211 membrane and a Pt/C anode at 0.1 mg_{Pt}/cm^2.
    b. 1/1 – Nafion/PVDF sprayed cathodes with 70% catalyst and 30% binder (15% PVDF and 15% Nafion) at 3.0 mg/cm^2 loading with a Nafion 211 membrane and a Pt/C anode at 0.1 mg_{Pt}/cm^2.
    c. 1/1 – Nafion/PVDF electrospun nanofiber cathodes with 70% catalyst and 30% binder (15% PVDF and 15% Nafion) at 3.0 mg/cm^2 loading with a Nafion 211 membrane and a Pt/C anode at 0.1 mg_{Pt}/cm^2.
    d. 1/2 – Nafion/PVDF electrospun nanofiber cathodes with 70% catalyst and 30% binder (20% PVDF and 10% Nafion) at 3.0 mg/cm^2 loading with a Nafion 211 membrane and a Pt/C anode at 0.1 mg_{Pt}/cm^2.
2. Each PGM-free cathode MEA was tested at BOL with no break-in procedure for initial performance evaluation and was subjected to a 300 hour voltage hold at 0.5 V. The current output over time was monitored. The current was measured across the entire timespan at a rate of 1 point every 10 minutes. The resulting Neat Nafion

curve agreed well with the literature while the MEAs containing PVDF resulted in a completely different trend – an increase in power density with respect to time. The nanofiber MEAs remained stable over the course of 300 hours while the slurry with PVDF lost 10% of its peak power which occurred around 100 hours.

3. PGM-free MEAs were subjected to a carbon corrosion voltage cycling accelerated stress test which ran under H_2/N_2 feed gases and operated from 1.0 V – 1.5 V. Traditional PGM-free catalysts lose ~90% of their initial power after only several carbon corrosion voltage cycles due to their high carbon content. This was observed for the Neat Nafion slurry cathode with PGM-free catalyst, whereas MEAs that contained PVDF in the cathode compartment were seen to withstand up to 500 carbon corrosion voltage cycles. Nanofiber electrodes that contained PVDF actually increased in power after 50 and 150 cycles. For example, the 1/1 Nafion/PVDF nanofiber electrode MEA increased from 150 mW/cm^2 max power to 180 mW/cm^2 max power.
4. Platinum-based inks for H_2/air PEM fuel cells were prepared in two ways – (1) catalyst was sonicated in the presence of water and alcohol and (2) catalyst was sonicated in the presence of water only. These two methods of ink preparation resulted in significantly different structures. Sonicating first with water and alcohol in the presence of catalyst and then electrospinning the resultant ink yielded fibers that melted upon hot pressing. Fibers that were electrospun from an ink that was sonicated in water only first did not lose their structure after hot pressing.
5. PtCo/C and PtNi/C from TKK were used as cathode catalysts in fuel cell MEAs. Electrodes were either painted at Vanderbilt University, sprayed at Nissan

Technical Center of North America (NTCNA) or electrospun into nanofibers with Nafion/PAA as the binder. The catalyst/binder ratio ranged from 55% to 65% wt.%. Electrochemical data was collected at both Vanderbilt and NTCNA including polarization data, electrochemically active surface area, and mass activity. Rated power data at elevated temperature was also obtained. These results were also supplemented with verification from Los Alamos National Lab (LANL) by sending nanofiber electrode MEAs to their facility to test.

6. NTCNA performed limiting current analyses to determine gas transport resistance (GTR). This analysis used 5 different oxygen concentrations in an O_2/N_2 feed at 4 different total pressures to determine the pressure dependent and pressure independent contributions of the gas transport resistance and to decouple the catalyst layer GTR from the diffusion media and the flow channels. Nanofiber electrodes were shown to have lower GTR at BOL as well as a smaller increase in GTR at EOL compared to a baseline slurry electrode MEA.
7. Scanning electron microscopy and scanning transmission electron microscopy was performed at Oak Ridge National Laboratory (ORNL) to determine electrode microstructure and intra-fiber properties. The analyses included looking at porosity from microtomed nanofiber cross sections, taking a tilt-series sequence of images to form a 3D reconstruction, using energy dispersive x-ray spectroscopy to analyze the distribution of ionomer and catalyst, and looking at low-magnification images of both MEA cross sections and planar views of the electrode to determine the structure and quality of the nanofibers used in fuel cell experiments.

8. Two types of accelerated stress tests (ASTs) were performed on Nafion/PAA-based nanofiber electrodes. The first accelerated stress test was a carbon corrosion AST which is defined by the United States Department of Energy as a voltage cycling protocol from 1.0 V – 1.5 V for up to 5,000 cycles. The second type of accelerated stress test was designed to simulate acceleration and deceleration in an automotive setting and is a metal dissolution stress test in which the voltage is cycled from 0.6 V to 0.95 V for up to 30,000 cycles. At Vanderbilt, these experiments were run at both 100%RH and 80% RH.
9. An electrospinning ink containing catalyst powder, Nafion in the sodium form, and polyethylene oxide was used to create an electrospun nanofiber electrode with a removable carrier. Unsuccessful attempts were made to electrospin the in using proton-form Nafion as well. Eventually, the electrospinning conditions of 20 cm, 20%RH, and around 8 kV was determined after much experimentation. The resultant nanofiber mat was hot pressed to a membrane and soaked in acid and water to remove the carrier. The fibers retained their structure and the performance in the fuel cell was improved relative to a nanofiber that still retained its carrier (e.g. PAA)
10. Nuclear magnetic resonance (NMR) experiments were performed to determine the quantitative amount of PEO that was being leeched from the electrode structure during the 1 hour soak. NMR was performed after soaking an electrode for 1 hour and again after a second hour. The first soak water showed that 97% of the PEO is removed while the second soak showed that there was only a trace amount of PEO

that remained in the electrode material after the first hour. These two experiments combined to confirm that the PEO is being removed.

11. The Nafion/PEO electrodes were tested at both high and low RH and it was determined that the performance was essentially constant from 100% RH to 40% RH. These results were verified at both Nisan Technical Center of North America and at Los Alamos National Laboratory.
12. STEM imaging was performed on the Nafion/PEO electrodes and revealed that the Nafion in the fibers was drawn toward the edge of the fiber diameter, leaving an I/C in the core of the fiber around 0.4 and an I/C at the edge of the fiber closer to 2. This structure is not fully understood and more work needs to be done to understand how it is affecting the performance of the fibers. STEM analysis also showed that the average pore size of the Nafion/PEO nanofiber cross section was smaller compared to the pore size in the Nafion/PAA nanofiber. This lead to the hypothesis that water may be condensing in the small pores of the fibers. This was tested by changing the pressure at low RH to see if performance increases more with pressure.
13. Oxygen reduction kinetics were tested for Nafion/PEO nanofibers vs RH compared to a slurry baseline. These experiments involved running H_2/O_2 feed gases, correcting the current due to hydrogen crossover, and correcting the voltage based on the ohmic voltage losses associated with the HFR. These results showed that the Tafel slopes of the nanofiber electrodes were shallower than the slurry at low RH.
14. A structural study on Pt/C, Nafion, and PVDF based electrodes was performed by analyzing MEA cross sections at Oak Ridge National Laboratory. These analyses

included cathode thickness measurements and STEM porosity measurements both at BOL and after 1000 carbon corrosion voltage cycles. The analyses showed that the greater the PVDF content, the less the cathode layer thinned and that above 50% PVDF, there was essentially no cathode thinning. Additionally, there was very little decrease in the porosity of the nanofiber electrode with PVDF compared to a neat Nafion slurry that also underwent the carbon corrosion AST.

15. Using a sol-gel reaction during the electrospinning process, a hybrid organic/inorganic sulfonated silicate network was generated within the electrode structure. This structure showed an improvement at low RH compared to a neat Nafion slurry electrode. Experiments were performed at varying concentrations of the sulfonated silica component (CSPTC) vs. the un-sulfonated component (TEOS)

CHAPTER 9

CONCLUSIONS

1. The use of electrospinning and polyvinylidene fluoride as a binder for a PGM-free catalyst system significantly improves the power generation of the MEA after a 300 hour hold at 0.5 V vs SHE. After this voltage hold, the current generation of a nanofiber MEA with a 1/1 Nafion/PVDF binder was stable and was more than 60% higher compared to a neat Nafion slurry baseline. In addition, the Nafion/PVDF nanofiber electrode was able to maintain significant power output after 500 carbon corrosion voltage cycles while the neat Nafion slurry diminished by nearly 90%. The use of PVDF in a slurry decreased the BOL power density compared to a neat Nafion slurry, but did improve the EOL/BOL power density.
2. Platinum alloys can be electrospun into a nanofiber cathode mat. The benefit of the nanofiber structure is most evident at EOL. The ways that the nanofiber morphology improve the power density of an MEA were determined to be by (1) lowering the gas transport resistance (2) decreasing the ionomer resistance in the catalyst layer (3) increasing surface area by introducing significant void-space within the fiber structure (30% surface area comes from internal porosity determined by STEM) and (4) by improving resistance to metal dissolution (evidence from both polarization data and energy dispersive x-ray spectroscopy elemental analysis of cobalt retention in PtCo nanoparticles).
3. The use of polyethylene oxide (PEO) as a removable carrier polymer for nanofiber electrodes is possible. This is accomplished by protecting the PEO from the superacidity of the ionomer in the ink by performing a Na^+ ion-exchange with the

ionomer in the ink. The carrier was proved to be removed through the use of repeated NMR experiments that show 97% of the PEO is removed in an hour soak at 80 °C. The result of this carrier removal in an MEA that generates significantly more power compared to both a slurry and a nanofiber that retains its carrier polymer. This high power is seen at both full humidification as well as at low relative humidities. The power output is essentially constant, the high frequency resistance determined by electrochemical impedance spectroscopy does not significantly increase with decreasing RH, and the oxygen reduction kinetics do not decrease as much as predicted with decreasing RH. All of these results suggest that the MEA is holding onto water at elevated back pressure. To study this possibility, STEM cross sectional analysis was performed on the Nafion/PEO nanofiber electrode. The results show that the pore size is significantly smaller than the Nafion/PAA nanofibers and may be sufficient to condense water via capillary condensation. The pore sizes measured were compared to predicted pore sizes to condense water according to the Kelvin Equation and were found to have 25% of the pores that were sufficiently small to condense water. This effect is further illustrated by observing a more drastic decrease in power at low RH and ambient pressure compared to 200 kPa absolute whereas there is a more mild decrease in power at full humidification.

4. The Nafion/PVDF system in a Pt-based electrode was shown to improve EOL power density by decreasing the amount that the catalyst layer thinned as well as decreased the amount of porosity that was lost after carbon corrosion. The evidence suggests that the PVDF is acting as a scaffolding material to prevent the collapse

of the catalyst layer as the carbon support is corroded and leaves as CO_2. The measured increase in pore size at EOL is consistent with the loss of material since there is no catalyst layer thinning and CO_2 is measured to leave during the corrosion AST.

5. The use of a sol-gel sulfonated silicate network in a nanofiber electrode produced higher power at low RH compared to a nanofiber electrode MEA with neat PVDF as the binder. This is the first electrode to be made in this way. Increasing the of sulfonated silica precursor, 4-chlorosulfonylphenyl)ethyltrichlorosilane (CSPTC) to unsulfonated silica precursor, tetraethyl orthosilicate (TEOS) significantly decreased the power density observed at low relative humidity and decreased the EOL power density after 1000 carbon corrosion voltage cycles.

CHAPTER 10

FUTURE WORK

1. Only two different Nafion/PVDF ratios were prepared for nanofibers containing PGM-free catalysts. More work should be done to determine the optimal ratio of Nafion and PVDF for this system. Different ratios of Nafion and PVDF should be used to determine what the optimal ratio is.
2. Only one MEA was made using Nafion/PEO as a binder for PGM-free catalysts. More MEAs should be tested with this binder to determine its effectiveness in producing higher power with Pt-free systems.
3. Nafion/PEO nanofiber electrodes (anode and cathode) are still poorly understood. There are many experiments that must be done to answer important questions regarding why these nanofibers have increased performance at both high and low relative humidity. For example:
    a. A more careful quantification of PEO removal should be performed to determine the exact percentage of PEO that is removed in a water soak with varying time.
    b. Polarization loss analyses should be performed to de-couple the effects of the anode and cathode.
    c. More work needs to be done to understand the effect of the core/shell structure of fiber cathodes with Nafion/PEO binder, including modeling of the interactions of water in pores, the protons conducted through that water and how the distance of the ionomer to the catalyst sites affects ion transport.

d. Work should be done to understand how/why residual PAA increases flooding in a PtCo/C cathode, reduce proton conductivity of Nafion, and how it affects ORR kinetics. (The power density is observed to decrease from 80% RH to 100% RH).

e. Future work should also include examining homogeneous solution cast films and fiber mats of Nafion/PAA and Nafion/PEO mixtures: specifically, how these compare in terms of sorption, conductivity and other properties.

f. Hot pressing conditions should be examined for MEAs that use the sodium-form of Nafion. Nafion(Na^+) is known to have a higher glass transition temperature – work should be done to determine how this affects fuel cell power and at BOL and EOL as well as to answer what happens to the sodium ions after a Nafion(Na^+)/PEO electrode is placed into a fuel cell. The effect of these ions on EOL power density (after a metal dissolution AST as well as a carbon corrosion AST) should also be determined.

4. MEAs using higher loading Pt/C in PEO-based electrodes should be tested in an effort to meet the demands of automotive companies.
5. Scale-up processes should be optimized so that nanofibers containing Nafion/PEO can be produced on a mass-scale.
6. Sulfonated silica electrodes are not well understood or optimized. Future work should include:

    a. Continued physical characterization including elemental mapping of sulfur and silica throughout a (Pt/C)/PVDF-based nanofiber electrode.

b. More work should be done to both understand what causes differences in polarization behavior at different ratios of TEOS to CSPTC as well as total inorganic content.
c. Nanofiber electrodes using a total sulfonated silica network content of 15 wt.% or less should be fabricated. These should undergo all the treatments that have shown to improve conductivity and reduce swelling of membranes containing the same type of networks: i.e. base treatment and annealing.
d. Investigate sulfonated silica precursors that do not contain a phenyl group (such as 3-(trihydroxysilyl)-1-propanesulfonic acid) instead of CSPTC.